Development of Selective Ligands for the Removal of Caesium, Strontium and Corrosion Products for Nuclear Waste Reprocessing

A thesis submitted in partial fulfilment of the requirements for the degree of

Doctor of Philosophy

Department of Chemistry

University of Reading

Iain Hopkins

April 2019

Declaration

I confirm that this is my own work and the use of all material from other sources has been properly and fully acknowledged.

Iain Hopkins

April 2019

Acknowledgements

Firstly, I would like to thank Professor Laurence Harwood for giving me the opportunity to be part of his fantastic research group and the chance to complete my PhD. I am grateful for your patience, support and advice during my time at Reading helping me to stay on the right track. Weekly meetings were a chance to present break throughs in research or to ponder how we've managed to 'produce' caesium and were extremely helpful. Thank you for being so approachable, even after office hours *via* emails. I will miss the jokes even though I may have heard them all by now.

Thanks also to George Elder and Sabine Joubaire for the constant push to achieve my project goals. Their insight into the project was highly valuable as well as their support and encouragement. Thanks must be given to Andy Leask and Rogers Leask for funding the project.

I would like to acknowledge Dr Ashfaq Afsar, Dr Joe Cowell, Dr James Westwood and Dr Chris Smith for their general lab supervision and for making the lab a welcoming and fun environment. It was a pleasure to work alongside previous and existing members of the Harwood group in Lab 213: Andy (Rui) Gu, Diana Monir, Geungseok Jang, Jasraj Singh Babra and Zoe Selfe (even as Zoe turned Lab 213 into a disco). Meeting and supporting numerous MChem students was enjoyable and amusing with my favourite 'incident' being when a student made up brine solution with acetone (and another student used it). Thank you to everyone in G06 for the jokes, strange talks and push to complete the Thesis.

Use of the Chemical Analysis Facility (CAF) and its general maintenance is gratefully acknowledged. A special thanks to Andy Dodson for general maintenance of the ICP-MS and Amanpreet Kaur for running TEM and SEM for me.

I would like to thank my family, especially my parents Paul and Elspeth for constantly asking if I've finished yet but mainly their encouragement and support. Special thanks to Emily Orrin, my fiancée, for putting up with me throughout and the invaluable help you gave me.

Abstract

In order to increase the public approval of nuclear power as an alternative to fossil fuels, developments in waste management of high-level liquid waste must be made. Fission products, such as ^{137}Cs and ^{90}Sr, are highly radiotoxic and principal heat generators in high-level liquid waste. Removal of these fission products would reduce the radiotoxicity, the long-term heat generation and the volume of high-level liquid waste enabling the simplification of storage design for nuclear waste. ^{127}Cs and ^{90}Sr are also environmental contaminants caused by past nuclear disasters. Removal of these contaminants from the environment would reduce the risk of health complications in both animals and humans. This thesis outlines the synthesis and extraction capabilities of caesium and strontium selective ligands on solid-supported extractants including magnetic nanoparticles and macroscopic silica gel for the selective separation of caesium and strontium from other group I and II elements. Recovery of fission/corrosion products using *N*-donor extractants is also reported.

Abbreviations and Acronyms

3-IPTMS	3-iodopropyltrimethoxysilane
An	Actinide
BTP	*Bis*-triazinylpyridine
BTBP	*Bis*-triazinylbipyridine
BTPhen	*Bis*-triazinylphenanthroline
D	Distribution ratio
DIAMEX	Diamide extraction
DMAP	4-(dimethylamino)pyridine
DME	Dimethoxyethanol
DMDOHEMA	*N*,*N*'-dimethyl-*N*,*N*'-dioctyl[(hexyloxy)ethyl]malonamide
DMF	*N*,*N*-dimethylformamide
DMSO	Dimethylsulphoxide
EDTA	Ethylenediaminetetraacetic acid
EDX	Energy Dispersive X-ray Spectroscopy
GW	Gigawatt
HLW	High level waste
HOMO	Highest occupied molecular orbital
ICP-MS	Induction-coupled plasma mass spectrometry
ILW	Intermediate level waste
kBq	Kilobecquerel
kGy	Kilogray
LLW	Low level waste
Ln	Lanthanide
MNP	Magnetic nanoparticle
MOX	Mixed oxide fuel
PBq	Petabecquerel
PUREX	Plutonium uranium extraction
SANEX	Selective actinide extraction
SEM	Scanning electron microscopy
SF	Separation factor
SPE	Solid-phase extraction
TBP	Tributyl phosphate
TBq	Terabecquerel
TEM	Transmission electron microscopy
TEOS	Tetraethoxysilane
TERPY	2,2:6',2"-terpyridine
TGA	Thermogravimetric analysis
TODGA	*N*,*N*,*N*',*N*'-tetraoctyldiglycolamide
TPH	Hydrogenated tetrapropene
TPTZ	2,4,6-tri-2-pyridyl-1,3,5-triazine
VLLW	Very low level waste

Table of Contents

Chapter 1 – A Review of the Development of Ligands for Extraction of Fission and Corrosion Products

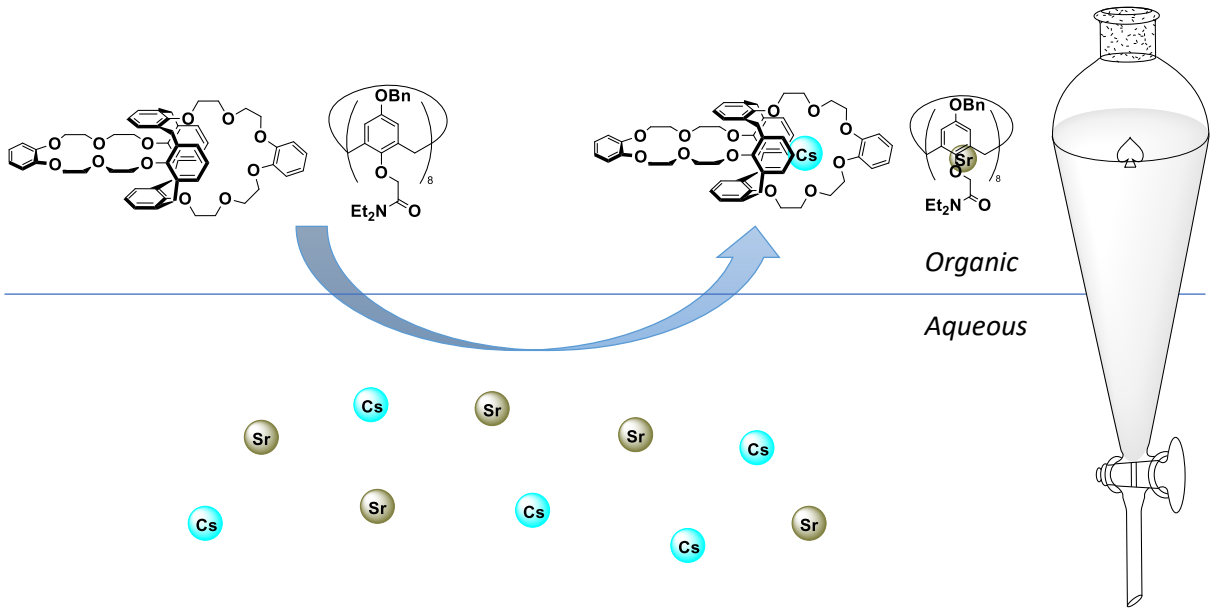

1.1 Introduction

Fossil fuels such as coal, oil or gas contribute greatly to global warming and are becoming increasingly scarce as they are non-renewable. Cleaner methods of power generation, particularly renewable methodologies, need to be adopted to maintain the supply of energy in developed countries, to withstand increased future demand and provide supply resilience to avoid political and social upheaval. Nuclear power, along with sources of renewable energy, remains the main focus in energy production. In 2016, Nuclear power generated 11% of the worlds energy, despite crude oil, coal and natural gas still dominating the provision.[1–3] Developed countries have invested the most into nuclear power. For example, the UK generated 21% of its energy in 2016 from nuclear reactors. Today 65 nuclear reactors are under construction around the world which will contribute 64 GW of energy per annum.[2] In many senses, nuclear energy is a clean energy source with no emissions of CO_2 or nitrogen and sulfur oxides, greenhouse gases associated with fossil fuel use. However, a major drawback with nuclear power is the toxic waste fuel that is produced and must be managed safely into the long distant future.[4] In 2013 an estimated 370,000 tonnes of spent fuel had been produced by nuclear reactors around the world.[5] Of the 370,000 tonnes of spent fuel, 120,000 tonnes has been reprocessed with the remainder in storage awaiting reprocessing or long term disposal.[5] Nuclear waste contains very low level waste (VLLW), low level waste (LLW), intermediate level waste (ILW) and high level waste (HLW). VLLW and LLW make up more than 95% of nuclear waste but more than 95% of the radioactivity is produced by ILW and HLW.[5] With inventories of nuclear waste increasing each year, long-term management and safe disposal of waste needs to be established to combat this issue.[6]

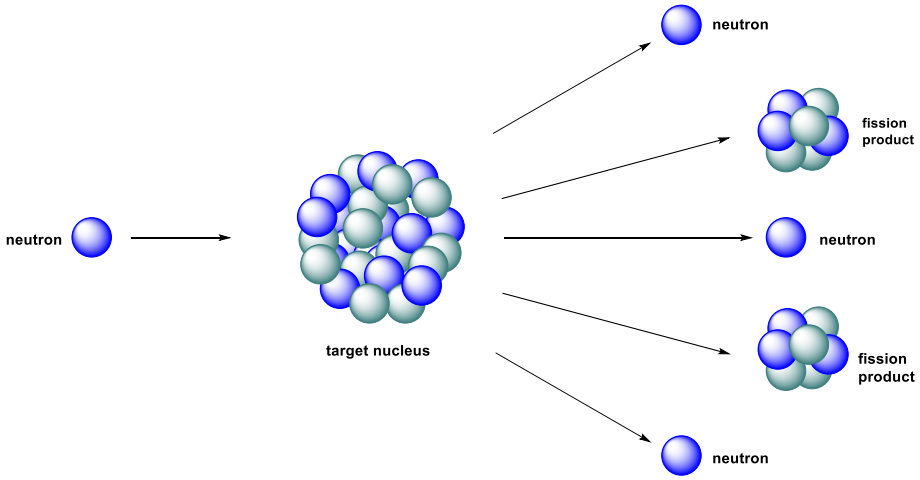

Figure 1.1 Fission of a nucleus

Nuclear power is created during the fission of $^{235}U_{92}$. Nuclear fission results from the action of thermal neutrons bombarding heavy nuclides leading to splitting of the original nucleus into fission products of smaller mass (Figure 1.1).[7] In nuclear reactors $^{235}U_{92}$ is bombarded with thermal neutrons, splitting the it into two smaller nuclides and more neutrons that continue the fission process.[7] The number of neutrons released per nucleus is between 2-3, producing energy (2×10^{10} kJmol^{-1} of ^{235}U) about two million times that obtained by burning an equal mass of coal.[7] Each neutron formed can initiate another nuclear reaction producing a branching chain reaction.[7] Left uncontrolled, this branching chain reaction would lead to a violent explosion producing a massive amount of energy.[7] Energy harnessed from the nuclear fission of $^{235}U_{92}$ must be a controlled process. Neutrons released from the fission of $^{235}U_{92}$ pass through a moderator (graphite or D_2O) that causes a loss of their kinetic energy.[7] The neutrons then either initiate further nuclear fission of $^{235}U_{92}$ or are captured by $^{238}U_{92}$. Of the uranium fuel source UF_6, only 5% contains $^{235}U_{92}$ after enrichment.[8] $^{238}U_{92}$ is the most abundant isotope

of uranium, which is converted to $^{239}U_{92}$ after neutron capture.[7] $^{239}U_{92}$ can then be partly converted to $^{239}Pu_{94}$ via β decay.[7,9]

$$^{238}U_{92} + {}^{1}n \rightarrow {}^{239}U_{92} + \gamma$$

$$^{239}U_{92} - \beta^{-} \rightarrow {}^{239}Np_{93} \rightarrow {}^{239}Pu_{94}$$

Equation 1.1 Nuclear fission of $^{238}U_{92}$

$^{239}Pu_{94}$ is a secondary nuclear fuel that is used in mixed oxide (MOX) reactors, consisting of a mixture of uranium(IV) oxide and plutonium(IV) oxides.[7,9–11] This process of isotope production is called bleeding.[7] Poisoning of the nuclear fuel source occurs when the fission products begin to absorb neutrons rather than releasing them.[7] This leads to a net decrease in neutron concentration leading to the need for replacement with new fuel.[7] Spent fuel contains mainly ^{238}U (94%) and short-lived fission products that constitute a low long-term hazard.[12] However, 4-5 wt% of the spent fuel consists of fission products including strontium, caesium, iodine and technetium, 1 wt% of plutonium and 0.1 wt% minor actinides (Am, Cm, Np), the latter being highly radiotoxic in the long-term (Figure 1.2).[12,13] These highly radiotoxic fission products are found in ILW and HLW and are the main concern in the disposal of spent fuel. Reprocessing of spent nuclear fuel leads to reduction in the radiotoxicity and long term heat production and reduces the total volume of HLW.[4] This would enable the simplification of storage design, increase the capacity of storage and increase public acceptance of nuclear power.[4]

1 Uranium ~ 94%

^{235}U	0.7%
^{238}U	93%

2 Fission Products ~4-5%

^{90}Sr	0.1%
^{137}Cs	0.2%
^{129}I	0.03%
^{99}Tc	0.1%

3 Plutonium ~1%

^{238}Pu	0.04%
^{239}Pu	0.7%
^{240}Pu	0.3%
^{241}Pu	0.2%
^{242}Pu	0.1%

4 Minor Actinides ~0.1%

^{237}Np	0.07%
^{241}Am	0.03%
^{244}Cm	0.01%

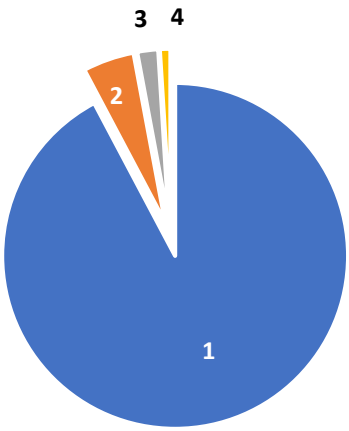

Figure 1.2 Composition of spent nuclear fuel

1.2 Reprocessing

1.2.1 PUREX Process

The first – and currently only - stage in reprocessing is the **P**lutonium and **UR**anium **EX**traction (PUREX) process that is utilised in current reprocessing plants. The purpose of this stage is to partition plutonium and uranium from the minor actinides and other fission products. This is so that the plutonium and uranium can be recycled and converted into uranium oxide or mixed oxide (MOX) fuels for reuse in nuclear reactors.[10,11] The PUREX process begins with the immersion of fuel rods in ponds of water for up to 3 months.[10,14] Short-lived and highly radioactive fission products such as ^{131}I decay during this time.[14] The fuel rods are then dissolved in concentrated nitric acid (7 M) forming $UO_2(NO_3)_2$, $Pu(NO_3)_4$ and other metal nitrates.[10,14] The uranium and plutonium nitrates are then extracted using a 20-30% solution of tributyl phosphate (TBP)(Figure 1.3) in kerosene.[10,14]

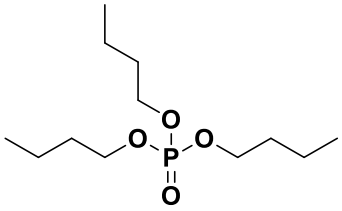

1

Figure 1.3 Tributyl phosphate (TBP) **1**

Uranium (VI) and plutonium (IV) are extracted into the organic kerosene via the complexes $[UO_2(NO_3)_2(tbp)_2]$ and $[Pu(NO_3)_4(tbp)_2]$, leaving lanthanides, minor actinides and fission products in the aqueous phase as they do not form strong complexes with TBP.[10,14] Uranium is then partitioned from plutonium by redox chemistry. A suitable reducing agent, typically uranous nitrate (U(IV)) is used to reduce Pu(IV) to Pu(III).[11,14]

$$2Pu(IV)_{(aq)} + U(IV)_{(aq)} + 2H_2O_{(l)} \rightarrow 2Pu(III)_{(aq)} + UO_2^{2+}{}_{(aq)} + 4H^+{}_{(aq)}$$

$$UO_2^{2+}{}_{(aq)} + 4H^+{}_{(aq)} + 2e^- \rightarrow U(IV)_{(aq)} + 2H_2O_{(l)} \qquad E = +0.27\ V$$

$$Pu(IV)_{(aq)} + e^- \rightarrow Pu(III)_{(aq)} \qquad E = +1.00\ V$$

Equation 1.2 Redox reaction of Pu(IV) and U(IV)

The reduction of Pu(IV) to Pu(III) facilitates the migration of plutonium into the aqueous phase as a result of weak complexation between TBP and Pu(III).[10,11,14] A possible complication is the re-oxidisation of Pu(III) to Pu(IV).[11] This proceeds in the presence of nitrous acid from nitric acid (Equation 1.3).[11] Hydrazine is added to the partitioning mixture to scavenge nitrous acid, which eliminates this issue.[11]

$$Pu(III)_{(aq)} + HNO_{2(aq)} + H^+{}_{(aq)} \rightarrow Pu(IV)_{(aq)} + NO_{(aq)} + H_2O_{(l)}$$

$$2NO_{(aq)} + HNO_{3(aq)} + H_2O_{(l)} \rightarrow 3HNO_{2(aq)}$$

$$N_2H_{4(aq)} + HNO_{2(aq)} \rightarrow HN_{3(aq)} + 2H_2O_{(l)}$$

Equation 1.3 Aqueous phase nitrous acid scavenging

Once uranium and plutonium are separated, the uranyl nitrate is extracted into the aqueous phase and crystallised as the hydrate $UO_2(NO_3)_2.6H_2O$.[14] The hydrate is thermally decomposed to UO_3 followed by hydrogen reduction to regain UO_2.[14] The plutonium is re-oxidised to Pu(IV) with HNO_3 and heated with oxalic acid, causing thermal decomposition to PuO_2.[14]

The current procedure for dealing with the remaining fission products is evaporation and pyrolysis to convert the residue into a mixture of oxides.[14] Fusion with silica and borax produces an inert borosilicate glass which encapsulates the radioactive materials, a process called vitrification.[14]

However, the post-PUREX raffinate could be further reprocessed to allow for more manageable storage. Minor actinides, lanthanides and fission products all remain in the PUREX raffinate.[6] Removal of the minor actinides from the raffinate would reduce storage time of the residual material from tens of thousands of years to a few hundred (Figure 1.5). If the minor actinides (americium and cerium) can be removed, the minor actinide oxides can be converted into shorter-lived ($T_{1/2}$ = 10^1 years) or stable isotopes by transmutation.[15,16] Transmutation involves the bombardment of the minor actinides with neutrons, resulting in their conversion to shorter-lived isotopes.[15,16] For transmutation to work, the minor actinides must be separated from the lanthanides.[6] The lanthanides have high neutron capture cross-sections and so will absorb neutrons preferentially, greatly reducing the efficiency of the transmutation of actinides. If it could be developed, a process of partitioning and transmutation would produce a more manageable waste form than that currently disposed.

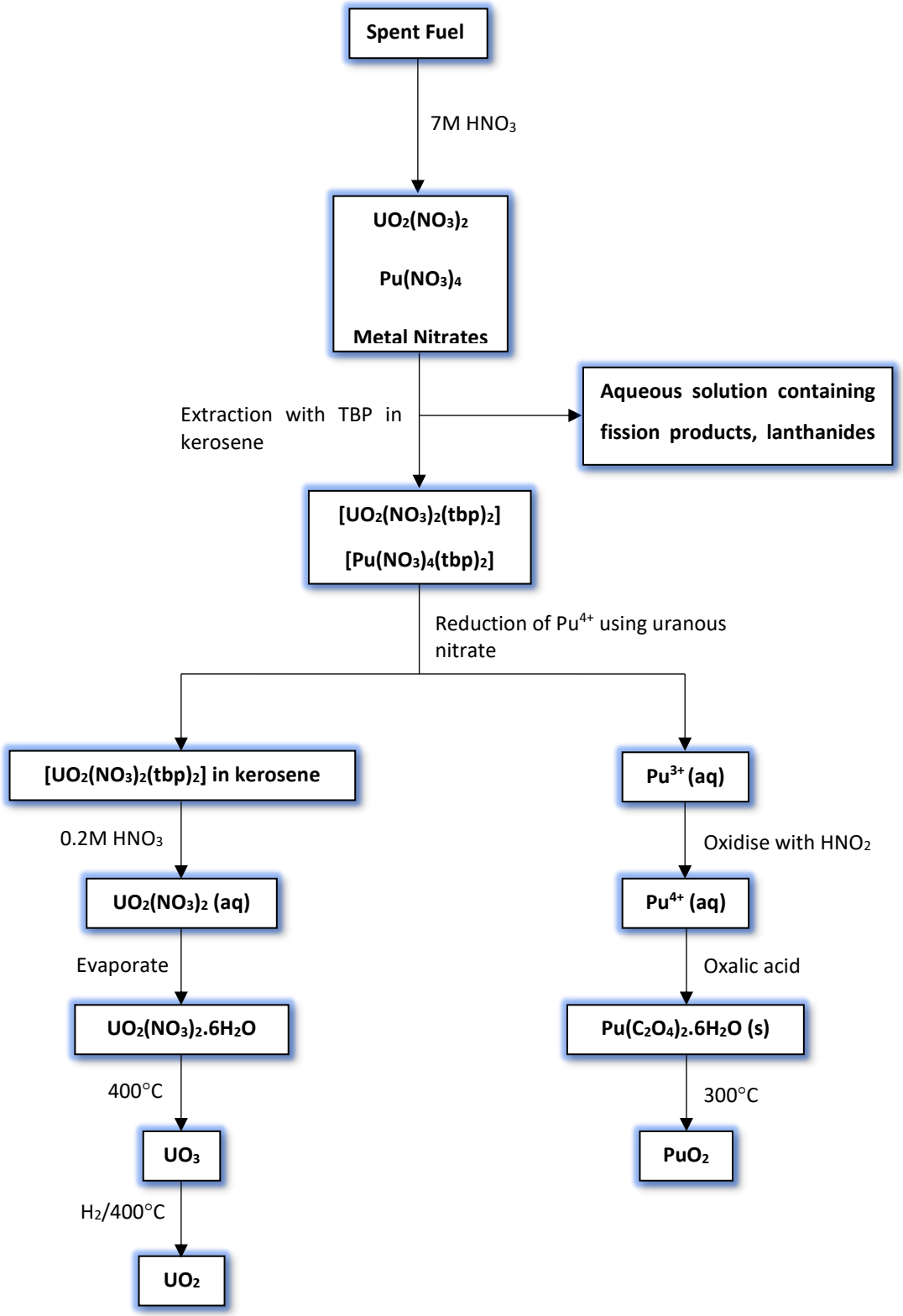

Figure 1.4 Flowsheet for PUREX

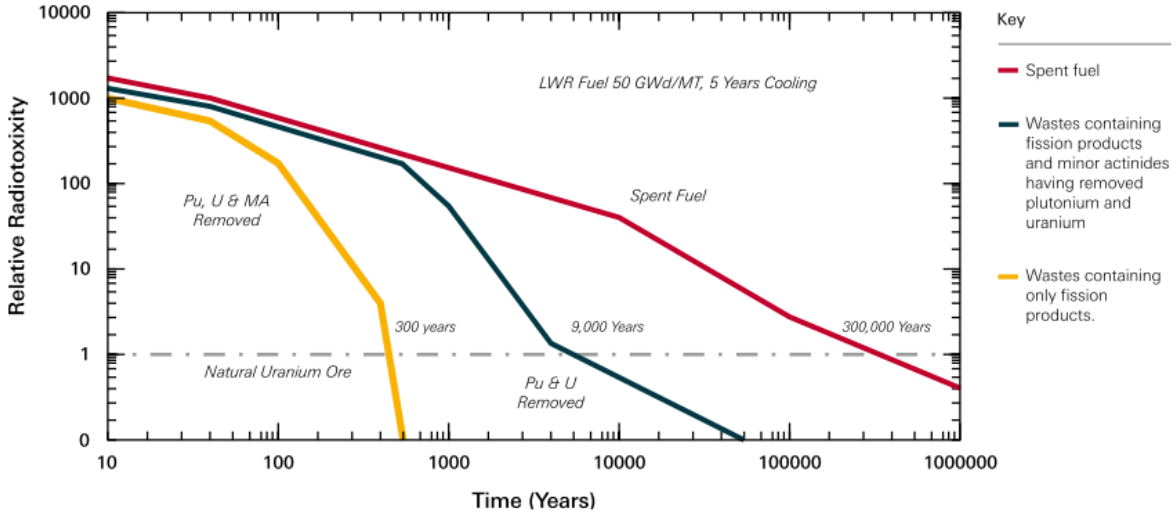

Figure 1.5 Relative radioactive decay of spent nuclear fuel as a function of time.[12]

1.2.2 DIAMEX Process

The PUREX raffinate contains minor actinides, lanthanides and fission products. The first step of partitioning and transmutation is to co-extract both actinides and lanthanides using a non-selective, diamide-based ligand.[6,17] This process was developed by the French CEA (Commissariat à l'Energie Atomique) and is called DIAMide EXtraction (DIAMEX) process.[6,17] Diamide-based ligands (malonamide molecules) were first identified by Musikas *et al.* in 1991.[15,18–20] Malonamide ligands have been reported to extract lanthanides (Ln^{III}) and actinides (An^{III}) efficiently from aqueous nitric acid.[15,18–20] The malonamide ligands also have the advantage of being solely composed of carbon, hydrogen, oxygen and nitrogen (therefore subscribing to the "CHON principle"), allowing for calcination without the formation of sulfur or phosphorous-based acidic wastes.[17] *N*, *N*'-dimethyl-*N*,*N*'- dioctyl[(hexyloxy)ethyl]-malonamide (DMDOHEMA, **2**) and *N,N,N',N'*-tetraoctyldiglycolamide (TODGA, **3**) are the benchmark ligands for the DIAMEX process, the latter showing high extraction efficiency for extraction of trivalent lanthanides and actinides, high solubility in paraffinic solvents (i.e. *n*-dodecane) and poor solubility in aqueous media.[21–26]

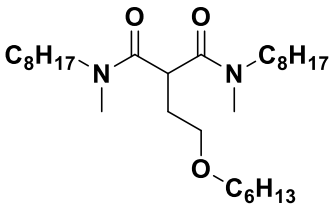

2

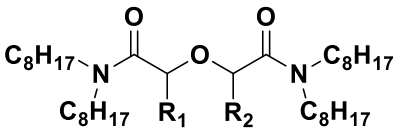

3 R_1=H, R_2=H
4 R_1=Me, R_2=H
5 R_1=Me, R_2=Me

Figure 1.6 DMDOHEMA **2** and TODGA **3-5**

Improvements to TODGA have been made with the substitution of methyl groups α- to the carbonyl in **3**. Furthermore, Me-TODGA **4** and Me_2-TODGA **5** display improved stability to high acidity and radiolytic flux in extraction processes.[27]

1.2.3 SANEX Process

The European approach to partitioning minor actinides from the lanthanides contained in DIAMEX raffinate is called the **S**elective **A**cti**N**ide **EX**traction (SANEX) process. Actinides and lanthanides share chemical similarities making separation difficult.[28,29] The characteristic that has been targeted is the slightly greater spatial extension of the 5*f* orbitals compared to the 6*d* orbitals in actinides than observed with the 4*f* and *5d* orbitals of the lanthanides as a result of a greater number of protons and electrons in the actinides series.[30] The electrons donated by the ligand to the metal show a greater tendency to bind covalently in the actinide series 5*f* orbitals than in the 4*f* orbitals of the lanthanides.[30] The 5*f* orbitals of actinides, being less shielded from the environment compared to 4*f* orbitals of the lanthanides, results in greater polarizability of the electrons that occupy the 5*f* orbitals.[30–33] This makes trivalent actinides more "soft" acceptors than the trivalent lanthanides.[30–33] Polydentate ligands containing "soft" *N*-donor sites have been found to exhibit good selectivity towards trivalent actinides. One of the first *N*-donor ligands investigated was 2,2:6',2''-terpyridine **6** (TERPY). TERPY **6** was

studied with 2-bromodecanoic acid **12** as a synergist, which acts as a lipophilic anion source allowing TERPY **6** to selectively extract Am(III) from weakly acidic aqueous solutions with $SF_{(Am/Eu)}$ of 7.2.[15]

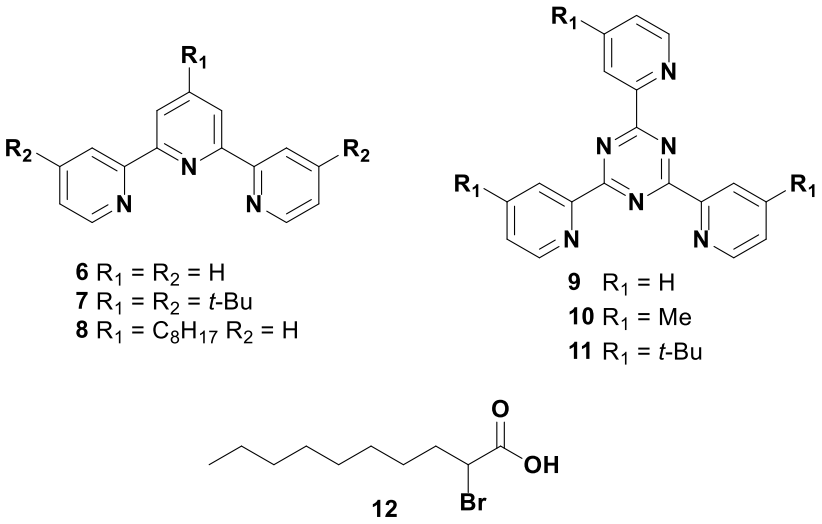

Figure 1.7 Structure of TERPY **6-8**, TPTZ **9-11** and 2-bromodecanoic acid **12**

However the *D* value for Am(III) decreases with increasing acidity because of protonation of the ligand causing solubility issues. Derivatives of TERPY with hydrophobic alkyl groups were investigated but lower distribution ratios for Am(III) were achieved. The increase of the basicity of the TERPY derivatives **7-8** led to competition between protonation of the donor atoms and metal ligation. Protonation of the ligands resulted in precipitation at the aqueous-organic interface.[6,15]

The central pyridine ring of TERPY was replaced with 1,3,5-triazine to reduce the basicity of the ligand leading to the formation of 2,4,6-tri-2-pyridyl-1,3,5-triazine **9** (TPTZ). TPTZs performed better than TERPY in solvent extraction studies. TPTZ **9**, used with 2-bromodecanoic acid **12** and hydrogenated tetrapropene (TPH) as the diluent, was one of the first *N*-donor ligands to achieve a $SF_{(Am/Eu)}$ of > 10. Despite the improved separation factor,

TPTZs were still protonated in highly acidic media greatly reducing the efficiency of the ligand.[34–36]

Introduction of a 1,2,4-triazine moiety allowed for extraction of both Am(III) and Eu(III) from highly concentrated solutions of HNO_3 (1-4M) without the need for additional synergists or phase transfer agents. High $SF_{(Am/Eu)}$ of > 100 were reported for alkyl substituted 2,6-bis(1,2,4-triazin-3-yl)pyridine (BTP) ligands **14-16**.[37,38]

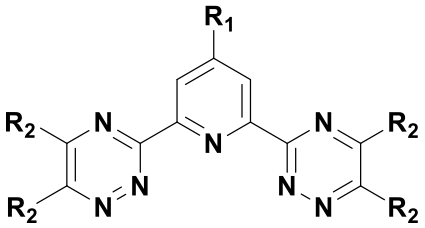

13 $R_1 = R_2 = H$
14 $R_1 = R_2 = Et$
15 $R_1 = R_2 = i\text{-Pr}$
16 $R_1 = R_2 = n\text{-Pr}$

17 $R_1 = H$, $R_2 =$

18 $R_1 = H$, $R_2 =$

Figure 1.8 Structure of BTP **13-18**

A key feature to this class of *N*-ligands is the "α-effect". The α-effect occurs when atoms with non-bonding electron pairs are adjacent and accounts for strong nucleophilic donors when a nucleophile with an unshared pair of electrons is adjacent to the nucleophilic centre. [39,40] Interactions between the unshared electrons on the adjacent atom raises its HOMO energy. This leads to *N*-donors having a decreased affinity for protons and increased affinity towards soft cations. The overlap between an adjacent non-bonding nitrogen lone pair with the bonding lone pair increases the covalent nature of the latter.[41]

The solubility of BTP was increased with tetra-*iso*-propyl **15** and tetra-propyl chains **16**.[38] In solvent extraction studies, the rate of extraction of Am(III) increased linearly as the concentration of BTP ligand increased. However, above 1M HNO_3 the rate of extraction decreased because of protonation of the ligand. BTP ligands were tested on genuine PUREX raffinate; however, major radiolytic degradation was observed.[18]

Harwood *et al.* hypothesised that the presence of benzylic hydrogen atoms on the side chains of BTP ligands were susceptible to degradation by reacting with hydroxyl radicals generated by radiolysis of water.[6,15] Introduction of a side group with solubilising alkyl groups but no benzylic hydrogen atoms was proposed, leading to the formation of $CyMe_4$ functionality. $CyMe_4$-BTP **17** showed stability towards acid hydrolysis, survived boiling in 3M HNO_3 and a benzannelated $CyMe_4$ ($BzCyMe_4$) derivative **18** was subject to γ-radiation up to 100 kGy showing good stability.[42] Solvent extraction tests on $CyMe_4$-BTP **17** produced high extraction efficiency ($D_{Am} \sim 500$) with a high $SF_{(Am/Eu)}$ of > 5000. The issue with $CyMe_4$-BTP **17** is the high binding efficiency between the ligand and An(III) which doesn't allow for back extraction (stripping). $CyMe_4$-BTP **17** binds in a 3:1 ratio with actinides, the metal centre being 9-coordinate with 3 tridentate BTP ligands. This complex doesn't allow for external stripping agents to complex with the actinides.[43,44]

6,6'-Bis(1,2,4-trianz-3-yl)-2,2'bipyridine ligands (BTBPs) have been investigated for use in the SANEX process. The tetradentate BTBP ligands allow for high affinity towards trivalent actinides in the presence of trivalent lanthanides and the ability for subsequent stripping. Having four *N*-donor groups induces a weaker ligand field resulting in 1:1 or 1:2 complexes and leaves room for a stripping species to interact.

$CyMe_4$-BTBP **25** is the current benchmark extractant for the SANEX process in Europe, synthesised by the Reading group from 2,2'-bypyridine **19**.[16,45] In spiked solvent extraction experiments, $^{241}Am(III)$ and $^{152}Eu(III)$ radioisotopes are used to represent the actinides and lanthanides, respectively.[6] An equilibrium ratio of metal concentration in the organic and aqueous phase (distribution ratio D_m) is used to quantify the effectiveness of a ligand.[6] The ratio of the *D* values for Am and Eu (separation factor SF) can be used as a measure the selectivity of the ligand.[6] $CyMe_4$-BTBP **25** shows strong selectivity for Am(III) over Eu(III) ($SF_{Am/Eu} \sim 150$) but exhibits slow kinetics.[36] Many BTBP analogues (Figure 1.7) have been investigated, but $CyMe_4$-BTBP has displayed the most promise.[16,36,43,44,46,47]

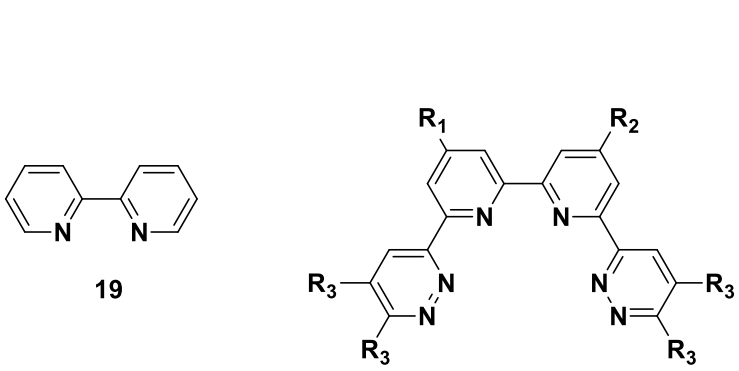

Figure 1.9 2,2'bypyridine **19** and BTBP analogues **20-28**

The slow kinetics for extraction with $CyMe_4$BTBP have been investigated, in particular looking closely at the conformations of the $CyMe_4$-BTBP ligand. The favoured conformation of the uncomplexed ligand is *trans*; whereas the *cis* conformation needed for extraction is 5.7 kcal mol^{-1} higher in energy than the *trans* conformation, with an activation energy of 8.1 kcal mol^{-1} causing the *trans* conformation to be favoured (Figure 1.9).[48]

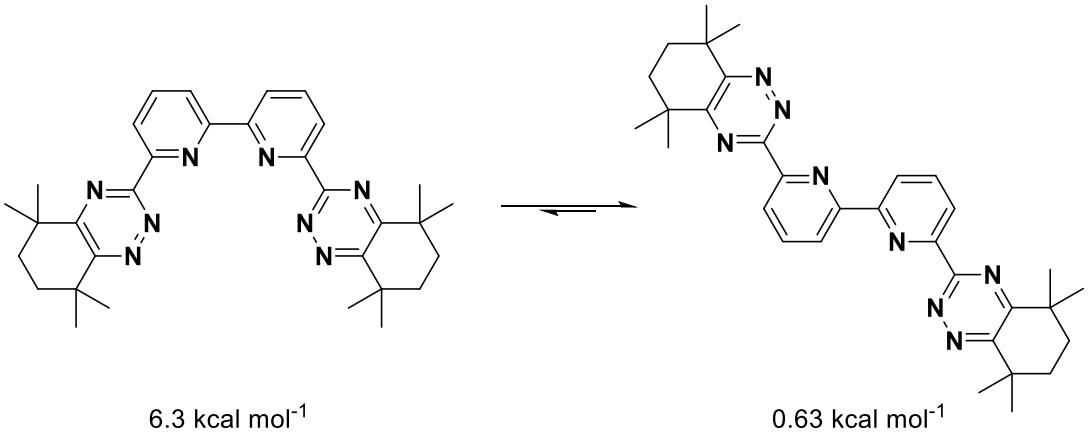

Figure 1.10 *cis* and *trans* conformation of $CyMe_4$-BTBP **25**

To improve the kinetics of extraction by $CyMe_4$-BTBP **25** the *cis*-locked 1,10-phenanthroline **29** was utilised as the precursor rather than 2,2'-bypyridine **19** used in the synthesis of BTBP. From neocuproine **30** the Harwood group developed a new class of ligands, the bis-triazine-phenanthrolines (BTPhens).[6,13,43]

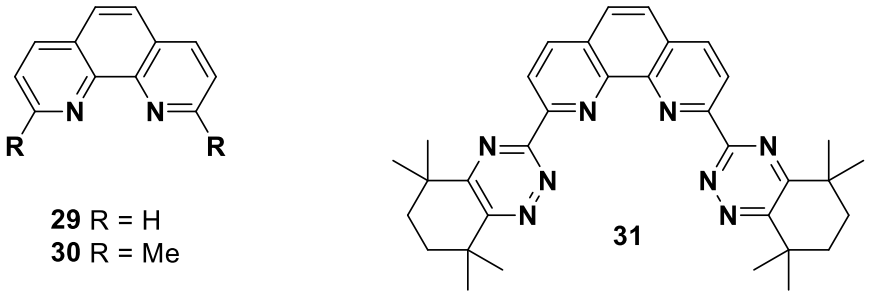

Figure 1.11 Neocuproine **30** and $CyMe_4$-BTPhen **31**

Extraction studies of $CyMe_4$-BTPhen **30** in 1-octanol proved it to be more efficient than $CyMe_4$-BTBP **25**. A high *D* value for Am(III) was obtained (D_{Am} > 1000) while the *D* value for Eu(III) were approximately 2 orders of magnitude lower (D_{Eu} < 10).[13] This resulted in high separation factors ($SF_{Am/Eu}$ ~ 68 - 400) showing that $CyMe_4$-PTPhen **30** extracts Am(III) in the presence of Eu(III) with high selectivity.[13] The rate of extraction was also significantly improved (< 15 mins)

compared to $CyMe_4$-BTBP **25** which displayed slow kinetics (> 60 mins) and, furthermore, no phase transfer agent DMDOHEMA was necessary.[13,49] $CyMe_4$-BTPhen **30** has been immobilised onto magnetic nanoparticles (MNPs) where its extraction abilities were explored in different nitric acid concentrations.[32] At 0.001M HNO_3 both Am(III) and Eu(III) were observed to be extracted (D_{Am} = 1162.8, D_{Eu} = 701.4, $SF_{Am/Eu}$ = 1.7) however at 4M HNO_3 separation was displayed (D_{Am} = 55.4, D_{Eu} = 0.03, $SF_{Am/Eu}$ = 1675.6).[32] This shows that it could be possible to first extract both actinides and lanthanides at low concentrations of nitric acid (DIAMEX) and then separate by increasing the concentration of nitric acid (SANEX).

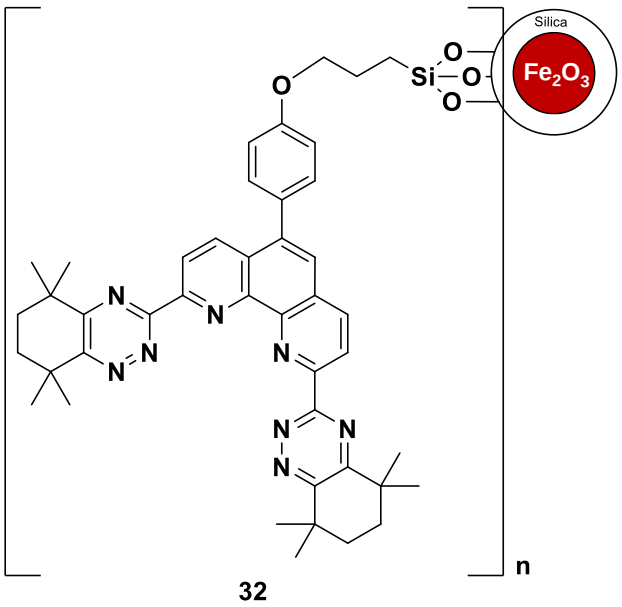

32

Figure 1.12 $CyMe_4$-BTPhen functionalised MNPs **32**

If a DIAMEX/SANEX process were to be adopted, the SANEX raffinate storage time would be significantly lower at ~300 years (Figure 1.5).[12] However fission products such as ^{137}Cs and ^{90}Sr are still present in the SANEX raffinate. Both radionuclides are principal heat generators in HLW with long half lives (^{137}Cs $t_{1/2}$ = 30.2 years, ^{90}Sr $t_{1/2}$ = 28.8 years).[50,51] ^{137}Cs and ^{90}Sr undergo β-decay producing energetic β-particles (~0.5 MeV), low energy recoil nuclei and γ-rays.[51] The

β-particles and γ-rays interact with solids producing defects.[51] Removal of ^{137}Cs and ^{90}Sr before vitrification would both reduce the volume of HLW and reduce the risk of matrix deformation caused by β-decay and heat generation.[50–56]

1.3 Environmental Impact

^{137}Caesium and ^{90}strontium are also present in the environment. Disasters such as Chernobyl (1986) and Fukushima (2011) released a large volume of radionuclides into the environment that need to be removed to prevent long term radioactive hazard. The steam explosion that occurred at the Chernobyl nuclear power plant resulted in the substantial release of radioactive materials into the atmosphere.[57] The estimated activity of the radionuclides ^{131}I, ^{134}Cs and ^{137}Cs released was 1760 PBq, 47 PBq and 85 PBq respectively (Table 1.1).[57,58] Radioactive contamination was found in every country in the northern hemisphere, with Europe most heavily affected.[57] As most of the radionuclides were released as aerosols into the atmosphere, Chernobyl radioactivity was observed in rain and air samples as far as Japan.[57] The highest ^{137}Cs deposition densities, exceeding 555 KBq/m^2, were found in Belarus (6400 Km^2), the Russian Federation (2400 Km^2) and the Ukraine (1500 Km^2).[57–59] Over a period from June 1986 to January 1989, approximately 85.1 TBq of ^{137}Cs and 51.8 TBq of ^{90}Sr were deposited into the Kiev reservoir, as well as 2.2 TBq of ^{137}Cs and 37 TBq of ^{90}Sr into the Black Sea.[60] From the overall radioactive contamination as a result of the Chernobyl incident, 237 cases of acute radiation sickness were reported with 31 deaths.[61]

Recently a large volume of radionuclides were released from the Fukushima nuclear power plant in 2011 after partial core melt-down of the nuclear fuel and hydrogen explosions caused by cooling systems failure. Approximately 21 PBq of ^{137}Cs and 28 PBq of ^{134}Cs were released

into the atmosphere, three times less than Chernobyl.[57,62] Within the 20 km zone evacuated at the time of the accident, surface activities of ^{137}Cs varied between less than 30 to 15000 kBq/m^2. Chernobyl saw contamination of ^{137}Cs greater than 600,000 Bq/m^2 over a surface area of 13,000 km^2 while Fukushima saw only 600 km^2. However, Fukushima is responsible for the largest one-off injection of artificial radionuclides into the marine environment estimated at 27×10^{15} Bq.[62]

Such releases of radionuclides from nuclear disasters must be addressed to decontaminate the surrounding environment. Humans and animals in contact with contaminated soil or water are more susceptible to radioactive health issues such thyroid cancer (^{131}I) and bone cancer or leukaemia (^{90}Sr).[63] Selective extraction methods for caesium and strontium need to be developed in order to decontaminate the environment in the presence of other group I and group II metal ions and to provide safety measures in the event of another nuclear disaster.

Radionuclide	*Half-life*	*Activity Released (PBq)*
Volatile elements		
^{129}Te	33.6 d	240
^{132}Te	3.26 d	1150
^{131}I	8.04 d	1760
^{133}I	20.8 h	910
^{134}Cs	2.06 y	47
^{136}Cs	3.1 d	36
^{137}Cs	30.2 y	85
Intermediate Volatility		
^{89}Sr	50.5 d	115
^{90}Sr	28.8 y	10
^{103}Ru	39.3 d	168
^{106}Ru	368 d	73
^{140}Ba	12.7 d	240
Refractory Elements		
^{95}Zr	64.0 d	84
^{99}Mo	2.75 d	72
^{141}Ce	32.5 d	84
^{144}Ce	284 d	50
^{239}Np	2.35 d	400

Table 1.1 Activity released of principle radionuclides during Chernobyl disaster

1.4 Group I and II Chemistry

1.4.1 Group I Chemistry

Group I elements, known as alkali metals, contain a single s electron outside of a noble gas core. The single s electron in its outer shell allows for M^+ cations and only M^+ cations exist because of the high second ionisation potentials shown in Table 1.2.[64] Group I elements mainly adopt ionic chemistry with a few covalent exceptions, for example: bonds to oxygen, carbon and nitrogen in chelates and organometallic compounds. Lithium shows the greatest tendency for covalent bonding, the least shown being from caesium because of the charge : radius ratio.[64]

Element	*Electronic Configuration*	*Metal Radius (Å)*	*1st Ionization Potential (eV)*	*2nd Ionization Potential (eV)*	*M.p. (°C)*	*B.p. (°C)*	*E° [a]* *(V)*	*E_{diss} [b]* *(kJ mol^{-1})*
Li	[He]2*s*	1.52	5.390	75.62	180.5	1326	-3.02	108.0
Na	[Ne]3*s*	1.86	5.138	47.29	97.8	883	-2.71	73.3
K	[Ar]4*s*	2.27	4.339	31.81	63.7	756	-2.92	49.9
Rb	[Kr]5*s*	2.48	4.176	27.36	38.98	688	-2.99	47.3
Cs	[Xe]6*s*	2.65	3.893	23.40	28.59	690	-3.02	43.6
Fr	[Rn]7*s*							

[a] For $M^+_{(aq)} + e = M_{(s)}$

[b] Energy of dissociation of the diatomic molecule M_2

Table 1.2 Properties of Group I elements.[64]

Francium is formed in natural radioactive decay series with all its isotopes having short half-lives. Precipitation, solubility and ion-exchange studies show that the ion correlates to its position in the periodic table. Increasing size of the group I elements results in a uniform effect

on chemical and physical properties. For example, the hydrated radii and hydration energies decrease down the group. Reactivity of the group I metals increases with increasing electropositive nature (Li → Cs). M^+ ions are easily hydrated or solvated, meaning that studies of extraction of group I ions must consider the hydrated radii rather than the 'naked' radii. Due to the increase in charge : radius ratio down the group, the hydration radii decrease down the group. The larger the cation, the less it is able to bind additional outer layers of water molecules.[64] For efficient extraction, high stability constants must be obtained with the active ligand. Complexes of the hydrated ions have reducing stability constants down the group (Li^+ >> Cs^+). Strength of absorption onto ion-exchange resins increases down the group (Li^+ << Cs^+) as the smallest hydrated radii will be held most strongly according to Coulomb's Law.[64]

1.4.2 Group II Chemistry

The Group II elements possess smaller atomic radii than those of Group I because of the increased nuclear charge. Beryllium and magnesium both demonstrate more covalent chemistry while the heavier elements (Ca, Sr, Ba and Ra) are ionic in nature.[7,64] Group II elements contain double the number of bonding electrons compared to group I, leading to their increased melting and boiling points and greater densities.[7,64] Values of IE_1 and IE_2 decrease down the group because of the increased size of the radius. This trend is broken in moving from Ba to Ra because of the thermodynamic 6s inert pair effect.[7] High values of IE_3 impede the formation of M^{3+} cation species, with group II ions predominately adopting M^{2+} ions. The M^{2+} cations are smaller than the isoelectronic M^+ group I species. Be^{2+} and Mg^{2+} and polarization of anions produces a degree of covalency for compounds of Be and Mg. The heavier group II elements follow similar trends to the group I elements with increasing size. For example, hydration tendencies of the crystalline salts increase, solubilities of sulfates,

nitrates and chlorides decrease, thermal stabilities of carbonates, nitrates and peroxides increase and rates of reaction with hydrogen increase.[64]

Element	*Electronic Configuration*	*Ionic Radius (Å)*[a]	*1st Ionization Potential (eV)*	*2nd Ionization Potential (eV)*	*M.p. (°C)*
Be	[He]2*s2*	0.34	9.32	18.21	1278
Mg	[Ne]3*s2*	0.78	7.64	15.03	651
Ca	[Ar]4*s2*	1.06	6.11	11.87	843
Sr	[Kr]5*s2*	1.27	5.69	10.98	769
Ba	[Xe]6*s2*	1.43	5.21	9.95	725
Ra	[Rn]7*s2*	1.57	5.28	10.10	700

[a]Ladd radii

Table 1.3 Properties of Group II elements.[64]

Group II oxides react with water to form hydroxides; however, it is only the heavier element (Ca-Ra) hydroxides that are soluble in water. The heavier group II ions can accommodate six or more water molecules in the first coordination sphere of the hydrated species.[7] Group II ions are hard acids and therefore coordinate with hard bases. O- or N-donor ligands are most suitable for coordination with cationic group II species, for example: $[EDTA]^{4-}$ and $[P_3O_{10}]^{5-}$ form water soluble complexes with group II ions and are sequestering agents used in water-softening to remove Mg^{2+} and Ca^{2+} ions.[7]

1.5 Metal Complexes

1.5.1 Crown ethers

Crown ethers, synthesised by Pedersen in 1967 are popular metal cation chelators and viewed as a potential selective chelators due to the size fit principle within the interior cavity of the macrocycle.[65–67] The size fit principle relates to the different size cavities of crown ethers capable of binding to different sized metal cations. The main factors of crown ethers' binding potential are preorganisation and complementarity, solvation and -significantly, - chelate ring size.[67–69] Flexibility of the crown ether can promote solubility in both aqueous and lipophilic solvents and rapid, reversible ion binding characteristics.[67] The flexibility enables exposure of either the hydrophilic ether oxygen atoms or lipophilic ethylenic groups to the surrounding solvent. For example 18-crown-6, which can be hydrophilic or lipophilic.[67]

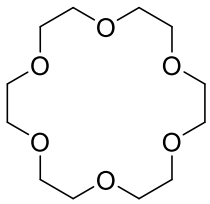

33

Figure 1.13 18-crown-6 **33**

Selectivity can be gained using the size fit criterion. The metal cations ionic radii must fit within the cavity of the crown ether. The crown ether 18-crown-6 **33** favours potassium cations, creating a complex with a high stability constant (log K = 6.10) in methanol.[67] Aqueous conditions cause solvation of the potassium cation, reducing the stability constant of the complex.[67] 18-Crown-6 **33** is a two-dimensional ligand, meaning the interactions between ligand and metal cation occur about the 'equator' and 'tropics'.[67] This leaves the 'North' and 'South' poles exposed, where water molecules can solvate the metal cation.[67] With the 'North'

and 'South' poles exposed, crown ethers are inefficient at removing metal cations from aqueous solutions. Complexes of 18-crown-6 **33** with the potassium cation often adopt a domed shape because of a conjugate anion pulling the potassium cation away from the most favourable intra-cavity site.[67] An example of this is [K(18-crown-6)]NO_3 **34**, where the nitrate anion binds to the cation as a bidentate ligand.

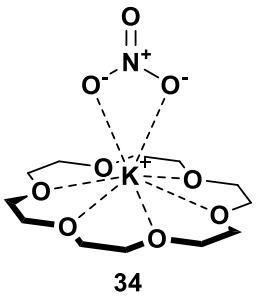

34

Figure 1.14 [K(18-crown-6)]NO_3 domed shape.

Sodium also complexes with 18-crown-6 **33** but there is a difference in behaviour because of the large non-complimentary macrocyclic ligand diameter.[67,70] Dunitz *et al.* provided four possible responses for complexation between a metal cation and a large non-complimentary macrocyclic ligand.[67,70] The four responses are:

1. Non-optimal M-O bonds lengths are formed with the metal cation sitting in the centre of the macrocyclic ligand: e.g. for Na^+ in 18-crown-6, the bond length is 2.8 Å.[71]
2. Deviation of metal cation away from the centre. Shorter interactions with some donor atoms and longer with others: e.g. the NaBr.2H_2O complex with dibenzo-18-crown-6 adopts this behaviour.[72]
3. The metal cation exhibits dynamic or static crystal disorder: e.g. [Na$(H_2O)_2$(18-crown-6)]N_3.[73]

4. Distortion of the crown ether occurs to form a more complimentary conformation for a metal cation: e.g. cis-anti-cis-dicyclohexyl-18-crown-6 distorts to an elliptical shape to complex with NaBr.[74]

These responses only apply when the crown ether is too large for the metal cation. Caesium has a larger ionic radius than sodium and potassium, requiring a larger crown ether than 18-crown-6 **33** to form a stable 1:1 complex. Caesium cations and 18-crown-6 **33** form ML_2 complexes with the cation 'sandwiched' in between two 18-crown-6 **33** ligands. A domed ML complex for Cs+ with 18-crown-6 **33** has been observed with $[N(PPh_3)_2]^-$ as the counter anion.[67] Caesium cations have a tendency to adopt cation-π interactions which helps to stabilise the ML complex with 18-crown-6 **33**.[67] Some degree of selectivity can be achieved utilising the size of the crown ether cavity. However, with the crown ethers' flexibility, a crown ether with a cavity size perfect for caesium cations would still be able to wrap around potassium and sodium cations. As sodium and potassium are in excess in nuclear waste and the environment, crown ethers do not offer suitable selectivity towards caesium over potassium and sodium. The exposed 'North' and 'South' poles also allow solvation of the metal cation by water molecules, reducing the stability constant of the cation/crown ether complex. Therefore, crown ethers are not suitable for caesium extraction from an aqueous medium.

1.5.2 Calixarenes

Calixarenes were first discovered by Alois Zinke in 1942 while investigating the 'curing' phase of the phenol-formaldehyde process in the formation of Bakelite.[75,76] Zinke synthesised a crystalline product with a high melting point, proposing the product to be a cyclic tetramer.[75–77] Cornforth repeated Zinke's synthesis isolating two products, both of which possessed characteristics of a cyclic oligomer.[75,76,78] However, it was not until the 1970s when Gutsche

was able to utilise new spectroscopic methods, chromatography and X-ray capabilities to uncover the structures of cyclic oligomers.[75,76] Gutsche developed procedures to acquire cyclic tetramers, cyclic hexamers and cyclic octamers in good yields using a base-induced reaction of *p-tert*-butylphenol and formaldehyde.[75,79]

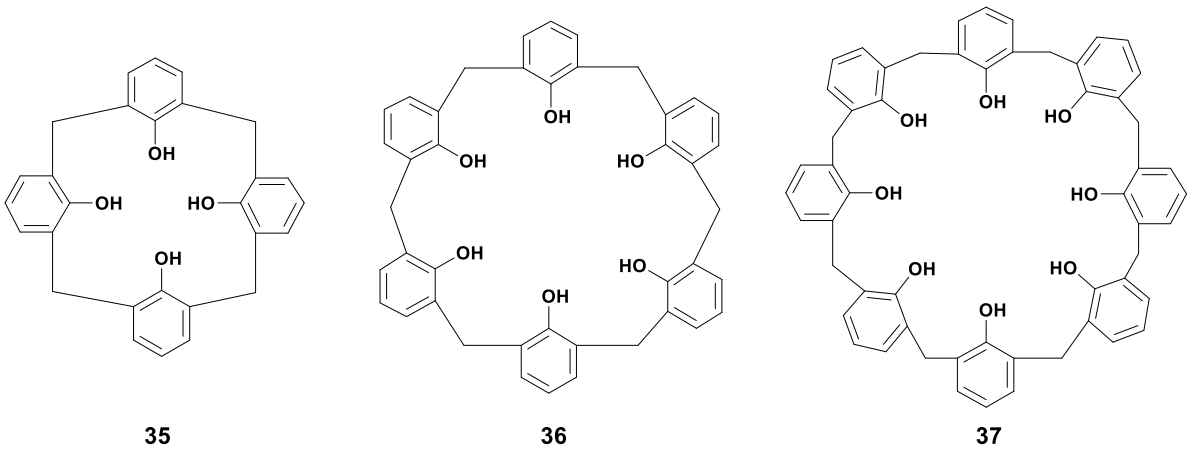

Figure 1.15 Structure of Calix[4]arene **35,** Calix[6]arene **36** and Calix[8]arene **37**

Gutsche gave the cyclic oligomers the name calixarenes because of their structural similarities to a Greek vase, *calix*.[75,76] The numerical prefix to the *arene* indicates the presence of aryl substituents in the macrocyclic compound. The structure of calixarenes is often depicted as having an annulus, an upper rim and a lower rim shown in Figure 1.15. The annulus corresponds to the aryl groups whilst the upper and lower rims are the hydroxide groups and the *para*-substituents of the calixarene respectively. The synthesis of pure calixarenes predominately follows a one step, base induced procedure. A mixture of *p-tert*-butylphenol, formalin (37% aq. formaldehyde) and sodium hydroxide is heated at 110-120 °C for 2 hours, leading to formation of a precipitate.[76,78] The precipitate is then heated to reflux in diphenyl ether for 2 hours, cooled and separated by filtration. The solid so formed is *p-tert*-butylcalix[4]arene. However, the hexamer can be formed by changing the concentration of the base. Approximately 0.03-0.04 equivalents of base favours the formation of tetramers;

whereas 0.3-0.5 equivalents favours hexamers.[76] Octamers can also be formed using the one step, based-induced procedure. A mixture of *p-tert*-butylphenol, paraformaldehyde and 0.03 equivalents of sodium hydroxide, on heating to reflux in xylene for 4 hours results in the octamer *p-tert*-butylcalix[8]arene.[76]

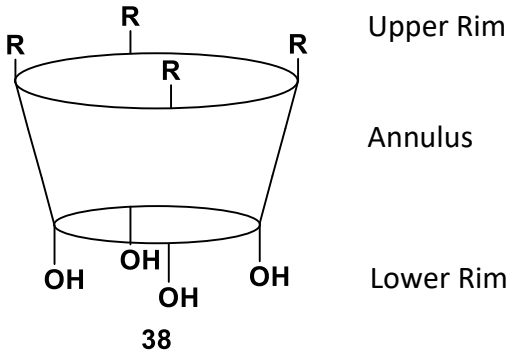

38

Figure 1.16 Simplified structure of calix[4]arene

Calixarenes can adopt several different conformations that either enhance or inhibit their extraction abilities. Calix[4]arenes **35** have four different conformations, observed in solid state and in solution. The four conformations are called 1,3-alternate **39**, 1,2-alternate **40**, partial cone **41** and cone **42**.

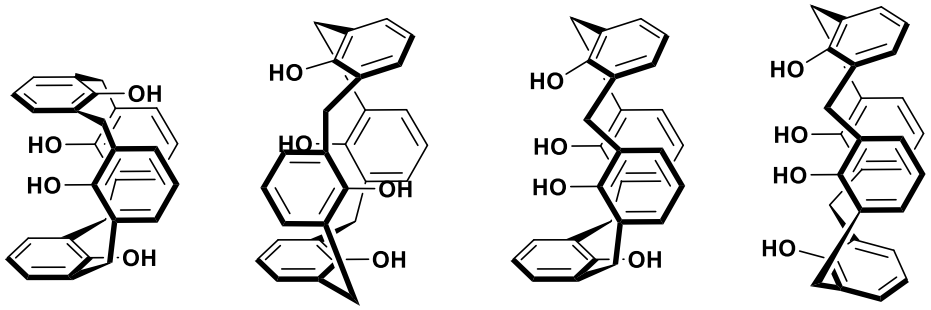

39 1,3-alternate

40 1,2-alternate

41 Partial Cone

42 Cone

Figure 1.17 Conformations of calix[4]arene **35**

The favoured conformation is the cone structure, due to the hydrogen bonding possible between each phenolic hydroxide group. However, the flexible nature of the calixarenes allows for inversion of the cone structure with two possible pathways of inversion. One pathway called the 'broken chain pathway' utilises the 1,3-alternate conformation during inversion.[76] Hydrogen bonding in the cone formation is disrupted during conversion to the 1,3-alternate conformer, with some hydrogen bonding being restored.

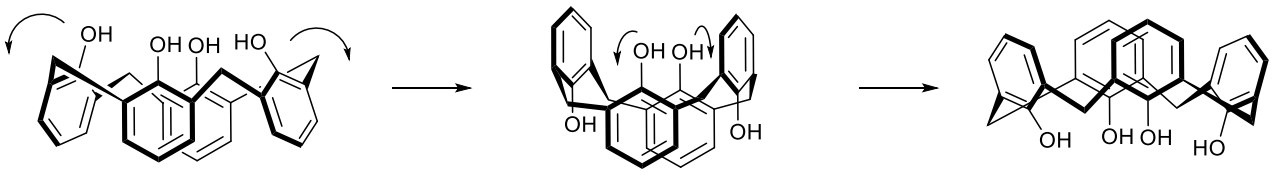

Figure 1.18 'Broken chain pathway' conversion.

The other pathway is called 'continuous chain pathway' where the aryl groups rotate 180° around the annulus in tandem, resulting in a conformer resembling a skewed 1,2-alternate conformation.[80]

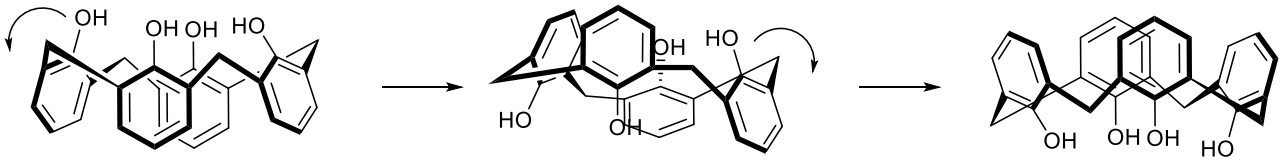

Figure 1.19 'Continuous chain pathway' conversion.

Calix[6]arene **36** can adopt eight 'up-down' conformations but the increased flexibility of the hexamer allows for additional conformations where one or more aryl groups assume an 'out' alignment.[76] An 'out' alignment is the positioning approximately in the average plane of the molecule.[76] There are sixteen 'up-down' conformations for calix[8]arene **37** with additional

forms adopting 'out' alignments.[76] Calix[8]arene **37** usually exists in a 'pleated loop' structure where the eight OH groups lie in a circular array ideal for hydrogen bonding.

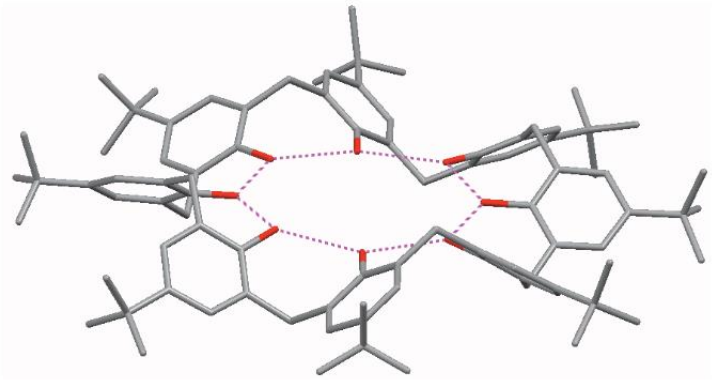

Figure 1.20 'Pleated loop' structure of *p-tert*-butylcalix[8]arene.[81]

Calix[4]arenes **35** have the ability to extract Group I cations from strongly basic aqueous solutions in a liquid-liquid extraction process, favouring caesium cations.[82,83] Caesium cations have been observed to adopt stable complexes utilising cation-π interactions with crown ethers and aromatic counter-anions.[67] Cation-π interactions with the aryl groups of calixarene stabilise the ML complex with caesium cations. The diameters of the calixarenes are ~ 1 Å for cyclic tetramers, ~ 2.4 Å for cyclic hexamers and ~ 4.8 Å for cyclic octamers.[76] Calix[4]arene is too small to fit the lithium cation and calix[8]arene is too large for the caesium cation. Therefore the calix[4]arene complex with caesium cations must adopt a 'domed' structure, where the cation complexes with the hydroxyl groups in the lower rim and is stabilised by cation-π interactions. However the ability of calix[4]arene **35** to extract is greatly affected by the solvation of the cations by water molecules. The calix[4]arene-cation complex can still be stripped by water molecules from the exposed upper and lower rim. Conversely, group II cations are not effectively extracted by calixarenes. Calix[4]arenes have become increasing popular ligands for the extraction of caesium and modifications to the calix[4]arene core

structure have been made to increase the binding with caesium cations. Conformation 'freezing' has been utilised where substituents have been added to lock the calixarene into the 1,3-alternate conformation.

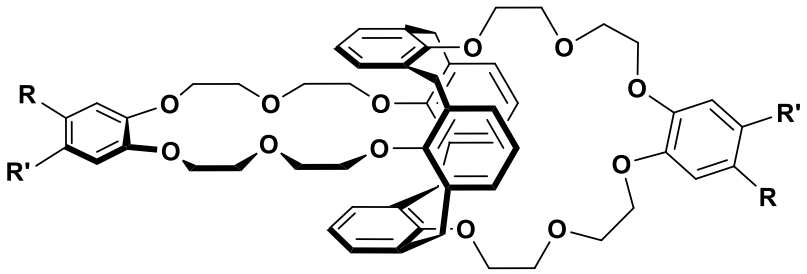

43 R = $C(CH_3)_2CH_2C(CH_3)_2CH_3$, R' = H
44 R = $CH_2CH(CH_2CH_3)(CH_2)_3CH_3$, R' = H
45 R = CH_3, R' = OH
46 R = CH_3, R' = CO_2H
47 R = CO_2H, R' = H
48 R = $CO_2(CH_2)_2OSO_3^-$ K^+, R' = H
49 R = $N(CH_2CH_2OH)_2$, R' = H

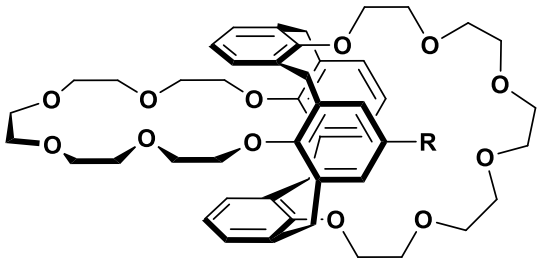

50 R = H
51 R = Br
52 R = CO_2H
53 R = $CONHSO_2CF_3$
54 R = $CONHSO_2Ph$
55 R = $CONHSO_2Me$

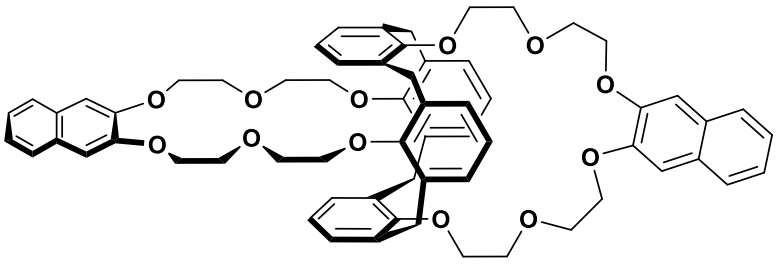

56

Figure 1.21 Examples of calix[4]bis-crown-6 ligands[84–91]

Etherification of the calix[4]arene **35** can form a calix[4]bis-crown using a polyethylene glycol unit. A polyethylene glycol with 5 repeat units will form a calix[4]bis-crown-6 that has shown promise in extracting caesium. This combination of crown ether and calixarene enables strong complexes with caesium cations because of dative covalent bonds from the ether oxygen atoms and π interactions from the aryl groups of the calixarene. Calix[4]bis-crown-6 ligands have been explored in their ability to extract caesium via liquid-liquid extraction methods, yielding a highly selective ligand for caesium over sodium.[84–91] Examples of calix[4]bis-crown-6 ligands are shown in Figure 1.17.

Haverlock *et al.* compared crown ethers to calix[4]bis-crown-6 derivatives with the most selective crown ethers providing a Cs/Na separation factor of $\sim 10^2$; whereas calix[4]bis-crown-6 produced Cs/Na separation factors exceeding 10^4.[89] Crown ethers are more flexible than calix[4]bis-crown-6 that have been locked into the 1,3-alternate conformation. This means that calix[4]bis-crown-6 compounds display a higher selectivity towards caesium over sodium because the compound is unable to distort around sodium cations.

Calix[6]arene **36** and calix[8]arene **37** have been studied for their ability to extract strontium cations. Calix[6]arene derivatives with tertiary amide groups have shown promising results in selectively extracting strontium over sodium, resulting in 83% extraction of strontium using *p*-*tert*-butylcalix[6]amide **57** ligand in a liquid-liquid method compared to 27% extraction for sodium.[92]

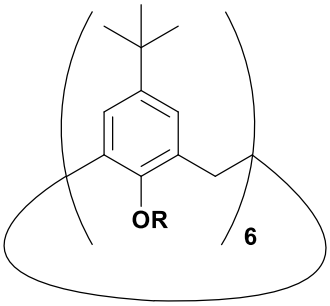

57 R = CH_2CONEt_2

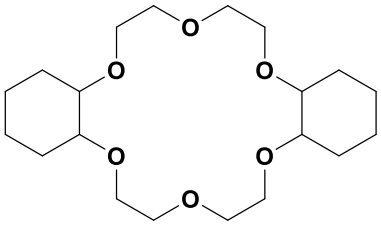

58

Figure 1.22 *p-tert*-butylcalix[6]amide **57** and dicyclohexyl-18-crown-6 **58**

The *p-tert*-butylcalix[6]amide **57** ligand demonstrates higher Sr/Na separation factors compared to dicyclohexyl-18-crown-6 **58**, one of the more selective extractants for strontium cations.[92] Development has been made to improve the Sr/Na separation factor further by modifying calix[8]arenes with tertiary amide groups. Casnati *et al.* compared various calix[6]arene and calix[8]arene derivatives in their ability to act as a strontium extractants achieving the highest Sr/Na separation factors of 51.3 from *p*-benzylcalix[8]amide.[93] This is significantly higher than dicyclohexyl-18-crown-6 **58** ($SP_{Sr/Na}$ = 12).

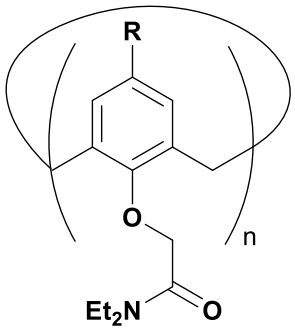

59 n = 6, R = H
60 n = 8, R = H
61 n = 8, R = *t*-Bu
62 n = 6, R = OCH_3
63 n = 8, R = OCH_3
64 n = 8, R = OBn

Figure 1.23 Structures of calix[8]amide **59-64**[93]

1.6 Solid-Phase Extraction (SPE)

1.6.1 Magnetic Nanoparticles (MNPs)

Different methods for waste water management include chemical precipitation, liquid-liquid extraction, use of ion exchange, cementation and electro-dialysis.[94–98] The problem with these treatment methods is the high cost and complexity of the processes as well as the large amounts of secondary waste produced.[98] Liquid-liquid extraction is predominantly used in the nuclear industry for reprocessing (PUREX process) but large volumes of solvent are needed with degradation of the solvent and extractant over time leading to loss of performance and efficiency.[99] Solid-phase extraction (SPE) is being increasingly used in such separations. The advantages of SPE over liquid-liquid extraction processes are high enrichment factors, absence of emulsification, safety with respect to hazardous samples, minimal costs (due to low consumption of reagents), flexibility and ease of automation.[100–104]

The introduction of magnetic separation technology (MACS process – Magnetically Assisted Chemical Separation) was reported at the Argonne National Laboratory in 1995.[105] A procedure utilising an extractant ligand immobilised onto magnetic particles was designed to reduce the complexity of waste treatment as the ligand immobilised magnetic particle is easily extracted using a weak external magnetic field.[106] Synthesis of mono-dispersed magnetic nanoparticles (MNPs) with particles sizes of less than 40 nm means that these can offer a large surface area for functionalisation. Iron oxide nanoparticles (Fe_3O_4 and γ-Fe_2O_3) have ferromagnetic and/or paramagnetic properties allowing for separation using a magnetic field.[32,95,107–109] Fe_3O_4 and γ-Fe_2O_3 nanoparticles can be generated using a co-precipitation method by mixing ferric and ferrous ions in a 1:2 molar ratio in highly basic solutions.[107–109] However, iron oxide nanoparticles have the potential to aggregate in liquid and so coating of the nanoparticles is needed. Silica coating allows for chemical stability and helps prevent

aggregation. Furthermore, the silanol groups from the silica layer can be easily covalently functionalised, providing a means of modifying the iron oxide MNPs.[107] The silica coating is produced using the Stöber process, where the silica coating is formed *in situ* through the hydrolysis and condensation of a sol-gel precursor.[107] In this protocol, iron oxide MNPs are homogenously dispersed in alcohol followed by addition of an appropriate silane and aqueous ammonia solution to produce the silica coating. Sonication allows even coating of the silane onto the homogenously dispersed iron oxide MNPs.

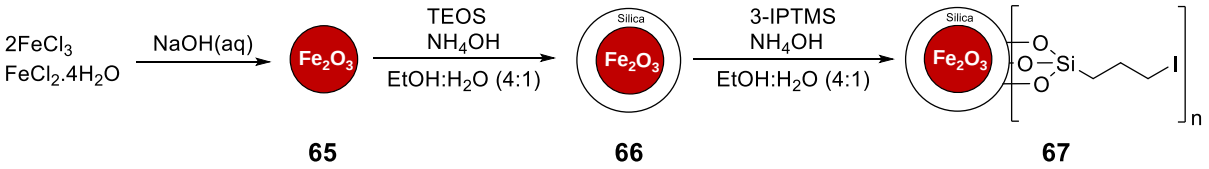

65 **66** **67**

Figure 1.24 Synthesis of Iodoalkyl-functionalised SiO_2 coated MNPs **67**

Tetraethoxysilane (TEOS) is the most common silane used in silica coating, where the OH groups bind onto the iron oxide MNPs.[107,110–112] Surface modification with organosilanes allows for additional functionalisation with extractant ligands due to organosilanes' bifunctional nature. The general formula for organosilanes is $X\text{-}(CH_2)_n\text{-}Si(OR)_3$, where X represents the headgroup functionality, $(CH_2)_n$ is the flexible spacer and $Si(OR)_3$ is the anchor group that couples with free Si-OH groups on the surface of silica-coated MNPs. Modification of the silica-coated surface with 3-iodopropyltrimethoxysilane (3-IPTMS) allows for functionalisation via displacement of the iodine group. The Harwood group has functionalised iodoalkyl-functionalized SiO_2-coated MNPs with different ligands: neocuproine for Cu(II) extraction, BTBP for An(III)/Ln(III) separation and BTPhen for An(III)/Ln(III) separation.[32,108]

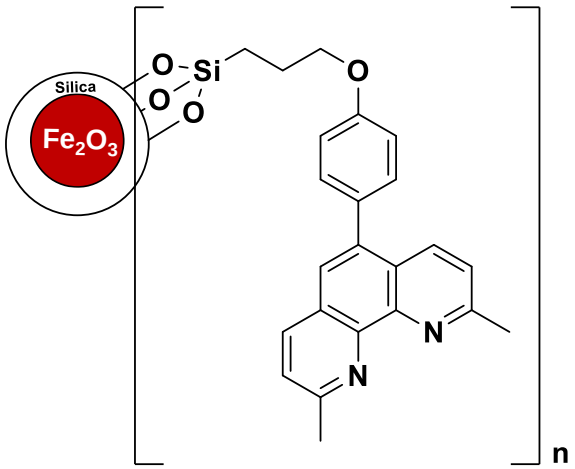

68

Figure 1.25 Neocuproine functionalised SiO_2-coated MNPs **68**

Neocuproine functionalised SiO_2-coated MNPs resulted in a system capable of highly efficient extraction (~99%) of Cu(II) at pH 2, while the precursor iodoalkyl-functionalised SiO_2 coated MNPs produced low extraction (~30%).[108]

Removal (%)		
SiO_2-coated MNPs	Iodoalkyl-functionalised SiO_2-coated MNPs	Neocuproine functionalised MNPs
17	30	99

Table 1.4 Extraction of Cu(II) from aqueous solution at pH 2 by SiO_2-coated Fe_2O_3 **66**, iodoalkyl-functionalized SiO_2-coated MNPs **67** and neocuproine functionalized MNPs **68**[108]

$CyMe_4$-BTPhen-functionalised SiO_2-coated MNPs have also been investigated for their ability to separate Am(III) from Eu(III) from HNO_3 solutions.[32] Extraction studies were carried out at nitric acid concentrations of 0.001, 0.1, 1 and 4M. At 0.001M HNO_3 high distribution ratios (D > 700) were achieved for both Am(III) and Eu(III) showing no separation ($SF_{Am/Eu}$ = 1.7 ± 0.1) for Am(III) over Eu(III). However, at 4M HNO_3 a decrease in D value for both Am(III) (D_{Am} = 55.4

$\pm$ 1.5) and Eu(III) (D_{Eu} = 0.03 $\pm$ 0.4) resulted in only Am(III) being retained on the functionalised MNPs. The separation factor at 4M HNO_3 ($SF_{Am/Eu}$ = estimated to be >1300) is much higher than that observed by $CyMe_4$-BTPhen ($SF_{Am/Eu}$ = 400) in liquid-liquid extraction.[13,32,113]

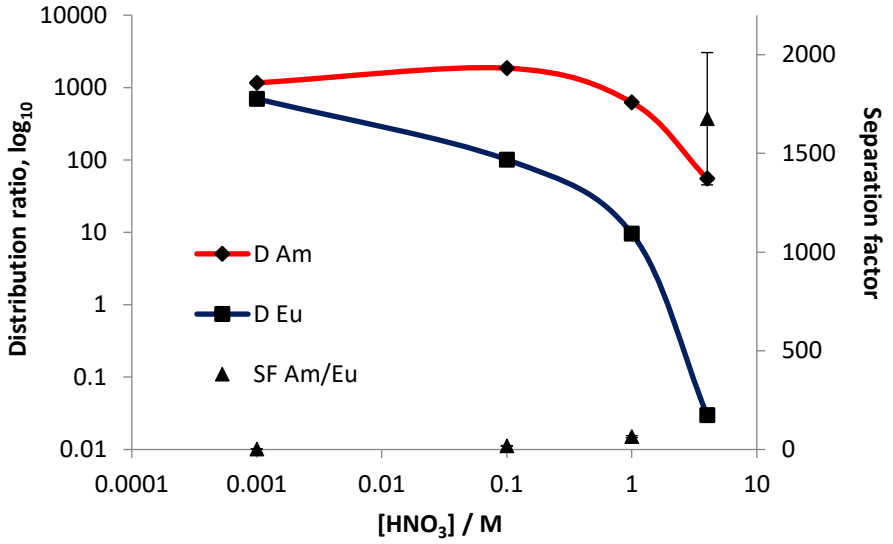

Figure 1.26 Extraction of Am(III) and Eu(III) by $CyMe_4$-BTPhen-functionalised SiO_2-coated MNPs as a function of nitric acid concentration.[32]

This demonstrated that, while iodoalkyl-functionalised SiO_2 coated MNPs are not effective extractants, they can be utilised as solid-state supports when functionalised with selective extractant ligands. It was therefore proposed that functionalisation of SiO_2-coated MNPs with demonstrated liquid-liquid caesium-selective ligands and strontium-selective ligands could provide a cheaper, more efficient alternative to liquid-liquid extraction.

1.6.2 Functionalised Silica Gel

Using selective chemisorption materials is another type of SPE that is becoming more popular in extraction processes. For an absorbing material to be efficient it should consist of a stable and insoluble porous matrix with suitable active groups that interact with a contaminant.[114] Silica gel has desirable characteristics for extraction and separation: for example silica gel is

stable under acidic conditions, is a non-swelling inorganic material and has high mass exchange characteristics and very high thermal resistance.[104,114–116] Functionalised silica gel can be utilised in a column separation protocol, extracting target species from eluents. The contaminant metal chelates to the selective ligand on the silica gel, while the eluent passes through the inert silica gel. This reduces the volume of secondary waste and allows for regeneration of the silica gel. Stripping of functionalised silica gel can provide a highly concentrated waste form that is easy to manage and permits recycling and reuse of the functionalised silica gel.

The silica gel can be first functionalised with an appropriate organosilane, like the organic coating of MNPs described in section 1.5.1. The $Si(OR)_3$ anchor group binds to the free Si-OH groups on the surface of the silica gel providing a good leaving headgroup (X) for further functionalisation. The Harwood group has immobilised BTBP and BTPhen onto silica gel to investigate extraction capabilities of such systems of minor actinides.[115] BTBP immobilised onto silica gel has also been investigated in its ability to extract transition metals. The uptake of various metals (Sc(III), Mn(II), Fe(III), Co(II), Ni(II), Cu(II), Zn(II), Mo(IV), Ag(I), Cd(II), Sb(V), Pb(II), Pd(II), Os(IV), Ir(III), Pt(IV), Au(III), Zr(IV), Nb(V), Hf(IV), Ta(V), W(VI) and Re(IV)) at pH 0.5 has shown > 80% extraction making BTBP-functionalised silica gel **69** a possible extractant for transition metals contaminants in nuclear waste or the environment.[117]

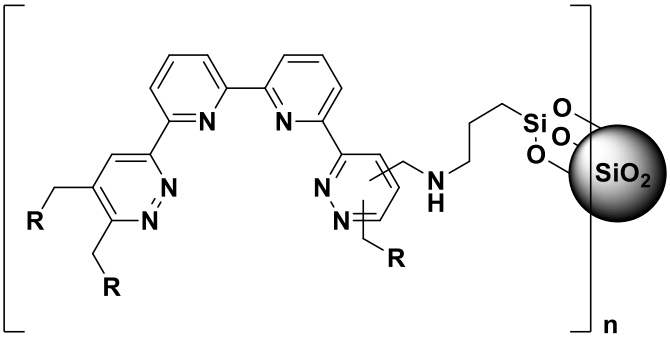

R = Br, Et_3N^+

69

Figure 1.27 BTBP-functionalised SiO_2 gel **69**

CyMe$_4$-BTPhen functionalised silica gel produced a high $SF_{Am/Eu}$ >154 at 4M HNO_3 and, at low HNO_3 concentration, extracted both Am(III) and Eu(III) similar to CyMe$_4$-BTPhen functionalised SiO_2-coated MNPs.[32,115,118]

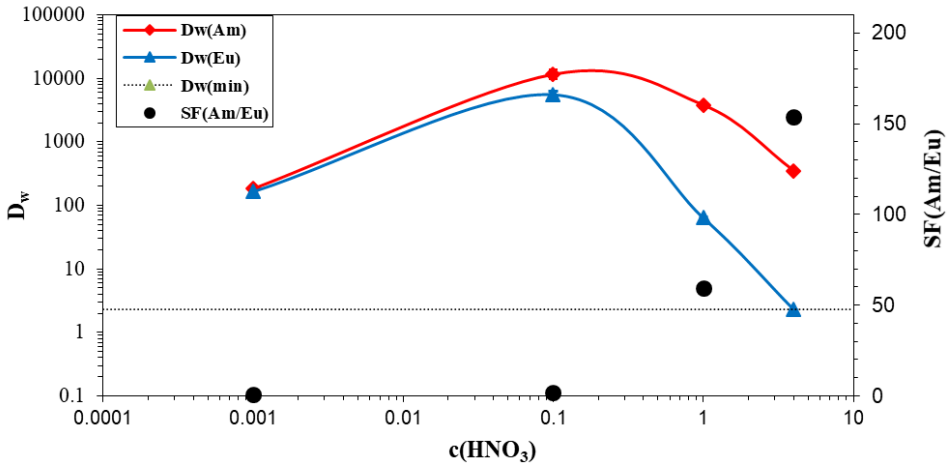

Figure 1.28 Extraction of Am(III) and Eu(III) by CyMe$_4$-BTPhen-functionalized SiO_2 gel as a function of nitric acid concentration.[32,115,118]

Just like SiO_2-coated MNPs, silica gel could well be functionalised with caesium and strontium selective ligands to provide a SPE protocol more manageable and cheaper than the widely used liquid-liquid extraction method.

Chapter 2 – Synthesis and Extraction Studies of a Caesium Selective Ligand

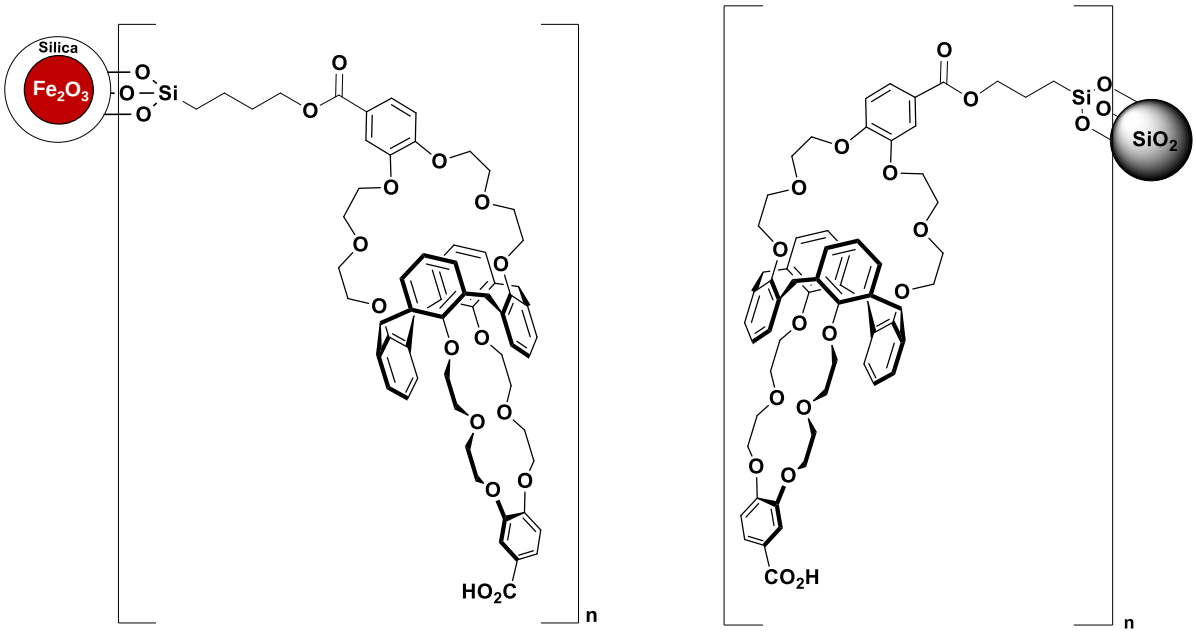

2.1 Synthesis of Calix[4]arene bis-[(4-carboxyl-1,2-phenylene)crown-6)]

Spent nuclear fuel is currently being encapsulated in borosilicate glass in a process called vitrification.[14] The encapsulated radioactive material can cause defects in the borosilicate glass by β-particles and γ-rays interacting with the solid.[51] Removal of the fission products before vitrification reduces the risk of matrix deformation caused by β-decay and heat generation and reduces the volume of HLW.[50–52,54,55] ^{137}Cs is a significant heat generator in spent nuclear fuel and has a half life of 30.2 years, releasing β-particles.[50,51] Therefore, the removal of ^{137}Cs is highly desirable to deliver a safer more manageable waste form.

In this study, the synthesis of calix[4]bis-crown functionalised MNPs and calix[4]bis-crown functionalised SiO_2 gel and their ability to extract Cs(I) in the presence of other alkali metals was investigated, the calix[4]bis-crown structures being derived from systems shown to extract caesium selectively from aqueous solutions.

2.1.1 Synthesis of Ethyl 3,4-bis(2-(2-hydroxyethoxy)ethoxy)benzoate ***72***

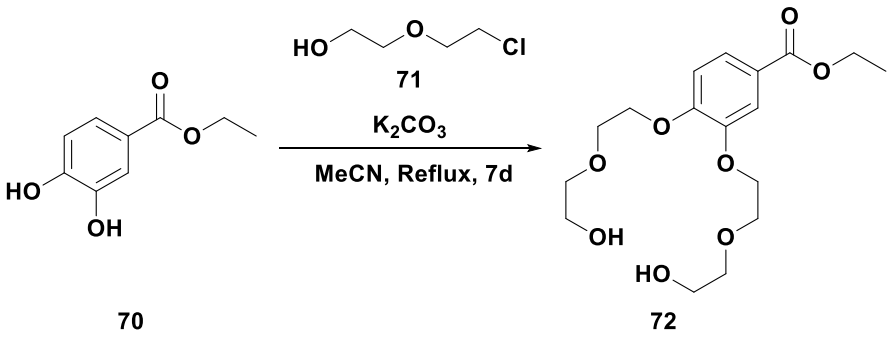

Scheme 2.1 Synthesis of Ethyl 3,4-bis(2-(2-hydroxyethoxy)ethoxy)benzoate **72**[85]

The first step of the synthetic route requires a nucleophilic reaction between ethyl 3,4-dihydroxybenzoate **70** and 2-(2-chloroethoxy)ethanol **71**[85] to provide the precursor to the

crown ether unit. The ethylene glycol chains on the product, when linked to calix[4]arene via macrocyclisation, will adopt a crown-6 structure with a cavity size that is suitable for complexation with caesium.[84,85,87–91] The phenolic group *para*- to the ester due to the stabilisation effect of the carbonyl group as shown in Figure 2.2. Acetonitrile was used as a polar aprotic solvent.

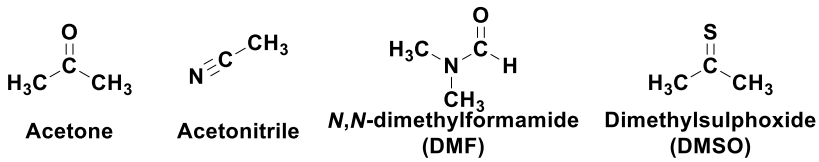

Figure 2.1 Polar aprotic solvents **73-76**

This allows the nucleophile to be un-solvated and free for nucleophilic substitution. Another benefit of using polar aprotic solvents is their ability to solvate cations. The base used to deprotonate the phenolic groups was potassium carbonate. Using acetonitrile also meant that the reaction was could be heated to reflux to speed up the reaction, while maintaining ease of workup due to acetonitrile's moderate boiling point (unlike DMF or DMSO).

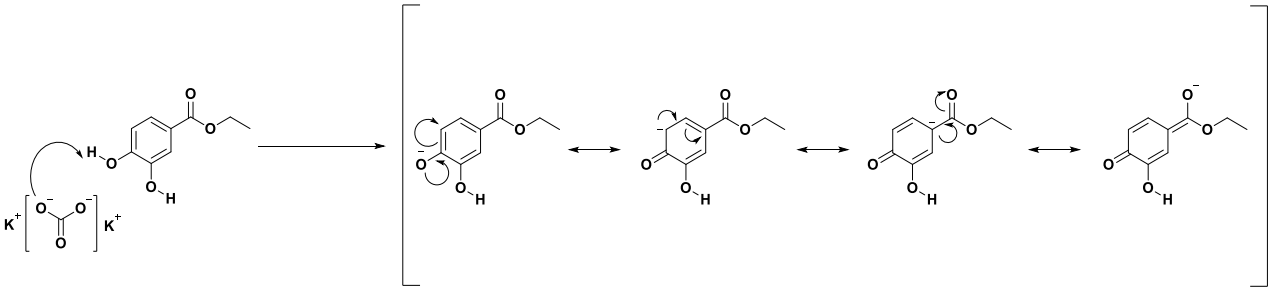

Figure 2.2 Acidifying effect of the ester group on the *para*- phenolic group.

2-(2-chloroethoxy)ethanol **71** may undergo an S_N1 pathway, losing the chlorine leaving group by neighbouring group participation of the central oxygen. The nucleophile then attacks the cationic epoxide species to form the ether bond. Labelling the adjacent carbon to the chlorine leaving group as ^{13}C could prove whether a S_N1 or S_N2 pathway is preferred. A S_N1 pathway would produce two products with different ^{13}C locations.

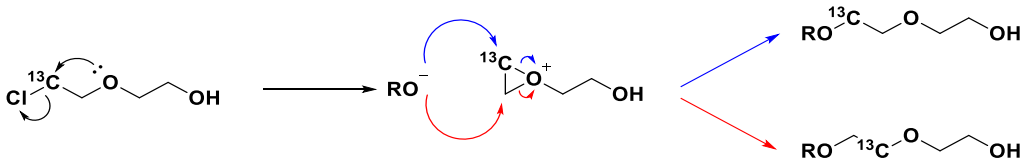

Figure 2.3 S_N1 mechanism with ^{13}C-labelling

In our hands a yield of 40% was achieved compared to the literature where a 30% yield was reported.[85] Changing the base to caesium carbonate improved the yield to 60%. However, introducing caesium to the synthetic route led to increases in Cs^+ concentrations in the aqueous phase when the final immobilized material was tested, presumably as a result of caesium uptake by the intermediate and the caesium being retained throughout the synthetic route. Changing the leaving group in the 2-(2-chloroethoxy)ethanol **71** could improve the yield. 2-(2-iodoethoxy)ethanol **77** is not available from chemical suppliers but can be made *in situ* by a Finkelstein reaction.[119]

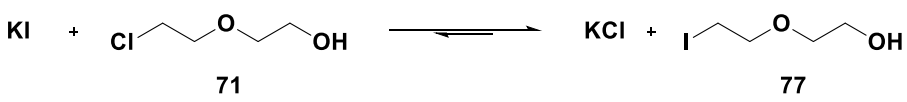

Figure 2.4 Finkelstein reaction

The Finkelstein reaction is an equilibrium but, in acetonitrile, the equilibrium is pushed towards the alkyl iodide product because of the insolubility of KCl, which precipitates out of solution, driving the reaction to completion.[120] When the Finkelstein reaction was carried out using 4.2 equivalents of KI, a yield of 93% was obtained after a period of reflux lasting 7 days (Scheme 2.2).

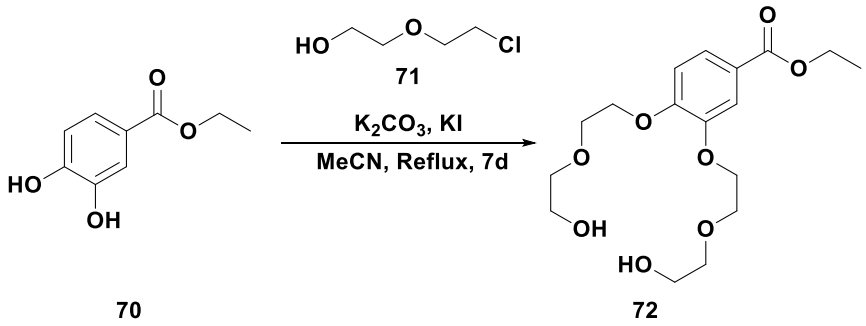

Scheme 2.2 Modified reaction Ethyl 3,4-bis(2-(2-hydroxyethoxy)ethoxy)benzoate **72**

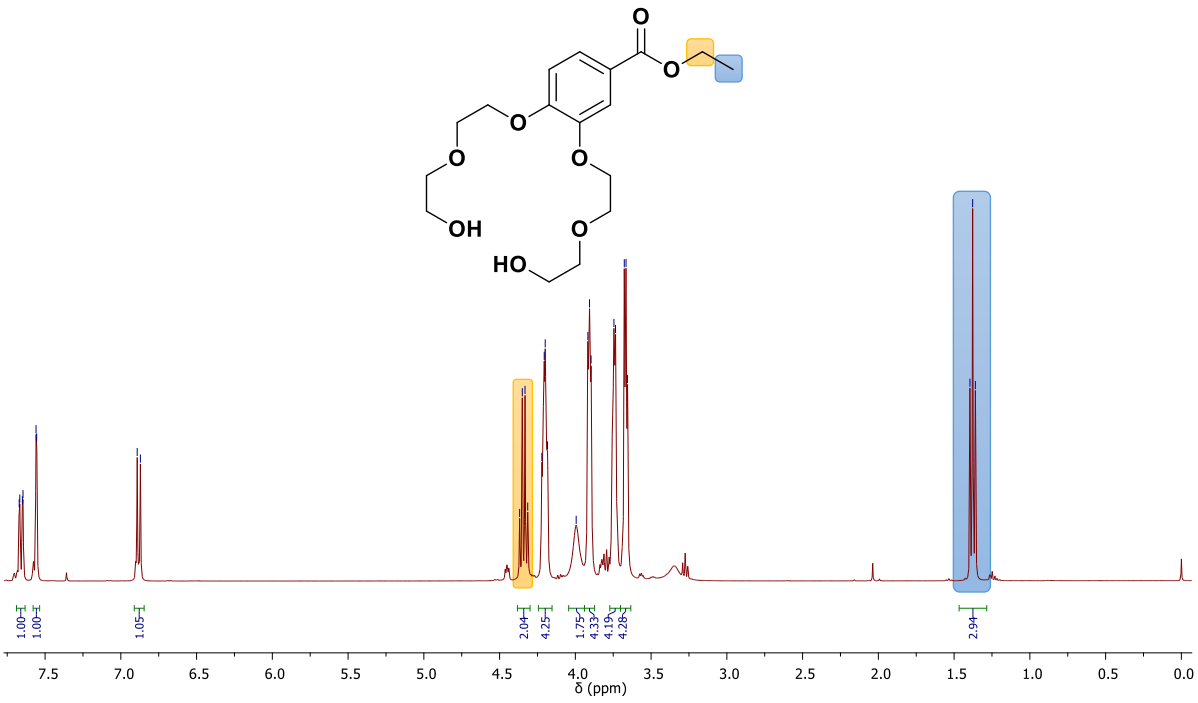

Figure 2.5 ^{1}H NMR spectrum of ethyl 3,4-bis(2-(2-hydroxyethoxy)ethoxy)benzoate **72**

The ^{1}H NMR spectrum of the product (Figure 2.5) shows the presence of the diethylene glycol units. The multiplets between δ 4.25 and 3.60 correspond to the two diethylene glycol units, with a broad resonance at δ 3.99 corresponding to the hydroxyl protons. The complex nature of the diethylene glycol resonances is because the molecule is asymmetric. However, the diethylene glycol units could be distinguished using 2-D NMR techniques such as COSY, HMBC and HMQC.

*2.1.2 Synthesis of Ethyl 3,4-bis(2-(2-(tosyloxy)ethoxy)ethoxy)benzoate **78***

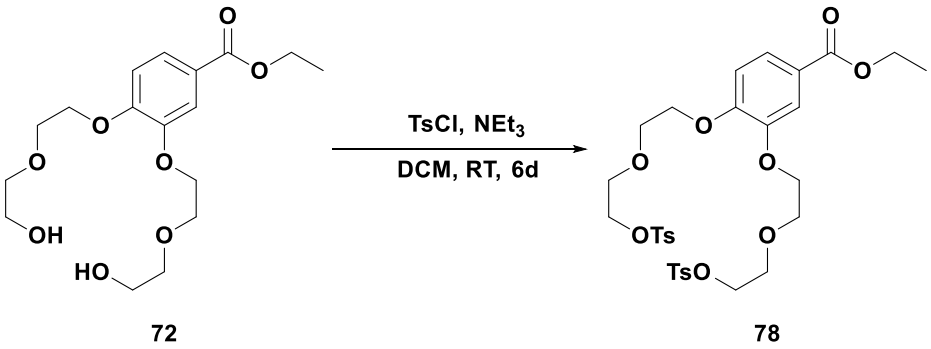

72 78

Scheme 2.3 Synthesis of Ethyl 3,4-bis(2-(2-(tosyloxy)ethoxy)ethoxy)benzoate **78**

The second step of the synthesis is to activate the hydroxyl groups and provide better leaving groups during nucleophilic substitution.[121] Tosylation with toluenesulfonyl chloride in the presence of an amine gives a tosyl ester that can then be reacted further with the appropriate nucleophile[122]. Ethyl 3,4-bis(2-(2-hydroxyethoxy)ethoxy)benzoate **72** was reacted with toluenesulfonyl chloride to provide the ditosylate product, ethyl 3,4-bis(2-(2-(tosyloxy)ethoxy)ethoxy)benzoate **78,** which can then undergo nucleophilic substitution with calix[4]arene **35**. The base used was triethylamine as previously reported by Lemaire *et al.* and the procedure resulted in a yield of 93% compared to a yield of 86% as reported in the literature.[85]

However, the rate of tosylation was slow resulting in a 6 day reaction. Therefore, the conditions were modified in an attempt to improve the kinetics. The base was changed to pyridine, which may act as a nucleophile, reacting with the toluenesulfonyl chloride, displacing the chlorine to provide a better leaving group. Excess pyridine will also remove HCl from the reaction.

Unfortunately, incomplete consumption of tosyl chloride was observed after 6 days using pyridine as the base. As triethylamine has a higher pKa than pyridine it may complex with the hydrogen of the primary alcohol of the diol. This would stretch the OH bond creating a greater dipole between the bond thus increasing the nucleophilicity of the oxygen. To ensure fast conversion, triethylamine could be used as the base with a catalytic amount of pyridine. This could allow the pyridine to displace the chlorine while the triethylamine facilitates the deprotonation. In fact, the pyridine was replaced with the acylation catalyst, 4-(dimethylamino)pyridine (DMAP), which has been used in previous tosylations.[123,124] DMAP is a more nucleophilic analogue of pyridine, activating the tosyl group, while triethylamine consumes the HCl by-product.

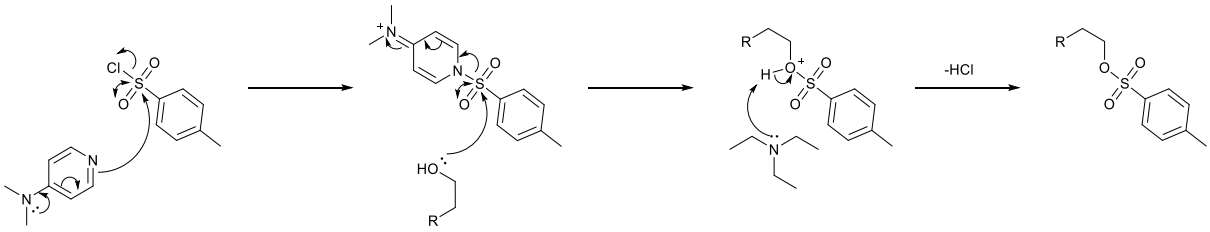

Figure 2.6 Tosylation mechanism with DMAP

Using a catalytic amount of DMAP with triethylamine decreased the reaction time from 6 to 4 days, while maintaining a high yield of 93% compared to the literature yield of 86%.[85] The DMAP catalyst could be simply removed by washing with saturated aqueous $CuSO_4$.

Recent studies into ultrasound-promoted tosylation of oligo(ethylene glycols) have seen yields being greatly improved and reaction times decreased. Triethylene glycol was shown to be tosylated successfully by Danjou *et al.* using triethylamine and toluenesulfonyl chloride in DCM with a yield of 95% after 30 minutes of sonication[125]. A similar approach was adopted for the tosylation of diol **72,** which contains two diethylene glycol units. Diol **72** and triethylamine were dissolved in DCM under nitrogen followed by the addition of 2 equivalence of toluenesulfonyl chloride. The mixture was subjected to sonication and completion of the reaction was achieved after 5 hours with a yield of 92%.[125]

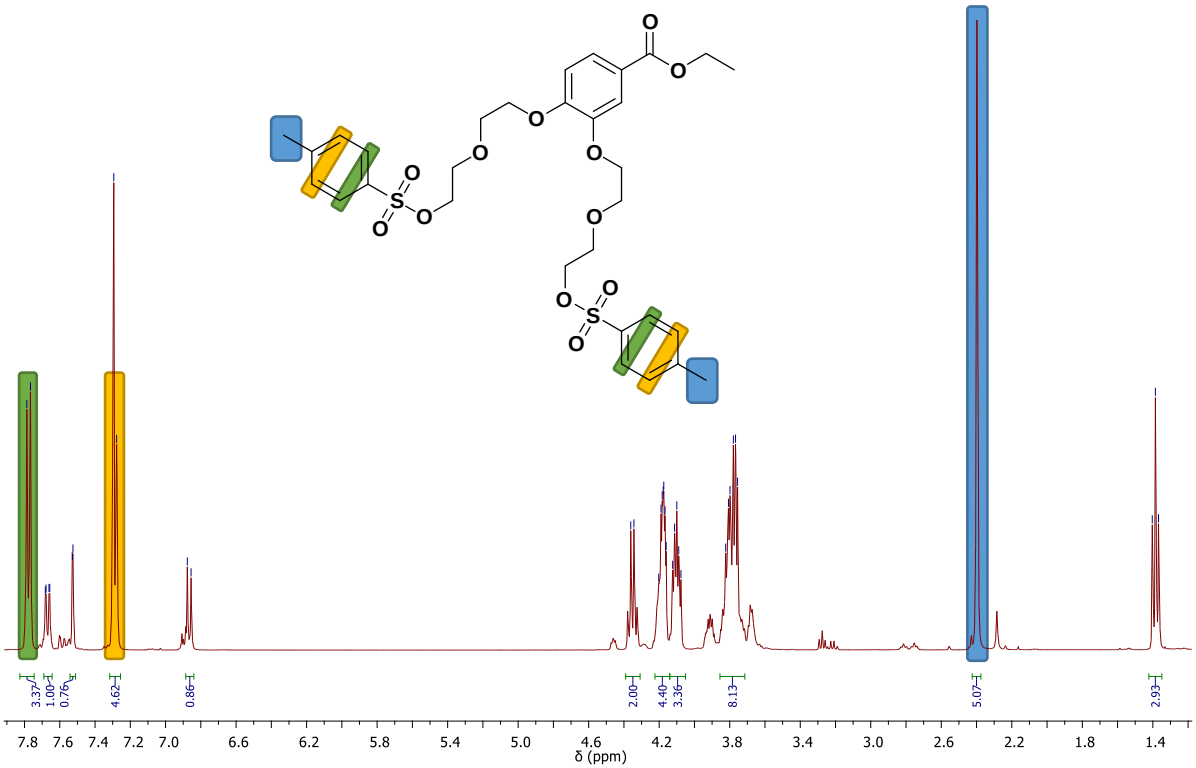

Figure 2.7 ^{1}H NMR spectrum of ethyl 3,4-bis(2-(2-(tosyloxy)ethoxy)ethoxy)benzoate **78**

The ^{1}H NMR spectrum of product **78** shows the presence of the toluenesulfonyl groups, With resonances centred on δ 7.78 and 7.29 corresponding to the aromatic protons and the methyl groups resonating at δ 2.40.

2.1.3 Synthesis of calix[4]arene-bis-[(4-ethoxycarbonyl-1,2-phenylene)crown-6] ***79***

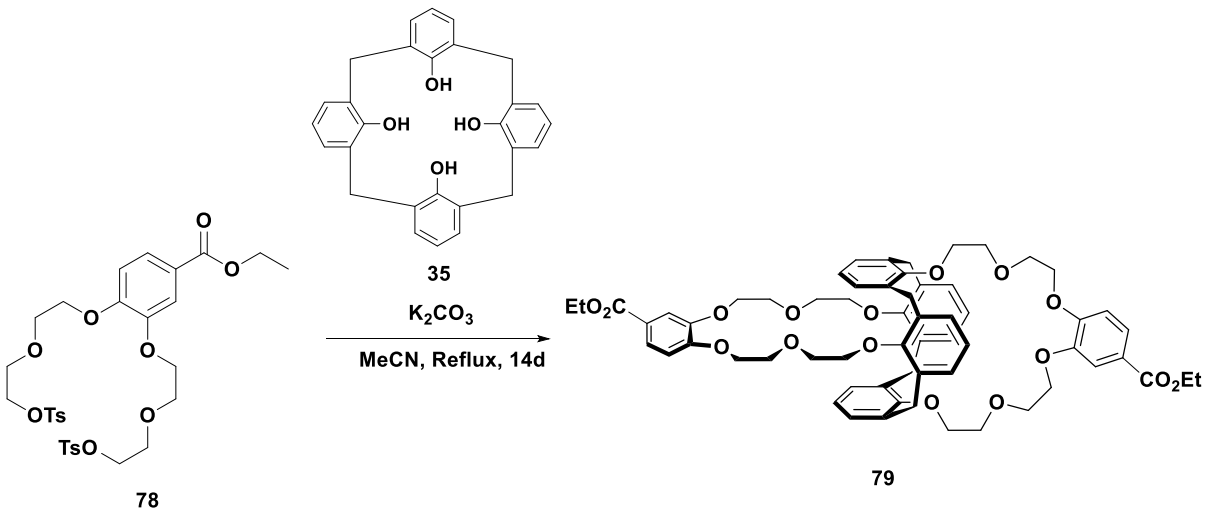

Scheme 2.4 Synthesis of calix[4]arene-bis-[(4-ethoxycarbonyl-1,2-phenylene)crown-6] **79**

The successful formation of the bis-calix[4]arene crown ether is dependent on the calix[4]arene adopting the 1,3-alternate conformation. Calix[4]arenes can adopt four different conformations shown in Figure 2.8.

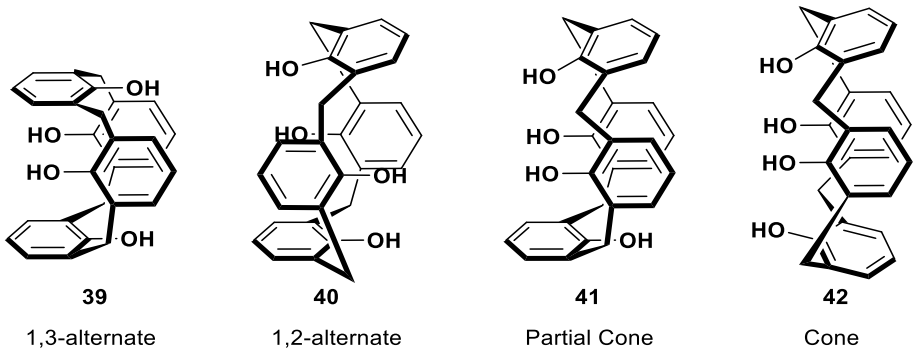

Figure 2.8 Conformations of calix[4]arene **35**

To form the calix[4]bis-crown **79** the ditosylate **78** must undergo macrocyclisation with calix[4]arene **35**.[85] The ditosylate **78** was added with calix[4]arene **35** as a 1:1 ratio to prevent oligomerisation of the ditosylate. After 7 days calix[4]mono crown was shown to be present, at which point additional potassium carbonate base and a further equivalent of ditosylate was added to complete formation of calix[4]bis-crown **79**. Acetonitrile was used as the solvent due to its polar aprotic nature, allowing solvation of the potassium cation from the carbonate base. It might be that the potassium cation also helps in templating the ditosylate to produce the calix[4]crown ether (Figure 2.9).

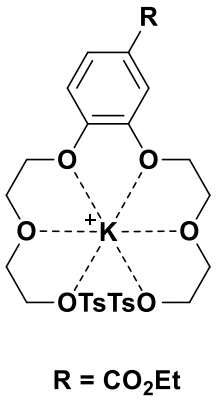

Figure 2.9 Possible templating effect of potassium cations

The base could be changed to Cs_2CO_3 allowing for better release of the carbonate anion. Caesium salts are far more dissociated than lithium, sodium and potassium salts because of their large ionic radius. Cs_2CO_3 is more soluble than other group I carbonates in aprotic organic solvents because the dissociated Cs^+ cation more easily solvated by the aprotic organic solvent. However, the Cs^+ cation would form a strong complex with the diethylene glycol units reducing the extraction capabilities of the final ligand.

The ^{1}H NMR spectrum of calix[4]bis-crown **79** possesses a triplet at δ 6.67 and a doublet at δ 7.07 corresponding to the aromatic protons of the calix[4]arene moiety. The ratio between the resonances corresponding to the ethyl ester and the calix[4]arene aromatic protons is 2:1 which supports the formation of the calix[4]bis-crown product and not calix[4]mono-crown.

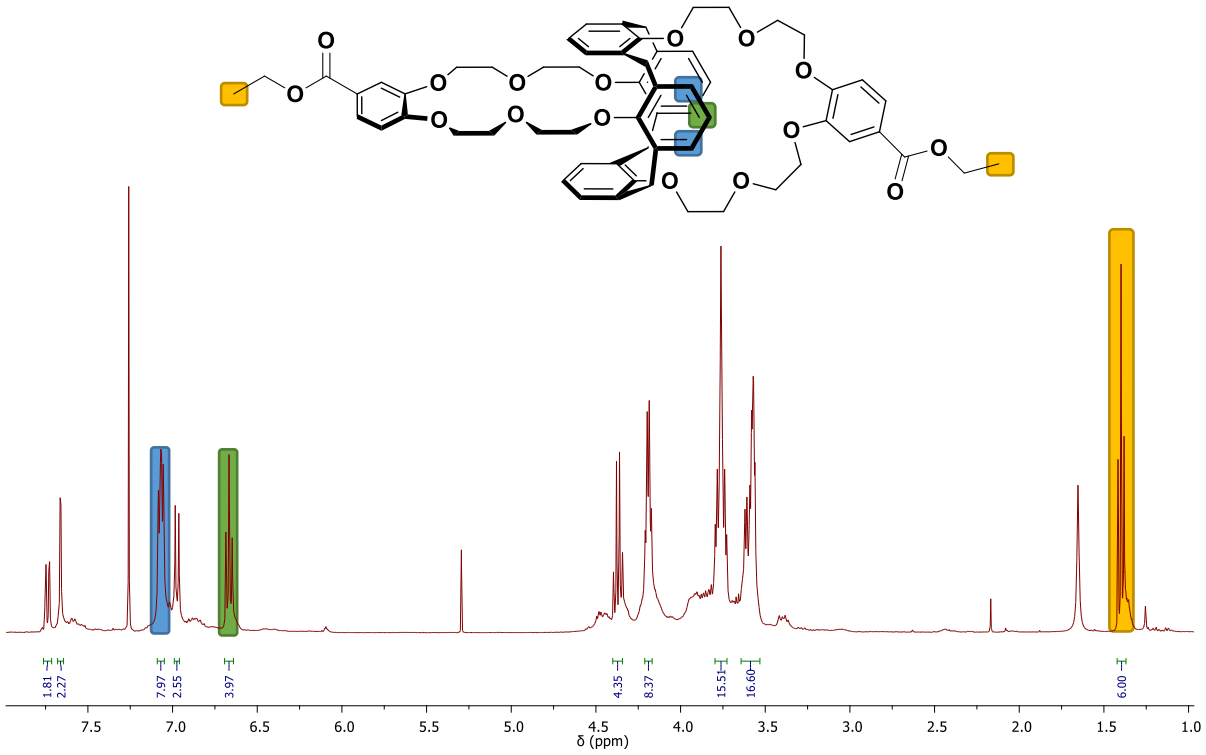

Figure 2.10 ^{1}H NMR spectrum of calix[4]arene-bis-[(4-ethoxycarbonyl-1,2-phenylene)crown-6] **79**

Calix[4]bis-crown is chiral by dissymmetric planes because of the position of the ester groups located on the crown ether units. In principle, this could be confirmed by the diastereotopic nature of any of the methylene resonances in the ^{1}H NMR; however, the Ar-C*H*$_2$-Ar linkages on the calixarene appear to have potentially the best defined magnetic environments. Upon closer inspection, the resonance for these methylene linkages is overlapped with other resonances from the molecule. A broad resonance at δ 3.75 could be consistent with either

with a singlet or a highly AB spin system. As the degree of diastereotopicity is variable between molecules and the solvent in which they are dissolved, whilst the appearance of diastereotopic resonances confirms the molecule's chirality, the absence of such changes does not discount the chirality.

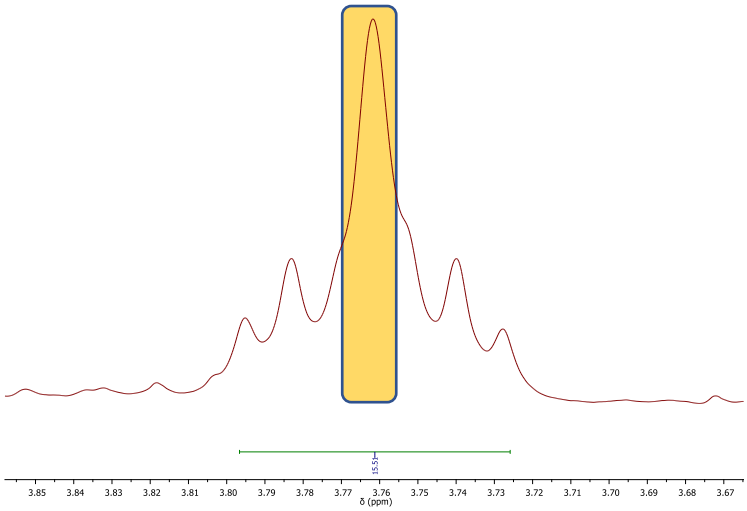

Figure 2.11 Possible singlet within ethylene multiplet.

Further investigation using a 700 MHz NMR spectrometer would be needed to distinguish whether the resonance at δ 3.75 is either a singlet or a diasterotopic environment.

2.1.4 Synthesis of calix[4]arene-bis-[(4-hydroxymethyl-1,2-phenyl-ene)crown-6] ***80***

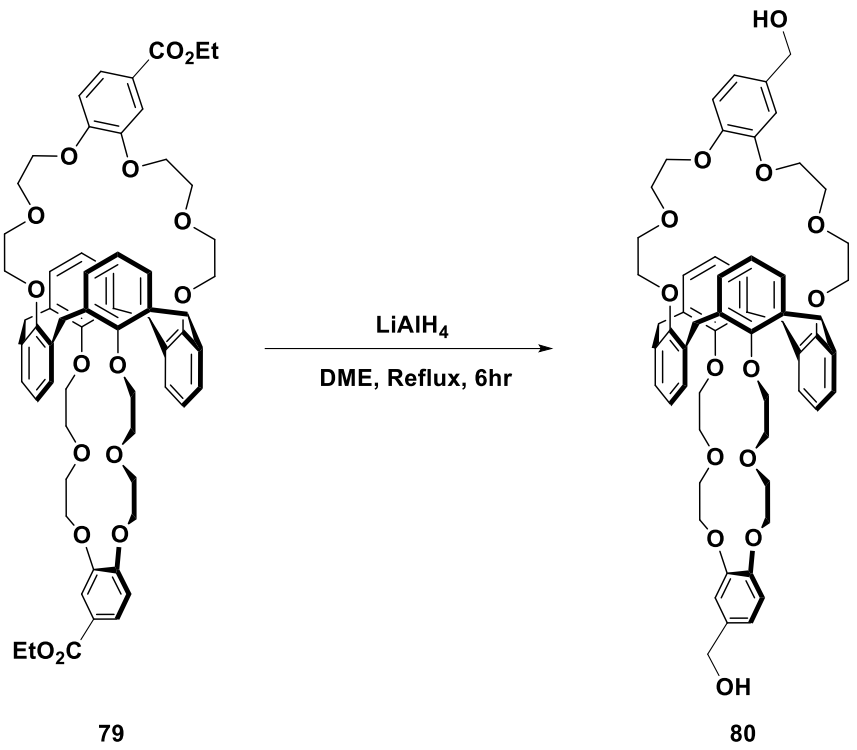

Scheme 2.5 Synthesis of calix[4]arene-bis-[(4-hydroxymethyl-1,2-phenyl-ene)crown-6] **80**

In order to immobilise the ligand onto a solid support an appropriate functional group must produced on the calix[4]bis-crown. A primary alcohol was initially chosen as a means of immobilisation via an ether linkage. The use of lithium aluminium hydride as a reducing agent is a common method in the reduction of esters to primary alcohols[126] and the reaction in Scheme 2.4 was reported by Lemaire *et al.* to occur with a yield of 80%.[85] However, when the reaction was attempted no conversion was observed. The procedure was repeated at varying reaction times all producing no reaction. Furthermore, the workup led to emulsions, making separation of the organic and aqueous phases difficult. Therefore, after quenching the reaction with water, the aluminium hydroxide emulsion was removed using an aqueous solution of Rochelle salt to form more soluble aluminium tartrate salts. However, while

improving the ease of workup, the reaction still yielded no product therefore the workup was not the issue with this reaction.

The substrate contains crown ethers and these might complex with the lithium cation of the lithium aluminium hydride. Smith *et al.* studied the kinetics and mechanisms of lithium aluminium hydride reactions and observed that, in the presence of a crown ether, the rate of reduction was significantly reduced.[127] The aluminium hydride anion without the lithium cation is a poor reducing agent causing no reduction of esters. Smith *et al.* found that, in THF, the lithium aluminium hydride in the presence of a crown ether was still able to act as a reducing agent but showed slower kinetics, suggesting that lithium aluminium hydride can reform from the lithium-crown ether complex, possibly by competition from the excess THF. However, when DME was replaced with THF for the reduction of calix[4]bis-crown **61** to a primary alcohol no reaction was observed. This may be because the complex between the calix[4]bis-crown and the lithium cation is too strong for the $LiAlH_4$ to reform. The crown ether moiety of the calix[4]bis-crown, while selective to Cs^+, is still a good complexing agent for other group I cations. Therefore Li^+ cation from $LiAlH_4$ coordinates to the calix[4]bis-crown stabilised by π electrons of calix[4]arene, a more stable complex than Li^+ and THF. This greatly reduces the efficiency of the reducing agent as Li^+ cation is less able to bind to the carbonyl of the ester during ester reduction.

2.1.5 Synthesis of calix[4]arene-bis-[(4-carboxyl-1,2-phenylene)-crown-6] ***47***

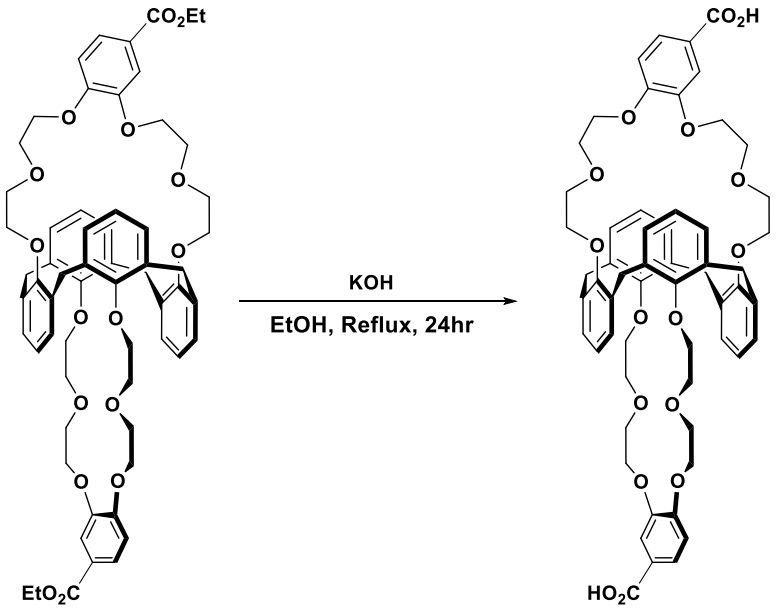

Scheme 2.6 Synthesis of calix[4]arene-bis-[(4-carboxyl-1,2-phenylene)-crown-6] **47**

Due to the unexpected failure of the attempted reduction of the ester, a hydrolysis reaction was chosen to form the carboxylic acid. Ester **79** was refluxed for 24 hours with potassium hydroxide to hydrolyse the ester. The carboxylate salt initially formed by alkaline hydrolysis of **79** was soluble in water but, once the reaction mixture was acidified, the carboxylic acid precipitated out of solution. To remove any water remaining in the solid after filtration, the carboxylic acid was dissolved in chloroform and the solution dried with magnesium sulfate. The solvent was then removed via rotary evaporation to afford pure carboxylic acid **47**. From the ^{1}H NMR spectrum, the ethyl ester resonances at δ 1.40 and 4.37 in **79** had disappeared, being replaced by a broad a resonance at δ 12.73 corresponding to the carboxylic acid proton.

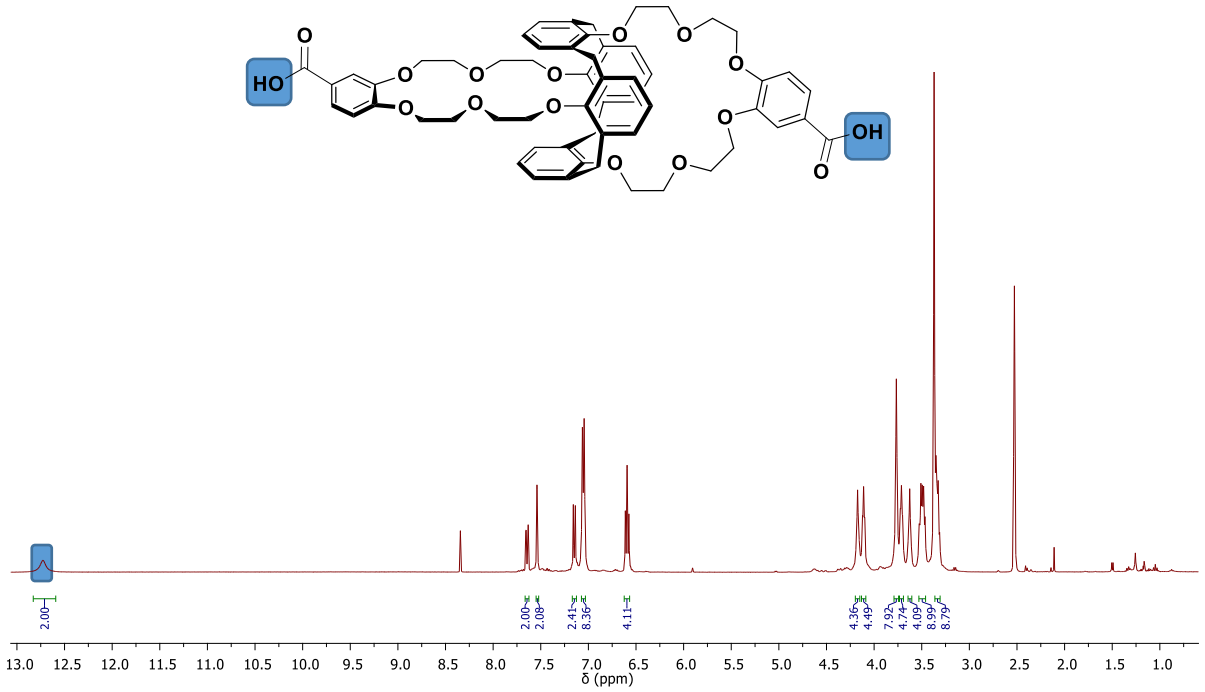

Figure 2.12 ^{1}H NMR of calix[4]arene-bis-[(4-carboxyl-1,2-phenylene)-crown-6] **47**

2.2 Calix[4]bis-crown silica-coated MNPs for extraction of Cs(I)

*2.2.1 Synthesis of calix[4]bis-crown silica-coated MNPs **81***

The magnetic core for the nanoparticles is an iron oxide (γ-Fe_2O_3), produced by co-precipitation from a mixture of aqueous iron(II) and iron(III) chlorides using sodium hydroxide.[108,109,128,129] The magnetic core is then coated with silica, enabling the nanoparticle to be functionalised covalently. The SiO_2 layer was applied to the γ-Fe_2O_3 MNPs by a sol-gel method using tetraethyl orthosilicate (TEOS).[108,130,131] The SiO_2 coating is further functionalised with 2-iodopropyltrimethoxysilane (3-IPTMS) as shown in Scheme 2.7.[108,132]

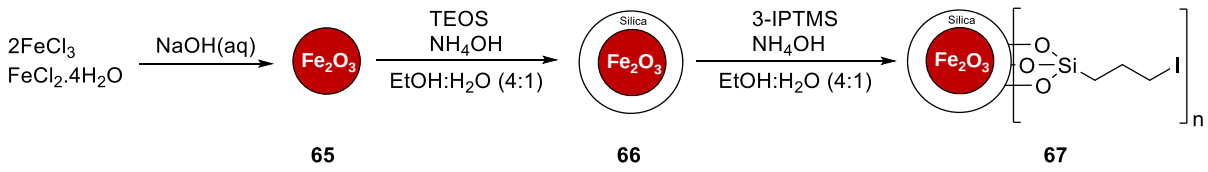

Scheme 2.7 Synthesis of SiO_2-coated γ-Fe_2O_3 MNPs

Calix[4]arene-bis-[(4-carboxyl-1,2-phenylene)-crown-6] was synthesised as previously described in Section 2.1 and then immobilised onto the MNPs by substitution of the iodo-moiety as shown in Scheme 2.8.

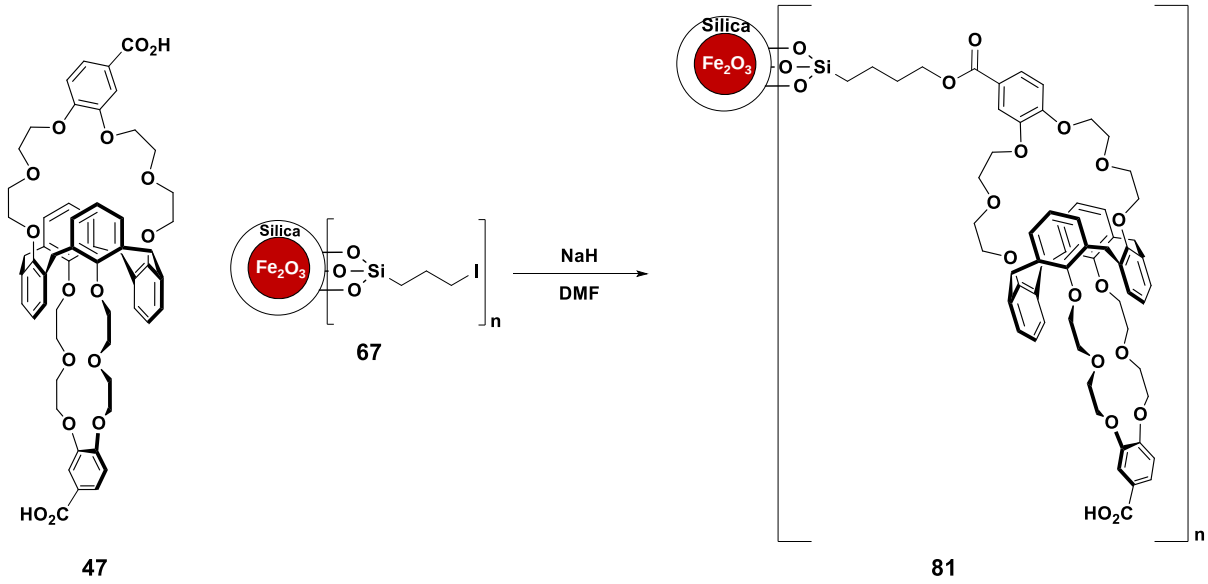

Scheme 2.8 Immobilisation of calix[4]bis-crown onto functionalised magnetic nanoparticles

*2.2.2 Characterisation of calix[4]bis-crown silica-coated MNPs **81***

During the formation of the MNPs, fourier-transform infrared spectroscopy (FT-IR) was used to characterise the products of each step. Figure 2.14 displays the FT-IR spectra of uncoated (γ-Fe_2O_3) MNPs **65**, silica-coated MNPs **66** and iodo-functionalised MNPs **67**. The γ-Fe_2O_3 MNPs **65** showed a strong absorption around 600 cm^{-1} caused by the Fe-O stretch. Coating the γ-Fe_2O_3 MNPs with silica resulted in appearance of absorptions at 3360 and 1070 cm^{-1}

caused by the O-H and Si-O stretching respectively. The silica coated MNPs **66** were then functionalised with 3-IPTMS, causing bands at 2960 and 689 cm^{-1} to appear corresponding to the C-H and C-I stretching of the iodopropyl functionalities on the SiO_2 coated MNPs. A small suppression of the O-H broad stretch at 3360 cm^{-1} was also observed, owing to the reduced number of Si-OH groups on the surface of the MNPs.

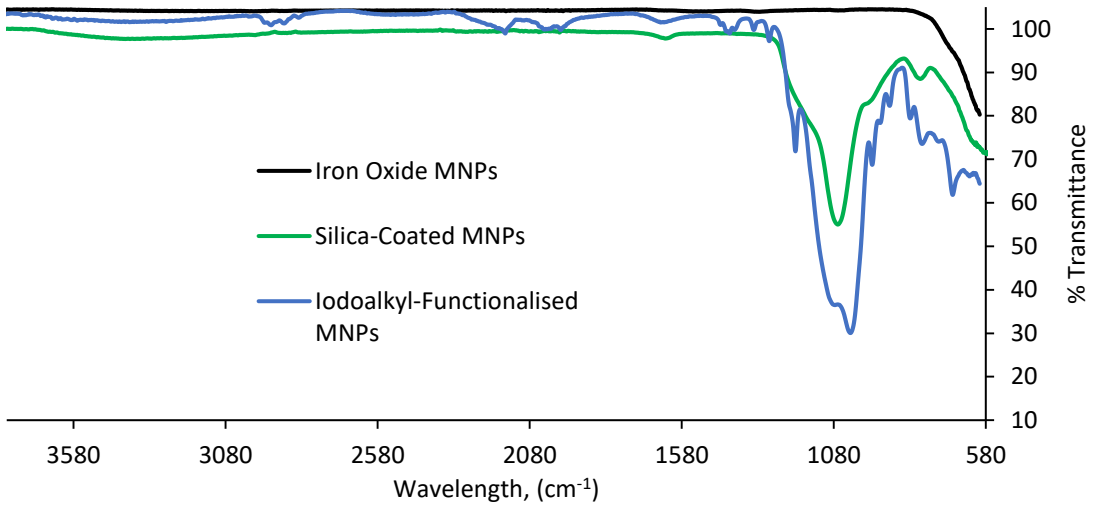

Figure 2.13 FT-IR spectra of γ-Fe_2O_3 **65**, SiO_2-coated Fe_2O_3 **66** and iodoalkyl-functionalised SiO_2-coated MNPs **67**

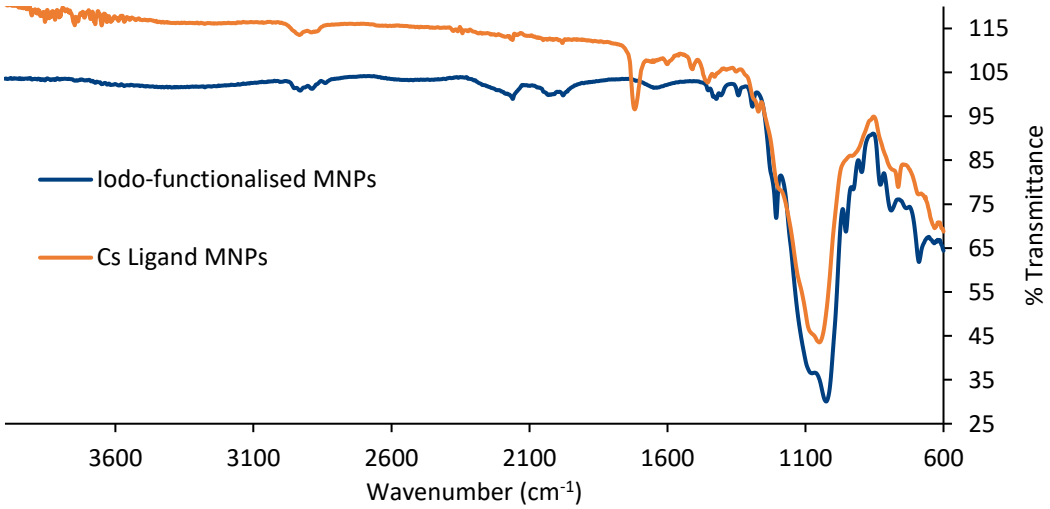

Figure 2.14 FT-IR spectra of iodoalkyl-functionalised SiO_2-coated MNPs **67** and calix[4]bis-crown functionalised SiO_2-coated MNPs **81**

The iodoalkyl-functionalised SiO_2 coated MNPs **67** were then functionalised with calix[4]bis-crown **47** in DMF, using sodium hydride to deprotonate the carboxylic acid of calix[4]bis-crown **47** initiating nucleophilic substitution to form an ester linkage. This resulted in suppression of the C-I stretching absorption at 689 cm^{-1} and the appearance of an absorption at 1716 cm^{-1} assigned to the carbonyl stretching frequency of the ester linkages.

SEM images shown in Figure 2.15 display the iodoalkyl-functionalised SiO_2-coated MNPs **67** and calix[4]bis-crown functionalised MNPs **81**. Little difference is seen in their appearance from SEM; however using elemental analysis during SEM imaging gave evidence for the degree of immobilisation of the calix[4]bis-crown. Table 2.1 shows the percentage of C, O and I in the iodoalkyl-functionalised SiO_2-coated MNPs and calix[4]bis-crown functionalised MNPs.

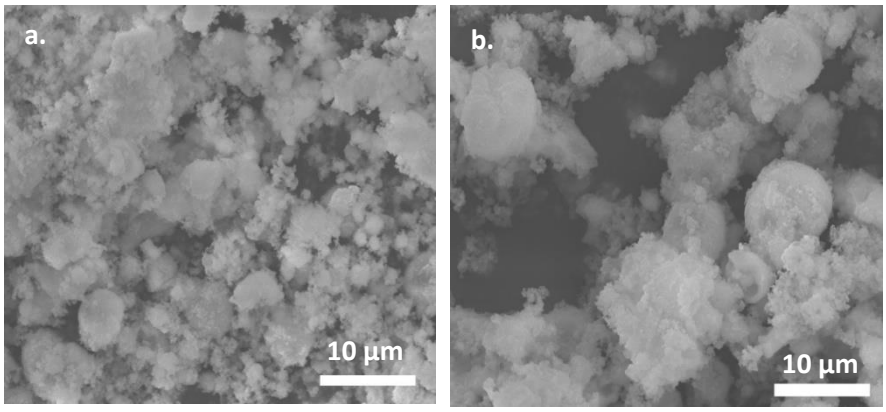

Figure 2.15 SEM images of (a) iodoalkyl-functionalised SiO_2-coated MNPs **67** and (b) calix[4]bis-crown functionalised SiO_2-coated MNPs **81**

	Iodoalkyl-functionalized SiO_2-coated MNP	*Calix[4]bis-crown functionalized SiO_2-coated MNP*
C (%)	39.29	52.6
O (%)	14.54	20.21
I (%)	36.91	15.47

Table 2.1 Elemental analysis of iodoalkyl-functionalised SiO_2-coated MNPs **67** and calix[4]bis-crown functionalised SiO_2-coated MNPs **81**

Immobilisation of calix[4]bis-crown **47** onto the surface of the SiO_2-coated MNPs is shown with the increase of carbon and oxygen (i.e. 39.29% carbon for iodoalkyl-functionalised MNPs and 52.6% carbon for calix[4]bis-crown functionalised MNPs). The loss of iodine also indicates immobilisation, resulting in circa 58% of the iodoalkyl groups having been substituted.

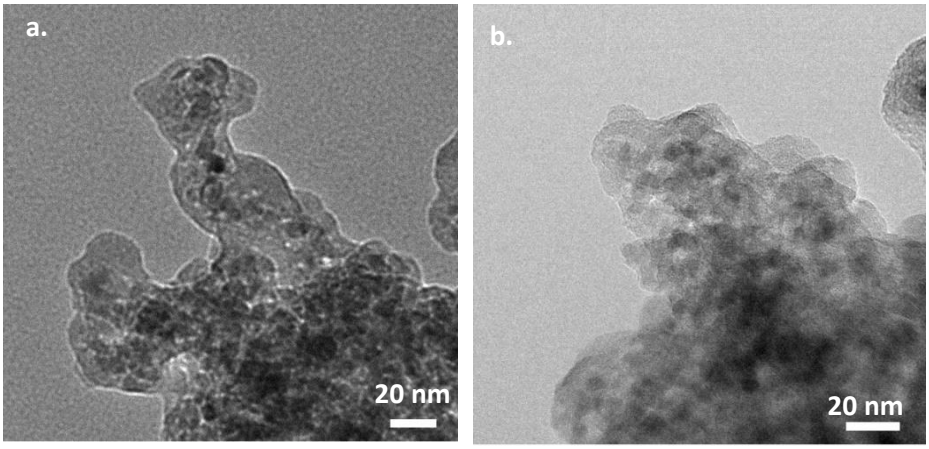

Figure 2.16 TEM images of (a) iodoalkyl-functionalised SiO_2-coated MNPs **67** and (b) calix[4]bis-crown functionalised SiO_2-coated MNPs **81**

TEM images of iodoalkyl-functionalised SiO_2-coated MNPs **67** and calix[4]bis-crown functionalised SiO_2-coated MNPs **81** are shown in Figure 2.16. Both TEM images show the γ-Fe_2O_3 core surrounded by an organic coating. The calix[4]bis-crown functionalised SiO_2-coated

MNPs [Figure 2.16 (b)] appear to show a greater thickness of organic coating around the darker γ-Fe_2O_3 cores.

Thermogravimetric analysis (TGA) can display the degree of organic coating around the Fe_2O_3 core by measuring the change in mass as a function of temperature. The changes of physical and chemical properties can be deduced from the change in mass at certain temperatures.

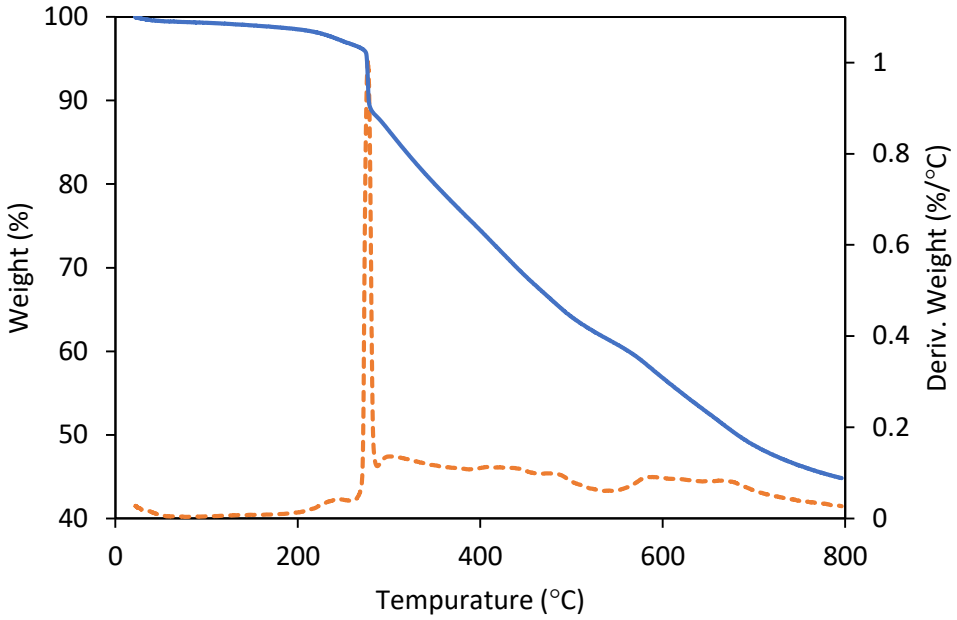

Figure 2.17 TGA curve of iodoalkyl-functionalised SiO_2-coated MNPs

The MNPs were investigated using TGA under nitrogen. The TGA curve of iodoalkyl-functionalised MNPs, shown in Figure 2.17, displayed a sharp loss of mass at 260-300 °C, presumed to correspond to the loss of the aliphatic iodoalkyl coating. The TGA curve of calix[4]bis-crown functionalised MNPs showed a three-step mass-loss (Figure 2.18). The loss in mass below 200 °C is attributed to the loss of absorbed water, while the significant loss in mass seen at 300-450 °C is proposed to correspond to decomposition of the largely aromatic

calix[4]bis-crown coating. The amount of calix[4]bis-crown immobilised onto the MNPs was estimated to be circa 18% w/w.

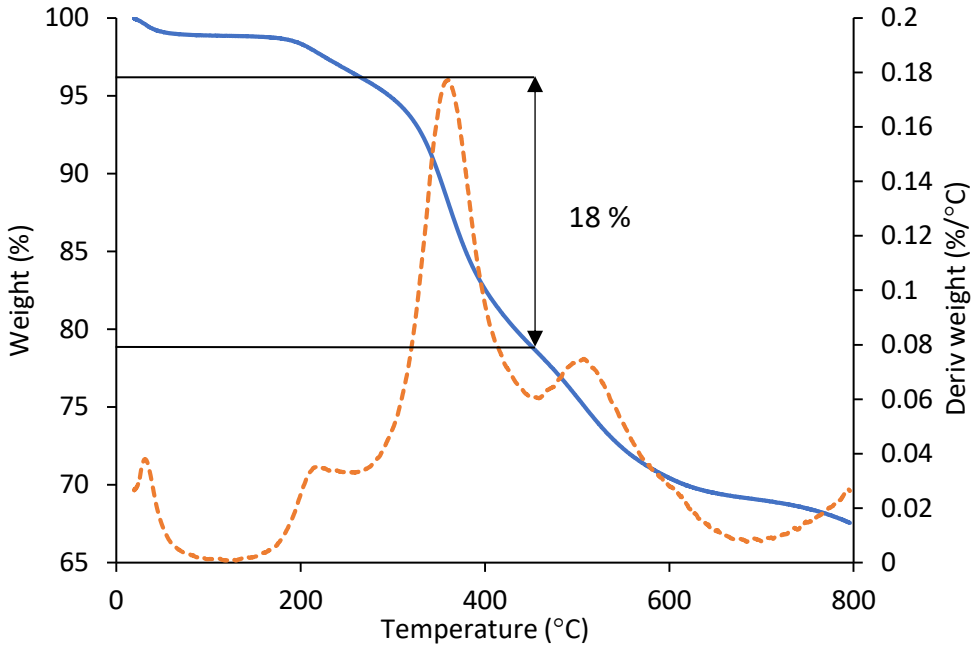

Figure 2.18 TGA curve of calix[4]bis-crown functionalised SiO_2-coated MNPs

2.2.3 Extraction studies

The calix[4]bis-crown functionalised MNPs were first compared to the precursor, iodo-functionalised MNPs to prove that the ligand was responsible for extracting the Cs^+ rather than the nanoparticles themselves. Equal amounts (5 mg) of calix[4]bis-crown functionalised MNPs and iodo-functionalised MNPs were tested on 10 mL samples of Cs^+ with a concentration of 10 ppb, with the analysis being carried out in triplicate. Before testing, samples were analysed using ICP-MS to measure the true starting concentration of Cs^+ in the samples. Once the samples were mixed with MNPs an external magnet was used to remove the MNPs, decanting off the supernatant.

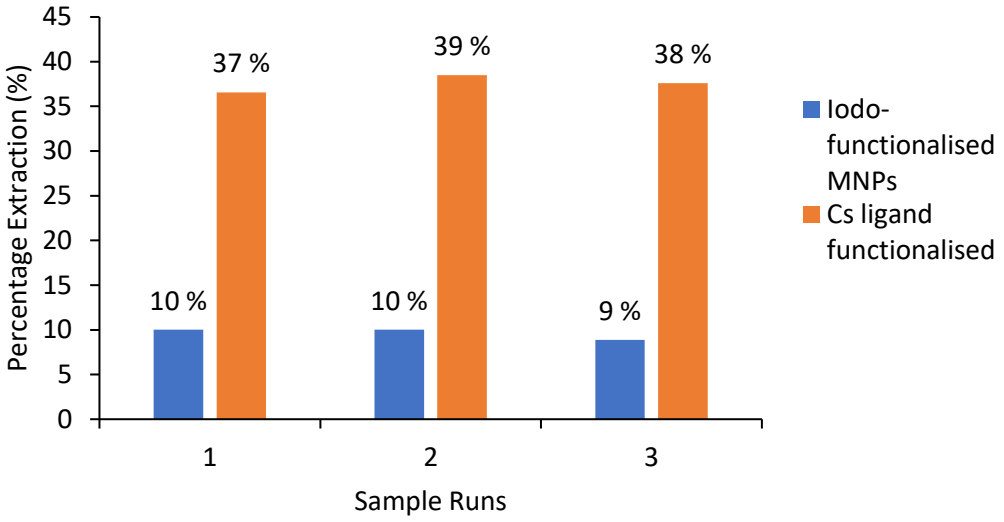

Figure 2.19 Extraction capabilities of iodoalkyl-functionalised SiO_2-coated MNPs **67** and calix[4]bis-crown functionalised SiO_2-coated MNPs **81**.

The supernatant was analysed by ICP-MS to measure the final concentration of Cs^+. A percentage extraction was then calculated from the starting and final concentration. Figure 2.19 shows that the iodo-functionalised only extracts 10% caesium; whereas the calix[4]bis-crown functionalised MNPs achieved extraction of >37%. This demonstrates that the ligand is responsible for a significant amount of Cs^+ extraction. To attempt to increase the percentage extraction of caesium, a higher dose of the functionalised nanoparticles was examined. However, the results from ICP-MS puzzlingly showed an increase in concentration of Cs^+ after testing shown in Figure 2.20. This was firstly thought to have been due to a calibration error but, on repeating the experiments, the same results were obtained. The results showed a linear correlation between the increased dose of MNPs and an increased concentration of caesium after testing.

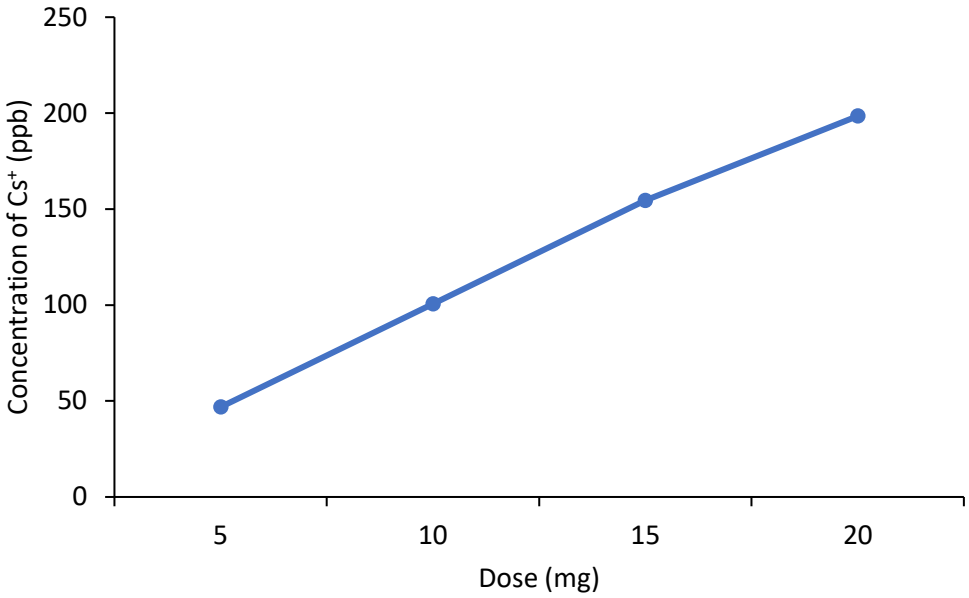

Figure 2.20 Increasing linear correlation between dose of MNPs and concentration of Cs^+ after exposure to caesium carbonate

It was proposed that the ligand was actually releasing caesium into the test samples rather than extracting due to retaining Cs^+ caused by early precursors in the synthetic route being exposed to caesium carbonate in the first step in the synthetic route involving ethyl 3,4-dihydroxybenzoate **70** and 2-(2-chloroethoxy)ethanol **71**.

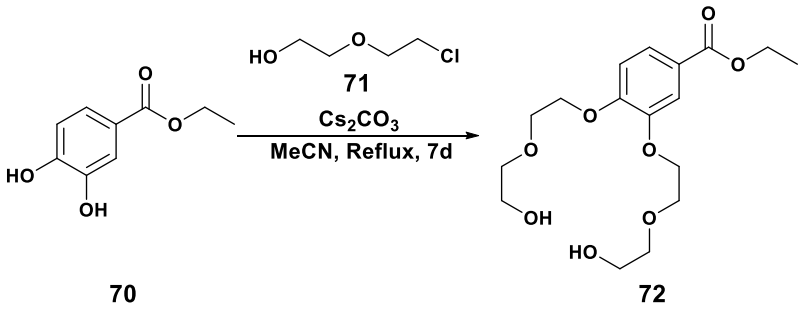

Scheme 2.9 Modified synthesis of Ethyl 3,4-bis(2-(2-hydroxyethoxy)ethoxy)benzoate

Caesium carbonate is highly dissociated which allows for solvation of Cs^+ by acetonitrile. However, because of the ethylene glycol units of diol **72**, Cs^+ also coordinates with early precursors. Exposure to nitrate anions in 2% HNO_3 solution used during extraction studies

leads to 'stripping' of Cs^+ causing the linear correlation between the increased dose of MNPs and an increased concentration of caesium after testing. Nitrate anions coordinate to Cs^+, disrupting the dative bonds between the calix[4]bis-crown and Cs^+. When reverting to potassium carbonate as the base in the first step of the synthesis to avoid exposure to caesium, an increase of caesium was still observed on carrying out the extraction analyses but at lower concentrations shown in Figure 2.21.

The reason for the increase of caesium at lower concentrations is a trace amount of Cs^+ is present in potassium carbonate. The trace caesium was again retained by early precursors in the synthetic route and stripped once exposed to nitrate anions from 2% HNO_3 solution from extraction studies. This shows calix[4]bis-crown **47** and early precursors strong affinity to Cs^+, and selectivity towards Cs^+ in the presence of a large excess of K^+. The stripping effect of nitrate anions could be a means of removing caesium from the calix[4]bis-crown functionalised SiO_2-coated MNPs after extraction.

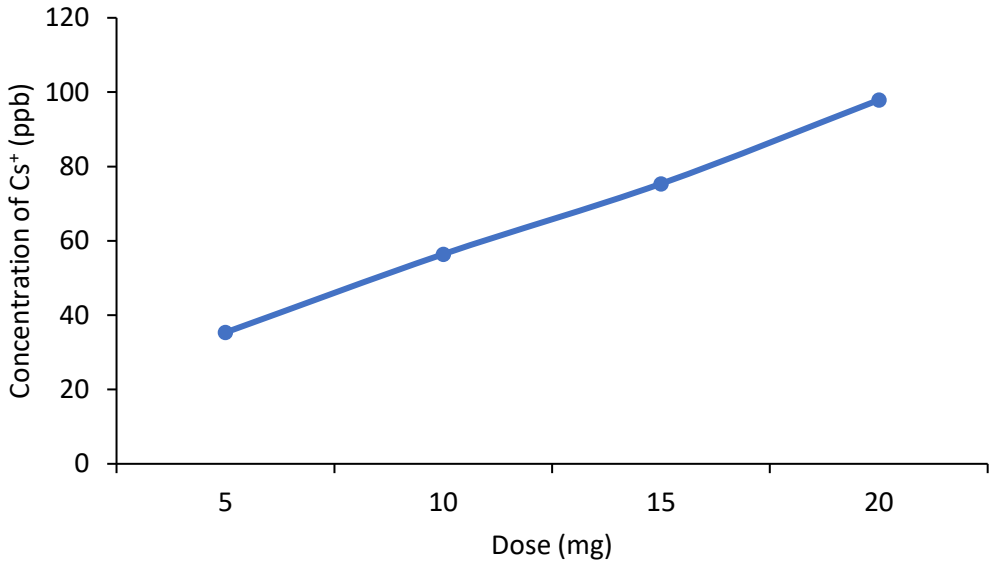

Figure 2.21 Increasing linear correlation between dose of MNPs and concentration of Cs^+ after exposure to trace caesium in potassium carbonate

The capacity of the calix[4]bis-crown functionalised SiO_2-coated MNPs to extract Cs^+ was then investigated at pH 7, the sample size was increased to 100 mL as was the concentration from 10 ppb to 100ppb to provide a greater range in dosage. Varying dose sizes (2 -100 mg) were tested, with 10 mL samples removed from each test run for ICP-MS analysis. Figure 2.22 shows the percentage extraction of Cs with increasing dosage of Cs ligand MNPs. From Figure 2.22 it is clear to see an increase in percentage extraction that correlates to an increase in the dose of calix[4]bis-crown functionalised MNPs. Between 10 – 50 mg there is a large increase in percentage extraction from 48% to 92%. Using the dose concentration of 0.5 mg mL^{-1}, an extrapolation leads to the conclusion that 250 g of calix[4]bis-crown functionalised MNPs would be needed for 500 L of Cs contaminated water, for example. Compared to a liquid-liquid extraction method that would require several litres of solvent to achieve high extraction, this shows the vast reduction in secondary waste when using solid-state supports.

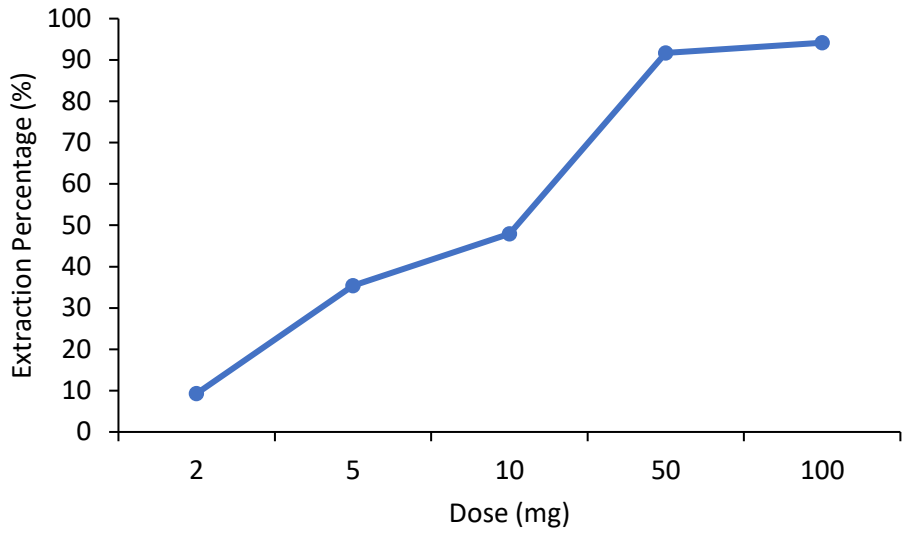

Figure 2.22 Capacity Test of calix[4]bis-crown functionalised MNPs from Cs Solutions (~100ppb)

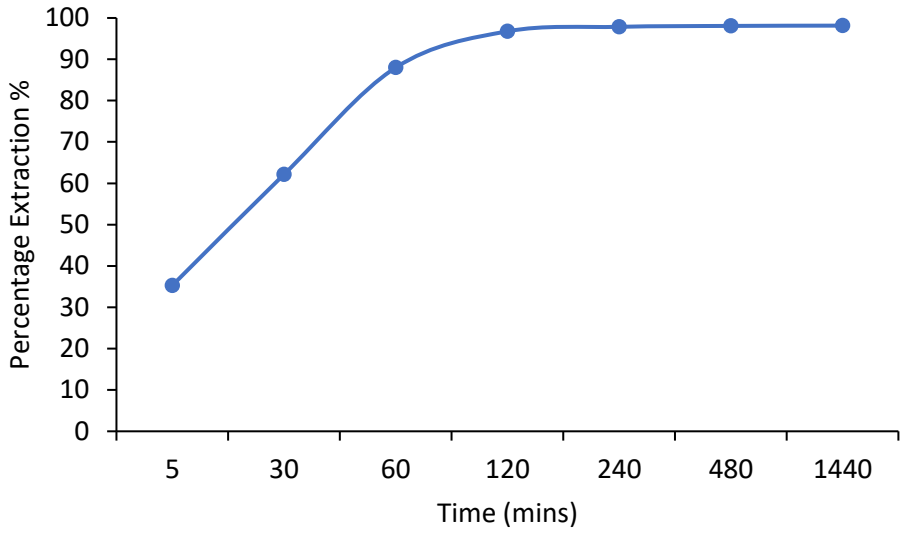

Figure 2.23 Kinetic study of calix[4]bis-crown functionalised MNPs

The kinetics of extraction were then tested to ensure extraction times appropriate for industrial application could be achieved. A 200 mL sample of caesium solution (100 ppb) was stirred with calix[4]bis-crown (100 mg). The dose of 0.5 mg/mL was chosen as high extraction had been achieved with the capacity assay. The extraction was left for a total of 24 hours, with small aliquots (10 mL) removed at various intervals to assess the level of extraction achieved at each stage. High extraction (>95%) was achieved after 2 hours of mixing (Figure 2.23). Presumably this could be improved with either increased loading of calix[4]bis-crown onto the magnetic nanoparticles or by increasing the dose used of the currently-prepared calix[4]bis-crown functionalised MNPs.

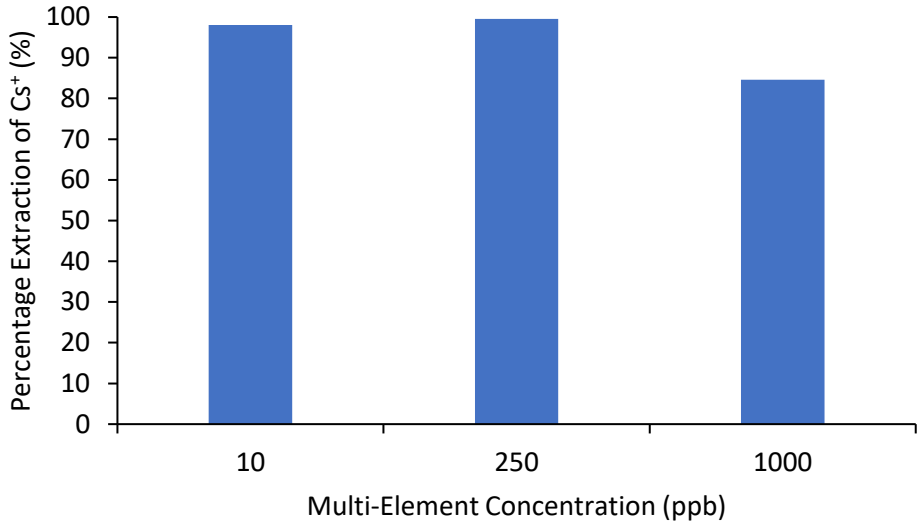

Figure 2.24 Percentage extraction of Cs^+ in the presence of competing ions.

The selectivity for caesium against other group I cations, as would be encountered in environmental conditions – such as extraction from seawater - was also tested through a competing ion test. Extraction of caesium from nuclear waste or from contaminated environmental samples needs to be selective due to the potentially high concentrations of alkali metals (Li^+, Na^+, K^+), group II metals (Ca^{2+}, Mg^{2+}) and the transition metals such as Fe^{3+} and Cu^{2+}. If the calix[4]bis-crown MNPs are not selective then their extraction capabilities will decrease in the presence of competing ions. The competing ions used in this assay were Al^{3+} , Sb^{3+}, Ba^{2+}, Pb^{2+}, B^{3+}, Ca^{2+}, Cd^{2+}, Cr^{3+}, Co^{2+}, Fe^{3+}, K^+, Cu^{2+}, Li^+ , Mg^{2+}, Mo^{4+} , Na^+ , Ni^{2+}, P^{3+}, Si, Ti^{4+}, V^{3+} and Zn^{2+}. Three model extraction samples were prepared with varying concentrations of the competing ions (10 ppb, 250 ppb and 1000 ppb). The concentration of caesium was kept constant at 100 ppb across all three samples. The amount of calix[4]bis-crown functionalised MNPs used was determined by the capacity test and so a ratio of 0.5 mg mL^{-1} was used as the dose concentration of extractant. Figure 2.24 presents the percentage extraction of caesium from the multi-element samples. Concentrations of multi-element mix below that of Cs^+ show

high extraction of Cs (>98%). A percentage extraction of >99% was achieved with competing ions at the same concentration as caesium. The sample containing higher concentrations of competing ions (1000ppb) still showed high selectivity towards Cs^+ with a level of extraction of 85%. To improve the level of extraction of Cs^+, the extraction process could be left longer to ensure achievement of equilibrium or a second dose of fresh calix[4]bis-crown MNPs could be utilised to remove the remaining 15% of caesium. The latter possibility was tested with the same dose concentration (1 mg/mL) of calix[4]bis-crown MNPs when complete extraction of the remaining caesium was achieved.

2.3 Calix[4]bis-crown functionalised SiO_2 gel for extraction of Cs(I)

2.3.1 Synthesis of Calix[4]bis-crown functionalised SiO_2 gel ***83***

Another possible solid-state supported extraction system is functionalised SiO_2 gel that can be used in column separation, allowing for long contact time with the absorbent moiety. As with MNPs, the use of functionalised SiO_2 gel reduces the amount of secondary waste and has the possibility for subsequent stripping of the loaded support to reduce the volume of waste further while recycling the absorbent material. Calix[4]arene-bis-[(4-carboxyl-1,2-phenylene)-crown-6] was synthesised as previously described in Section 2.1 and then immobilised onto commercially available macroscopic chloropropyl-functionalised silica gel by stirring calix[4]arene-bis-[(4-carboxyl-1,2-phenylene)-crown-6] and sodium hydride in DMF. Chloropropyl-functionalized silica gel was purchased from Sigma Aldrich (particle size 230-400 mesh and a pore size of 60 Å) and used as supplied. The extent of chloropropyl labelling of the purchased substrate was ~ 2.5 % loading and the matrix active group was ~ 8 % functionalised.

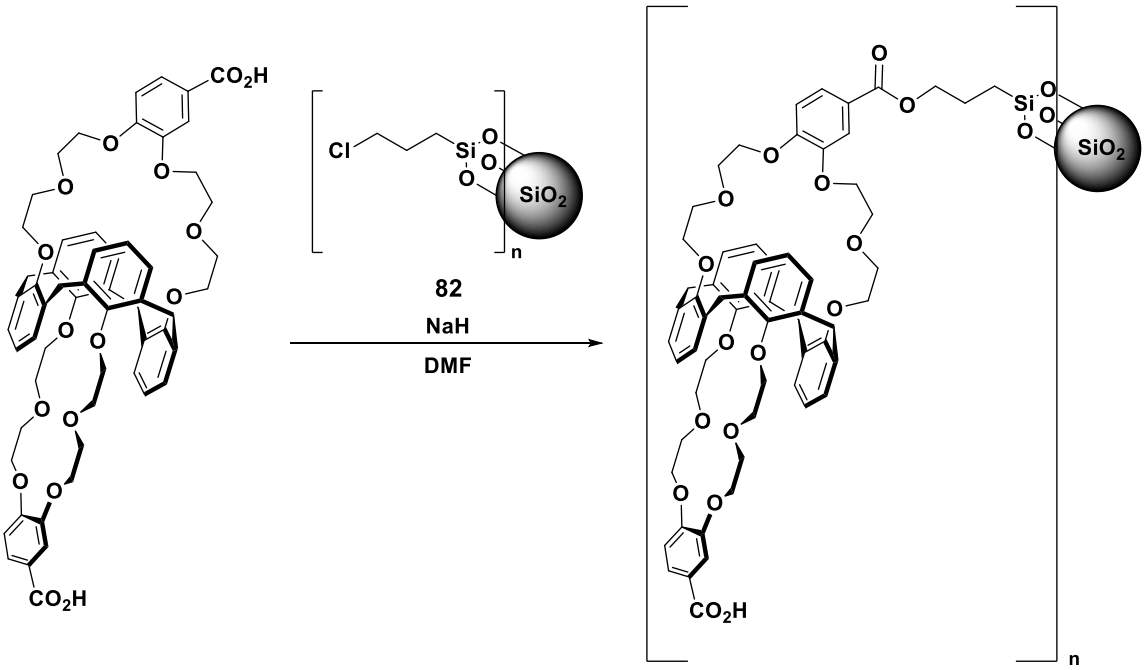

Scheme 2.10 Immobilisation of calix[4]bis-crown onto chloropropyl-functionalised SiO_2 gel

2.3.2 Characterisation of Calix[4]bis-crown functionalised silica gel

The degree of functionalisation of calix[4]bis-crown onto the surface of the silicagel was monitored using several analytical techniques. FT-IR was utilised to compare the commercial chloro-functionalised SiO_2 gel with the calix[4]bis-crown-functionalised silicagel. Both show the strong Si-O-Si stretch at 1059 cm^{-1} but only the calix[4]bis-crown functionalised SiO_2 gel shows a C=O stretch at 1717 cm^{-1}.

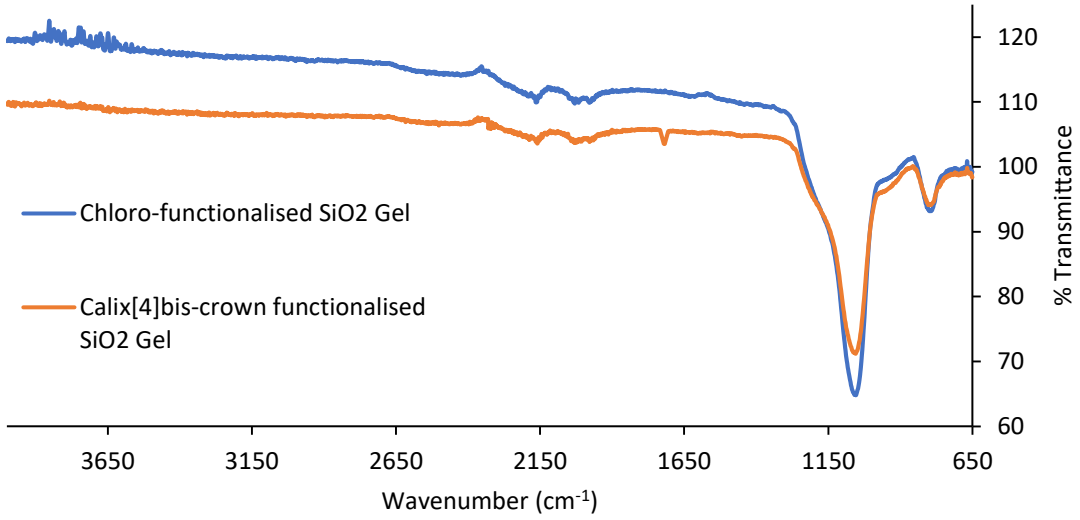

Figure 2.25 FT-IR comparison of chloro-functionalised silica gel **82** and calix[4]bis-crown functionalised silica gel **83**.

Energy dispersive X-ray (EDX) spectroscopy of both chloro-functionalised silica gel and calix[4]bis-crown functionalised silica gel show an increase of O content as a result of incorporation of the oxygen rich calix[4]bis-crown and a decrease in Si and Cl (Table 2.2). Roughly half of the chlorine has been lost, correlating to circa 51% immobilisation of calix[4]bis-crown onto the available sites. The margin for error for EDX is ±0.1% for uniform flat surfaces; however, here the error could be greater as the silica gel isn't uniformly flat. This reduces the reliability of EDX spectroscopy. TGA analysis of the chloro-functionalised SiO_2 gel shows a mass loss around 125 °C, proposed to correspond to the loss of absorbed water, followed by a near-linear loss between 250-700 °C relating to decomposition of organic matter. TGA analysis of calix[4]bis-crown silica gel (Appendix A2) shows a similar trend as the chloro-functionalised SiO_2 (Appendix A1), with the greater near linear loss occurring at 300-700 °C relating to *circa* 10% w/w.

	Chloro-functionalised SiO_2 Gel	*Calix[4]bis-crown functionalised SiO_2 Gel*
C (%)	21.34	19.70
O (%)	46.58	56.00
Si (%)	31.53	24.02
Cl (%)	0.55	0.28

Table 2.2 Elemental analysis of chloro-functionalised silica gel **82** and calix[4]bis-crown-functionalised silica gel **83**.

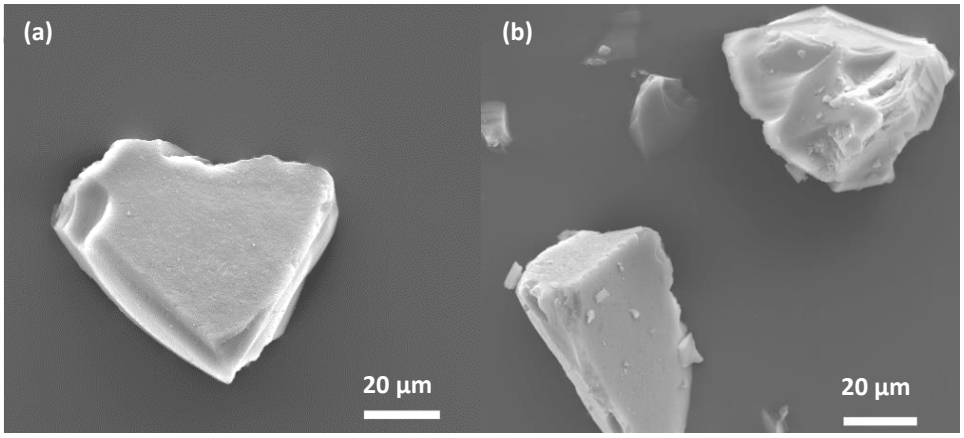

Figure 2.26 SEM images of (a) chloro-functionalised silica gel **82** and (b) calix[4]bis-crown-functionalised silica gel **83**.

The surface morphology of the chloro-functionalised silica gel and calix[4]bis-crown functionalised silica gel, shown in Figure 2.26, was examined by SEM. Comparison of the SEM images highlights the increased surface roughness thought to be a result of the possible incorporation of calix[4]bis-crown onto the surface of the silica gel.

2.3.3 Extraction studies of Calix[4]bis-crown functionalised silica gel 83

As previously reported in Section 2.2.3 the calix[4]bis-crown functionalised silica gel was compared with the commercial chloro-functionalised silica gel to ensure that it was indeed the ligand that was responsible for the caesium extraction. A column extraction technique was simulated using both calix[4]bis-crown functionalised silica gel and chloro-functionalised silica gel. The extraction efficiencies of chloro-functionalised silica gel and calix[4]bis-crown functionalised silica gel were found to be 18% and 99% respectively (Table 2.3). This proves that the majority of the extraction capacity of calix[4]bis-crown-functionalised silica gel is due to the calix[4]bis-crown ligand and that calix[4]bis-crown-functionalised silica gel is a viable option in removing caesium.

Extraction %	
Chloro-functionalised SiO_2 gel	Calix[4]bis-crown functionalised SiO_2 gel
18	99

Table 2.3 Extraction of Cs^+ from aqueous solution at pH 7 by column extraction loaded with chloro-functionalised silica gel and calix[4]bis-crown-functionalised silica gel.

The capacity of the calix[4]bis-crown functionalised silica gel was investigated. A column was loaded with 500 mg of calix[4]bis-crown-functionalised silica gel and 5 mL samples of Cs^+ (100 ppb) at pH 7 were passed through at a rate of 5 mL min^{-1}. After five runs, all saw >90% extraction of Cs^+, however the extraction efficiency dramatically dropped to <20% on the 6^{th} run. From the previous capacity test, comparison to chloro-functionalised SiO_2 gel showed that standard silica was able to extract near 20% of Cs^+ which is what is being observed after the fifth run. Therefore the capacity of calix[4]bis-crown functionalised SiO_2 gel for caesium was approximately 5 µg g^{-1}.

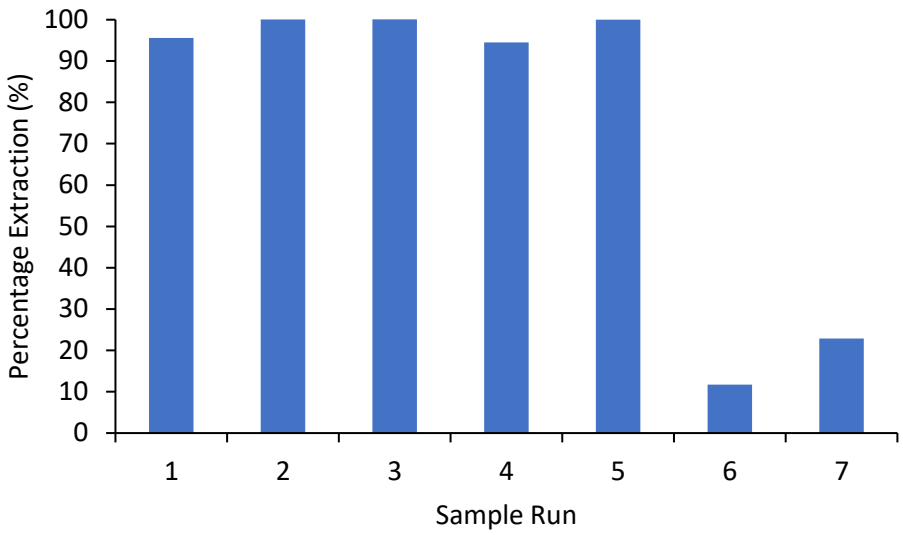

Figure 2.27 Capacity test for calix[4]bis-crown functionalised SiO_2 gel.

With a flow rate of 5 mL min^{-1}, the maximum capacity of the calix[4]bis-crown-functionalised silica gel was achieved after 5 minutes. This is a vast improvement compared to the calix[4]bis-crown functionalised MNPs, where high extraction was only attained after 1 hour. This could be because the 5 mL samples were being actively forced through a higher concentration of functionalised solid-state support compared to the dispersion of MNPs in a sample. A possible improvement for calix[4]bis-crown-functionalised silica gel **83** is to improve immobilisation of the ligand onto the silica gel. Utilising a Finkelstein reaction with the addition of potassium iodide could greatly increase both the rate and yield of immobilisation by replacing the chlorine of chloro-functionalised silica gel **82** with iodine which is a far superior leaving group.

Chapter 3 – Synthesis and Extraction Studies of a Strontium Selective Ligand

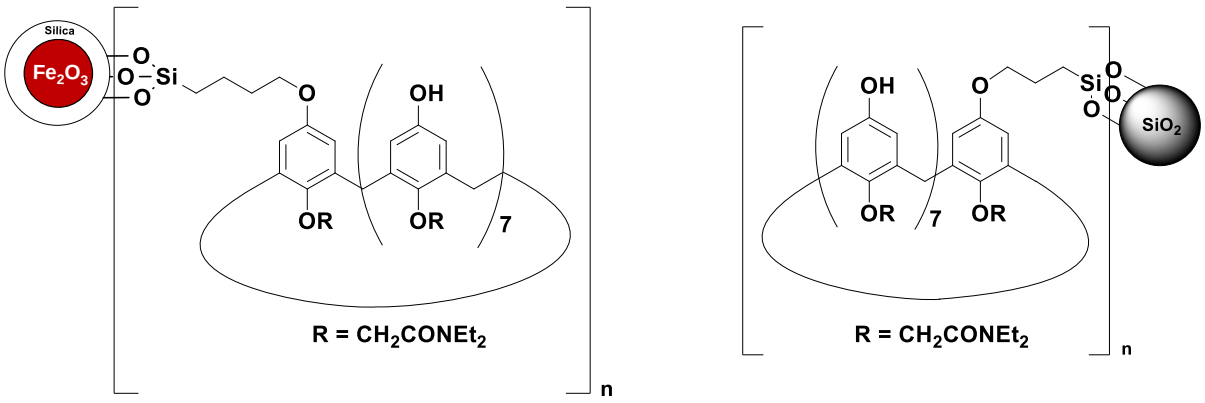

3.1 Synthesis of 5,11,17,23,29,35,41,47-octahydroxy-49,50,51,52,53,54,55,56-octakis[(*N*,*N*-diethylaminocarbonyl)methoxy]calix[8]arene

3.1.1 Synthesis of 5,11,17,23,29,35,41,47-octakis(benzyloxy)-49,50,51,52, 53,54,55,56-octahydroxycalix[8]arene ***85***

The target molecule chosen as a potential strontium-selective ligand was a functionalised calix[8]arene. Calix[8]arenes have been shown to extract strontium selectively over sodium when possessing amide functionalisation on the lower rim.[93] Therefore these octa-amides were chosen for investigation of their extraction abilities when immobilised onto solid supports.

The first step of the synthesis was to produce the octamer as shown in Scheme 3.1.

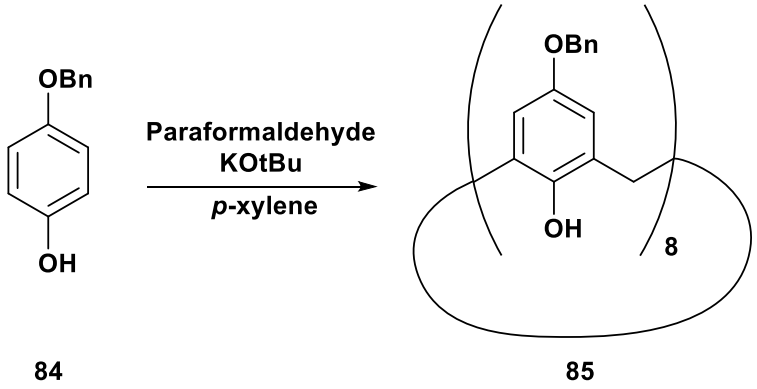

Scheme 3.1 Synthesis of 5,11,17,23,29,35,41,47-octakis(benzyloxy)-49,50,51,52, 53,54,55,56-octahydroxycalix[8]arene **85**

A base-induced reaction was utilised for the synthesis of calix[8]arenes as the reaction can proceed in one pot. The precursor 4-benzyloxyphenol **84** was heated to reflux in *p*-xylene with potassium *tert*-butoxide as the base. This reaction produces a mixture of cyclic oligomers from the hexamer to the octamer. In this process, the potassium *tert*-butoxide initiates the formation of the phenoxide ion, which acting as a carbon nucleophile under the apolar conditions, attacks the formaldehyde.

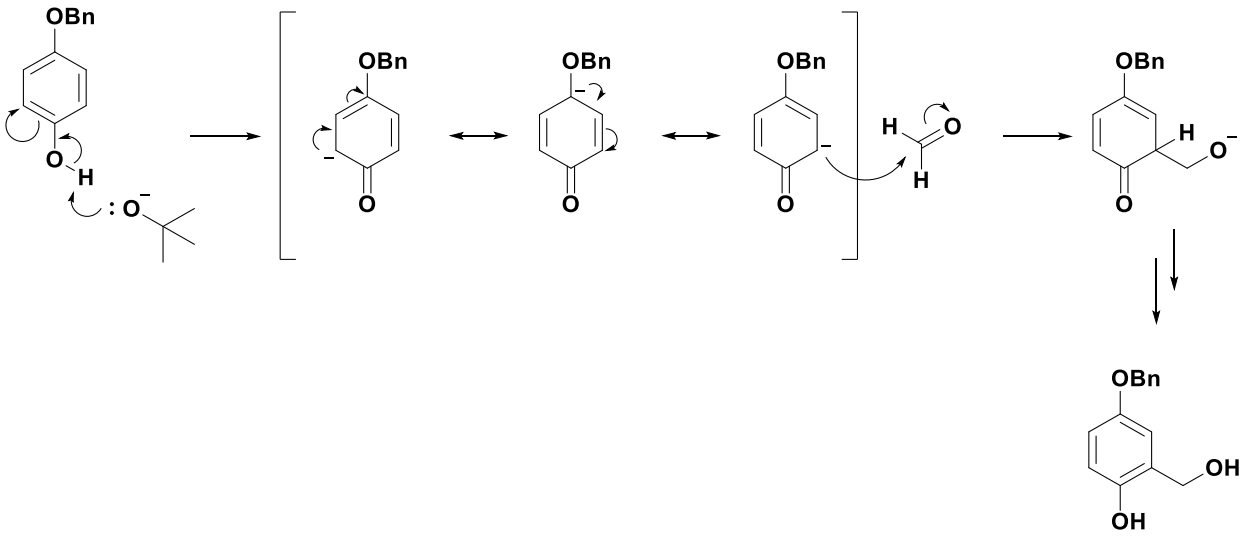

Figure 3.1 Mechanism for formation of 4-(benzyloxy)-2-(hydroxymethyl)phenol

Mild conditions allow the 4-(benzyloxy)-2-(hydroxymethyl)phenol to be isolated. However, heating to reflux in *p*-xylene pushes the reaction further via elimination to form as series of *o*-quinonemethide intermediates. A phenoxide ion reacts with the *o*-quinonemethide intermediate to form the methylene bridge. These steps are repeated to form linear oligomers that, at the hexamer level, can also undergo an intramolecular cyclisation.

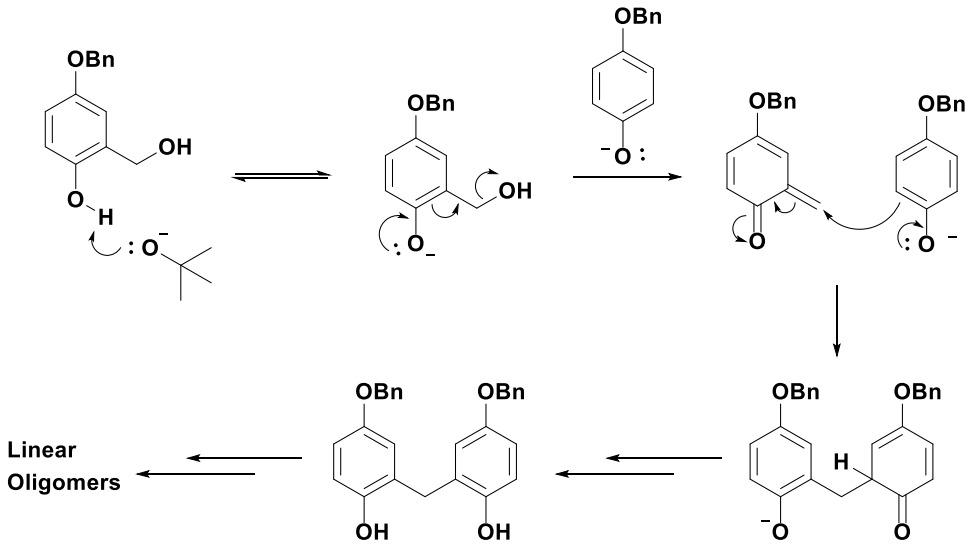

Figure 3.2 Mechanism for the formation of linear oligomers.

Linear octamers have not been detected during the synthesis of calix[8]arenes, with tetramers being the dominant linear oligomer identified. Therefore calix[8]arenes would appear to be formed via a pathway in which a pair of linear tetramers form an intermolecularly hydrogen-bonded dimer termed a hemicalix[8]arene. Reaction of the termini links the tetramers to form the cyclic octamer. During the synthesis of calix[8]arenes, small proportions of calix[6]arenes and calix[7]arenes are produced but the desired calix[8]arene could be purified by heating the crude mixture to reflux in chloroform for 3 hours and hot filtering the homogeneous mixture. Calix[6]arene and calix[7]arene dissolve in hot chloroform, leaving insoluble calix[8]arene as the residue on the filter.

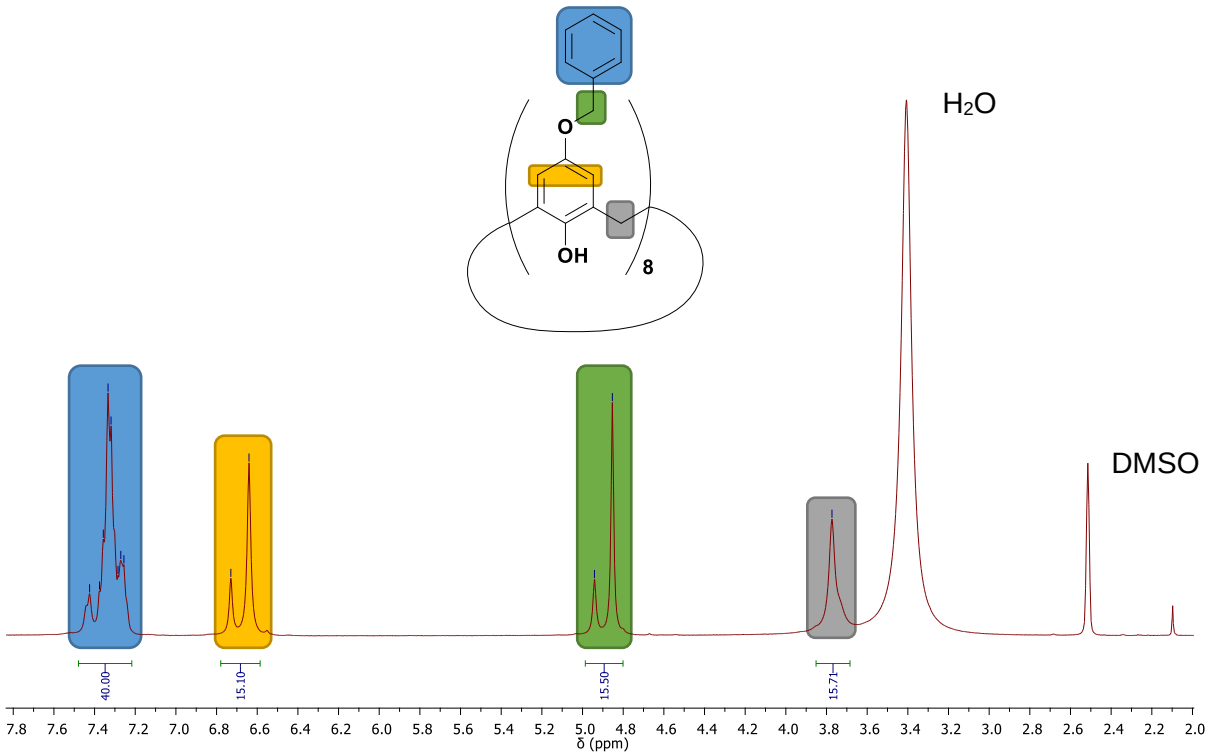

Figure 3.3 ^{1}H NMR spectrum of 5,11,17,23,29,35,41,47-octakis(benzyloxy)-49,50,51,52,53,54,55,56-octahydroxycalix[8]arene **85** in d_6-DMSO.

The ^{1}H NMR spectrum shown in Figure 3.3 indicates the successful formation of the octamer by the appearance of the methylene bridge resonance at δ 3.77. Mass spectroscopy confirmed the cyclic octamer was formed displaying a $[M-H]^-$ peak at 1695.6626 corresponding to the cyclic octamer and not the linear octamer.

3.1.2 Synthesis of 5,11,17,23,29,35,41,47-octakis(benzyloxy)-49,50,51,52,53,54,55,56-octakis[(N,N-diethylaminocarbonyl)methoxy]calix[8]arene 86[133]

The amide functionality was then added onto the lower rim of the calix[8]arene to provide the *N*-donor moiety needed to complex with strontium cations. Reaction of the calix[8]arene **85** with 2-chloro-*N*,*N*-diethylacetamide **86** provided the desired amide functionality.

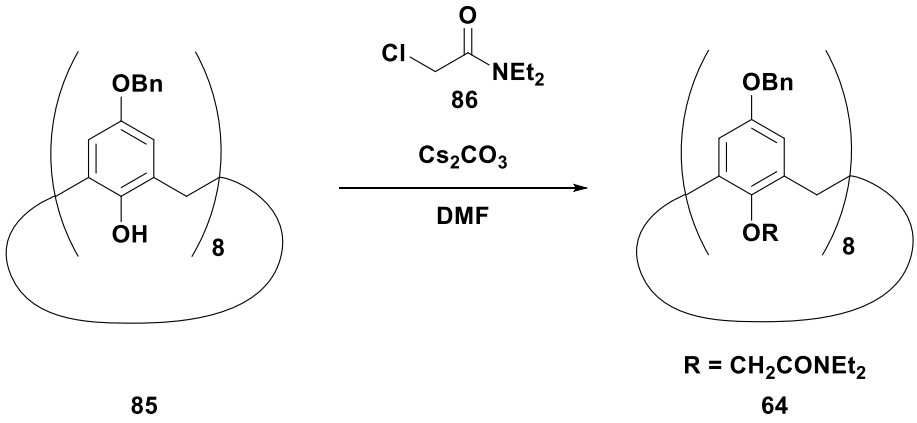

Scheme 3.2 Synthesis of 5,11,17,23,29,35,41,47-octakis(benzyloxy)-49,50,51, 52,53,54,55,56-octa-*N*,*N*-diethylacetamide calix[8]arene **64**.

The pure product was obtained by dissolving the crude product in hot methanol and precipitating with hexane.

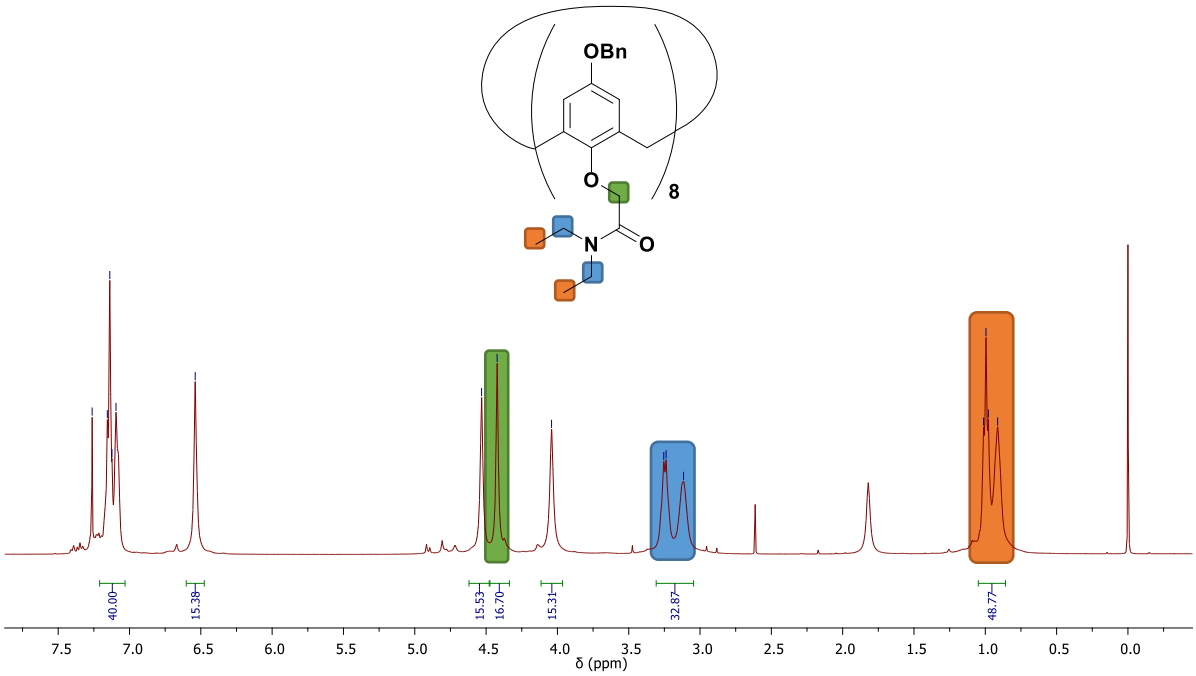

Figure 3.4 ^{1}H NMR spectrum of 5,11,17,23,29,35,41,47-octakis(benzyloxy)-49,50,51, 52,53,54,55,56-octa-*N*,*N*-diethylacetamide calix[8]arene **64**.

The presence of the diethylacetamide groups is evident from the ^{1}H NMR spectrum shown in Figure 3.4. The ethyl group protons appear as doubled multiplet resonances at δ 3.34 – 3.03 and 1.09 – 0.84 as a result of hindered rotation around the amide bond.

*3.1.3 Synthesis of 5,11,17,23,29,35,41,47-octahydroxy-49,50,51,-52,53,54,55,56-octakis[(N,N-diethylaminocarbonyl)-methoxy]calix[8]arene **87***[133]

Once the amide functionality had been appended the benzylated hydroxyl groups on the upper rim of the calixarene needed to be deprotected to allow for immobilisation onto solid-state supports.

The benzyl group was successfully cleaved via a palladium-catalysed hydrogenation. Cyclohexene was used as the hydrogen source with $Pd(OH)_2/C$ to produce the deprotected calix[8]amide **87**.

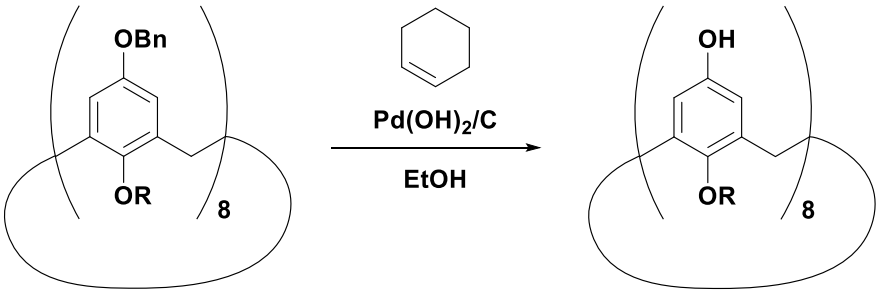

Scheme 3.3 Synthesis of calix[8]amide **87**.

The crude product was triturated with methanol to remove unwanted by-products, leaving pure calix[8]amide **87**.

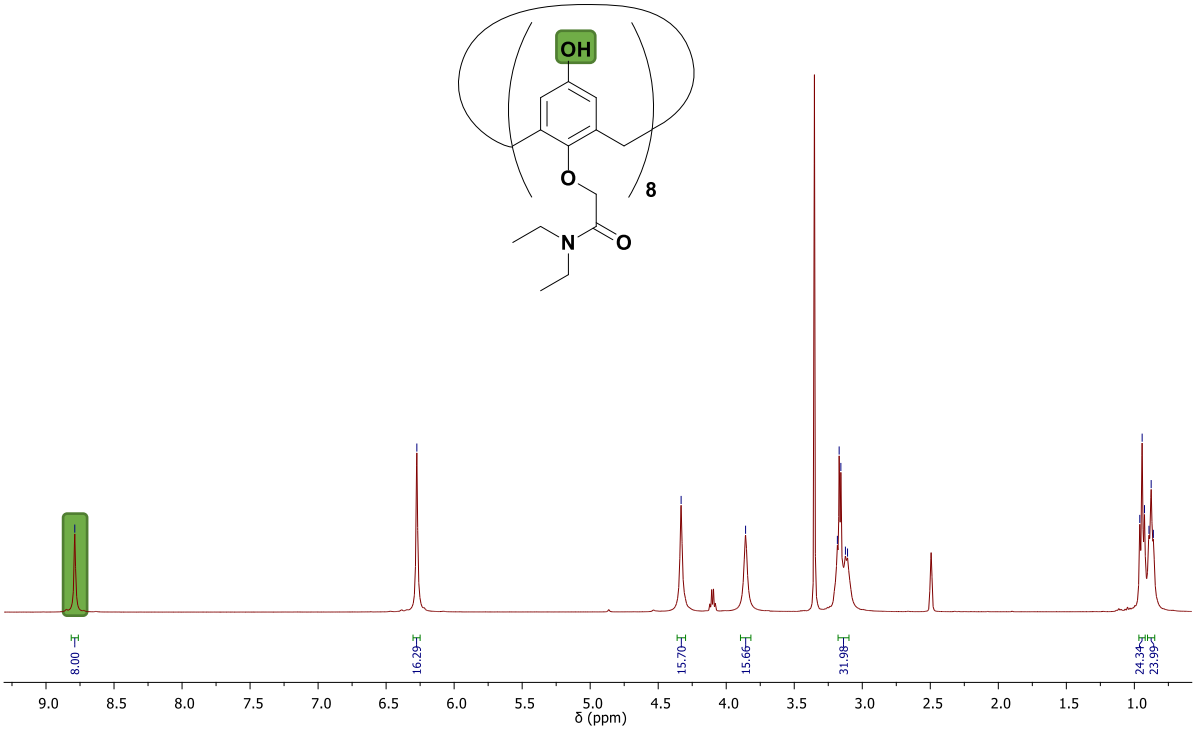

Figure 3.5 ^{1}H NMR spectrum of 5,11,17,23,29,35,41,47-octahydroxy-49,50,51,52,53,54,55,56-octakis[(*N*,*N*-diethylaminocarbonyl)methoxy]calix[8]arene **87**.

In the ^{1}H NMR spectrum, shown in Figure 3.5, the loss of the benzyl aromatic resonances at δ 7.47 – 7.22 and the appearance of a resonance attributable to the hydroxyl groups on the upper rim shown as a singlet resonance at δ 8.79 indicated that debenzylation had been successful. In addition, the CH_3 resonances of the two diethyl groups showed greater definition, appearing as two triplets rather than two multiplets.

3.2 Preparation of calix[8]amide silica-coated MNPs for extraction of Sr^{2+}

3.2.1 Synthesis of calix[8]amide silica-coated MNPs 88

Calix[8]amide **87** was immobilised onto iodopropyl-functionalised SiO_2 coated MNPs **67**, synthesised as described in Section 2.2.1. Deprotonation of the hydroxyl groups of calix[8]amide **87** using sodium hydride allowed for nucleophilic substitution onto the iodo-

functionalised SiO_2-coated MNPs. Calix[8]amide functionalised silica-coated MNPs **88** were washed with degassed ethanol and dried at 120 °C.

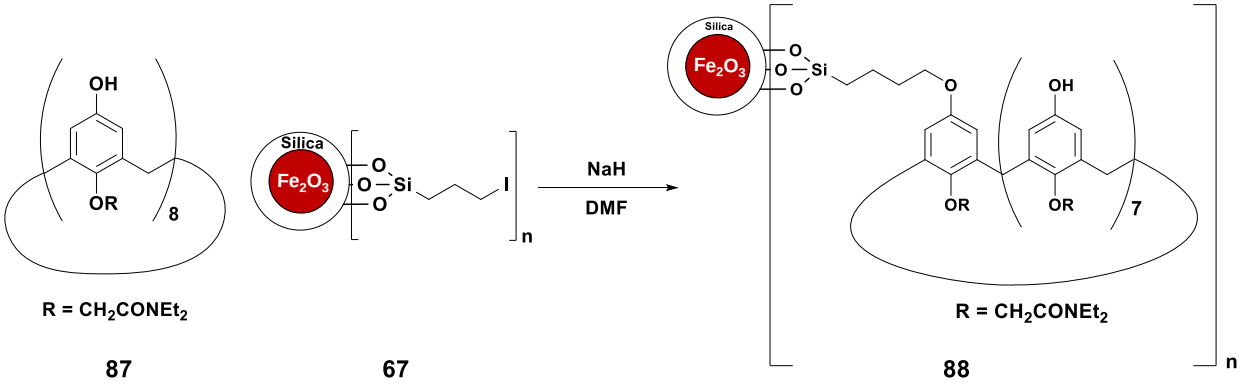

Scheme 3.4 Immobilisation of calix[8]amide **87** onto iodopropyl-functionalised SiO_2 coated MNPs **67**

*3.2.2 Characterisation of calix[8]amide silica-coated MNPs **88***

The success of the immobilisation of calix[8]amide **87** onto the iodo-functionalised SiO_2-coated MNPs **67** was evidenced by FT-IR analysis. Figure 3.7 shows that immobilisation of calix[8]amide **87** onto iodopropyl-functionalised SiO_2 coated MNPs **67** results in suppression of the C-I stretching absorption at 689 cm^{-1} and the appearance of an absorption at 1671 cm^{-1} owing to the carbonyls of the lower rim amide groups.

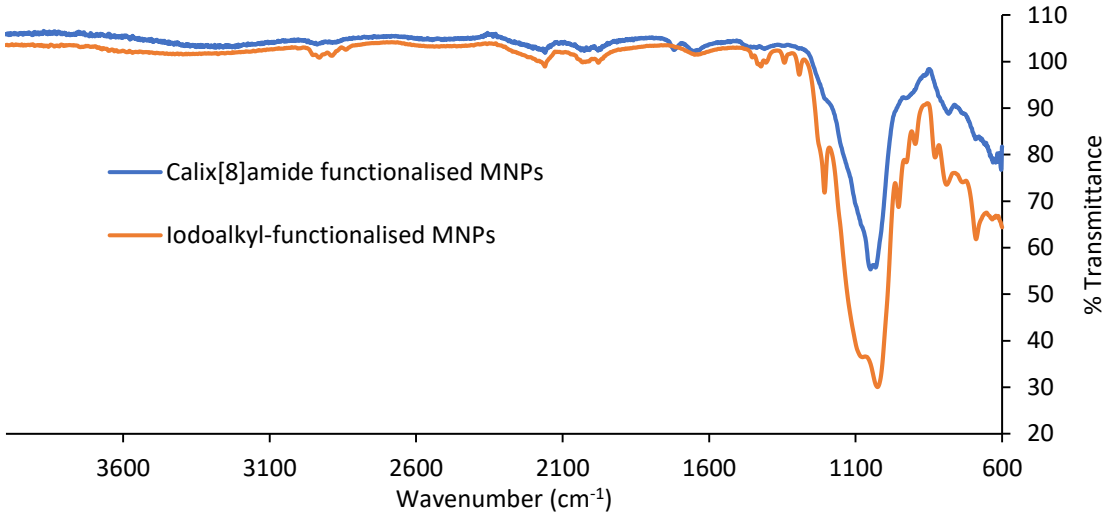

Figure 3.6 FT-IR of Calix[8]amide functionalised SiO_2 coated MNPs **88** and iodopropyl-functionalised SiO_2 coated MNPs **67**.

SEM images of the iodopropyl-functionalised SiO_2-coated MNPs **67** and calix[8]amide functionalised MNP **88** (Figure 3.7) show little visual difference, but energy dispersive X-ray spectroscopy taken during the SEM imaging showed an increase in oxygen and carbon for the calix[8]amide-functionalised MNPs compared to the iodopropyl-functionalised MNPs (14.54% oxygen for iodopropyl-functionalised MNPs **67** and 28.33% oxygen for calix[8]amide functionalised MNPs **88**). The reduction in iodine also indicated significant immobilisation of calix[8]amide **87** as ~84% of the iodopropyl groups had been successfully displaced.

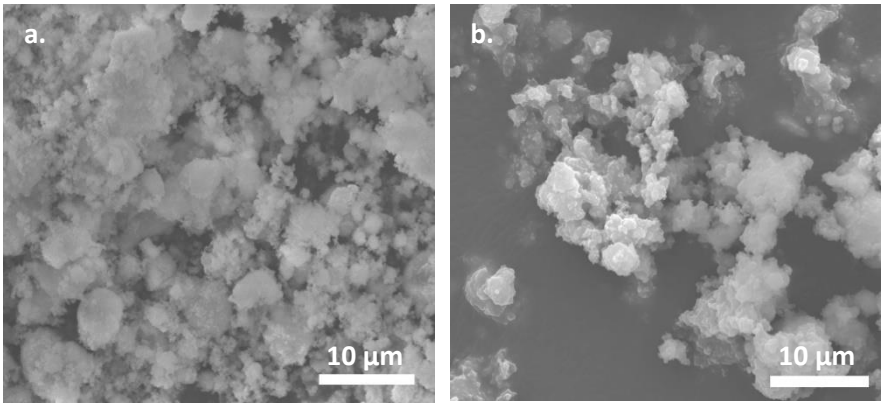

Figure 3.7 SEM images of (a) iodo-functionalised SiO_2-coated MNPs **67** and (b) calix[8]amide functionalised SiO_2-coated MNPs **88**

	Iodopropyl-functionalized SiO_2-coated MNP	*Calix[8]amide functionalized SiO_2-coated MNP*
C (%)	39.29	54.02
O (%)	14.54	28.33
I (%)	36.91	6.03

Table 3.1 Energy dispersive X-ray spectroscopic analysis of iodopropyl-functionalised SiO_2-coated MNPs **67** and calix[8]amide functionalised SiO_2-coated MNPs **88**

TEM images of iodopropyl-functionalised SiO_2-coated MNPs **67** and calix[8]amide functionalised SiO_2-coated MNPs **88** are shown in Figure 3.8. Both TEM images show the γ-Fe_2O_3 core surrounded by an organic coating. However, the degree of organic coating around the Fe_2O_3 cores appears to have increased on the calix[8]amide functionalised SiO_2-coated MNPs **88**.

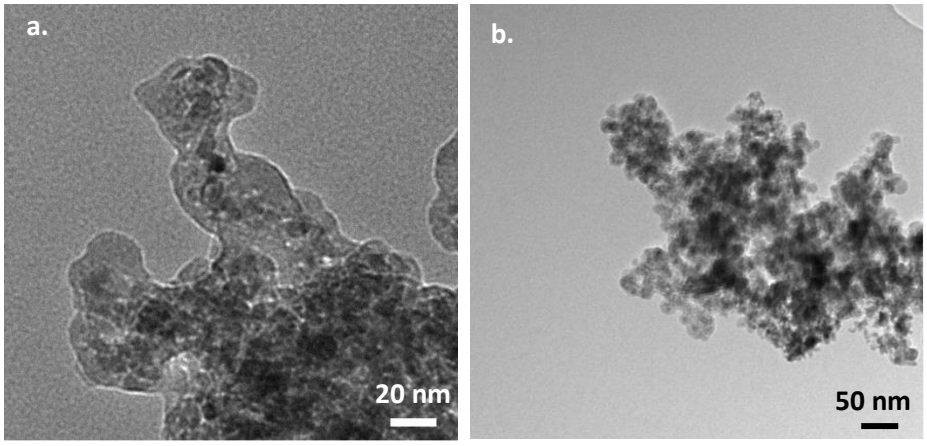

Figure 3.8 TEM images of (a) iodopropyl-functionalised SiO_2-coated MNPs **67** and (b) calix[8]amide functionalised SiO_2-coated MNPs **88**

The organic coating on the MNPs was further investigated using thermogravimetric analysis (TGA) under nitrogen. The loss in mass below 100 °C can be attributed to the loss of absorbed water and the significant loss in mass at 200-600 °C is most likely due to decomposition of the organic content. Comparison of the TGA analysis between **67** and **88** revealed the content of calix[8]amide **87** in the calix[8]amide functionalised SiO_2-coated MNPs **88** to be ~26% w/w.

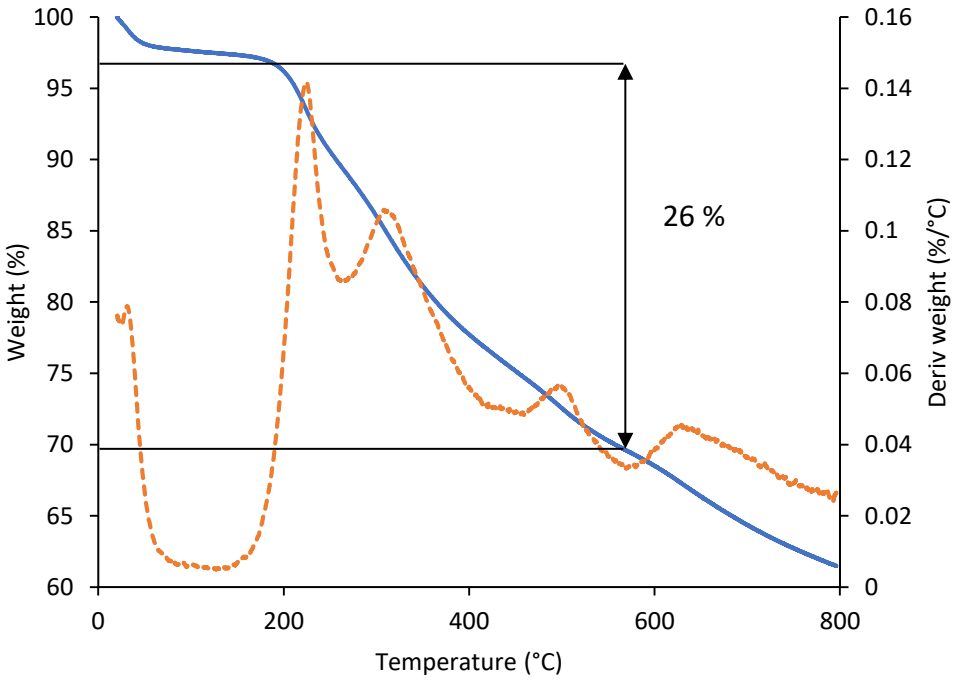

Figure 3.9 TGA curve of calix[8]amide functionalised SiO_2-coated MNPs **88**.

3.2.3 Extraction Studies

As with calix[4]bis-crown functionalised MNPs **81**, the calix[8]amide functionalised SiO_2-coated MNPs **88** were tested against the precursor iodopropyl-functionalised SiO_2-coated MNPs **67** to assess the extent to which the calix[8]amide is responsible for Sr^{2+} extraction and against the precursor MNPs. Equal weights (10 mg) of calix[8]amide functionalised SiO_2-coated MNPs **88** and iodopropyl-functionalised SiO_2-coated MNPs **67** were added to 10 mL

samples of aqueous strontium nitrate with a concentration of 10 ppb Sr^{2+}. Initial studies were carried out at pH 2 using nitric acid to acidify the samples.

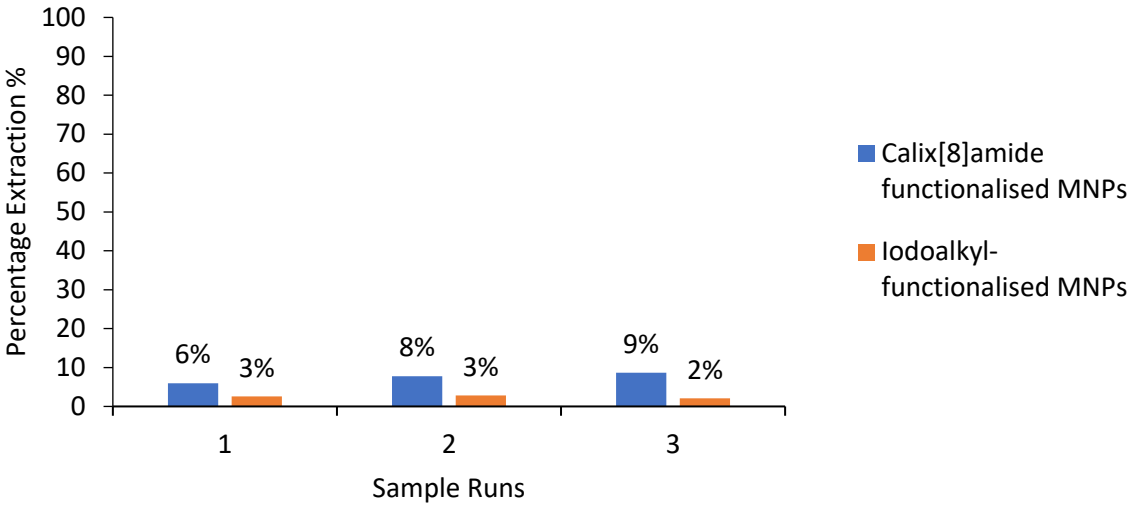

Figure 3.10 Extraction capabilities of iodopropyl-functionalised SiO_2-coated MNPs **67** and calix[8]amide functionalised SiO_2-coated MNPs **88**.

Figure 3.10 shows the poor extraction of Sr^{2+} with both calix[8]amide functionalised MNPs **88** and iodopropyl-functionalised MNPs **67**. Calix[8]amide functionalised MNPs **88** display a minimal improvement in extraction compared to iodopropyl-functionalised MNPs **67**. The pH was changed to neutral to test whether the system was pH sensitive. The samples were subjected to the same conditions as the pH 2 samples, which resulted in a decrease in percentage extraction. The calix[8]amide functionalised MNPs **88** showed an average of 3% extraction in neutral pH, the same as the precursor. The amide functionality of the calix[8]amide provides the *N*-donor moiety needed to complex with the strontium cations, but this is limited to the lower rim of the calix[8]arene. This leaves the upper rim open for water molecules to solvate the strontium cation, limiting the calix[8]amide's extraction ability.

3.3 Calix[8]amide functionalised SiO_2 gel for Extraction of Sr^{2+}

3.3.1 Synthesis of Calix[8]amide functionalised SiO_2 gel 89

Calix[8]amide **87** was immobilised onto SiO_2 gel to investigate whether the solid-state support is the reason for the poor extraction observed with the functionalised MNPs. Calix[8]amide **87** was synthesised as previously described in Section 3.1 and then immobilised onto commercially available macroscopic chloropropyl-functionalised SiO_2 gel **82**. Thus, calix[8]amide **87** was deprotonated with sodium hydride and then reacted with chloropropyl-functionalised SiO_2 gel **82**.

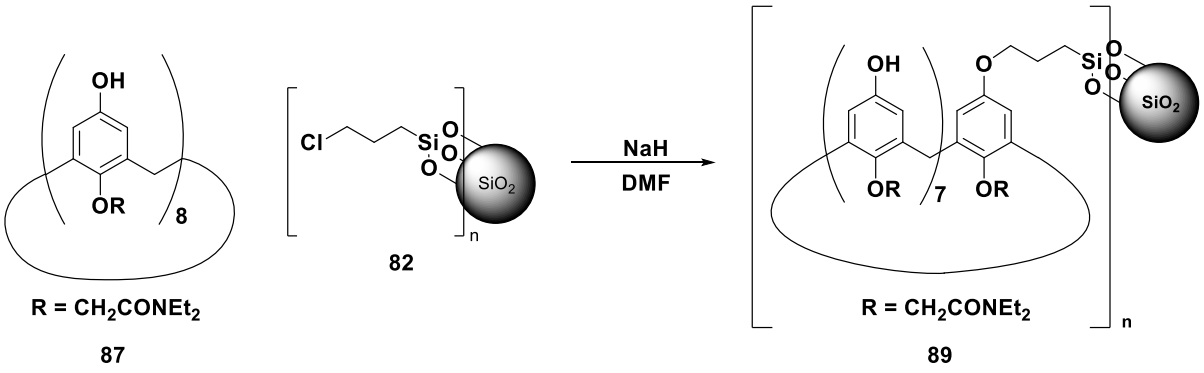

Scheme 3.5 Immobilisation of calix[8]amide onto chloro-functionalised SiO_2 gel **89**.

3.3.2 Characterisation of Calix[8]amide functionalised SiO_2 gel 89

The degree of functionalisation of calix[8]amide **87** onto the surface of the SiO_2 gel was monitored using several analytical techniques. FT-IR was utilised to compare chloro-functionalised SiO_2 gel **82** and calix[8]amide functionalised SiO_2 gel **89**. Both spectra showed a strong Si-O-Si stretch at 1053 cm^{-1} but only calix[8]amide functionalised SiO_2 gel **89** showed a C=O stretch of the amide functionality at 1612 cm^{-1}.

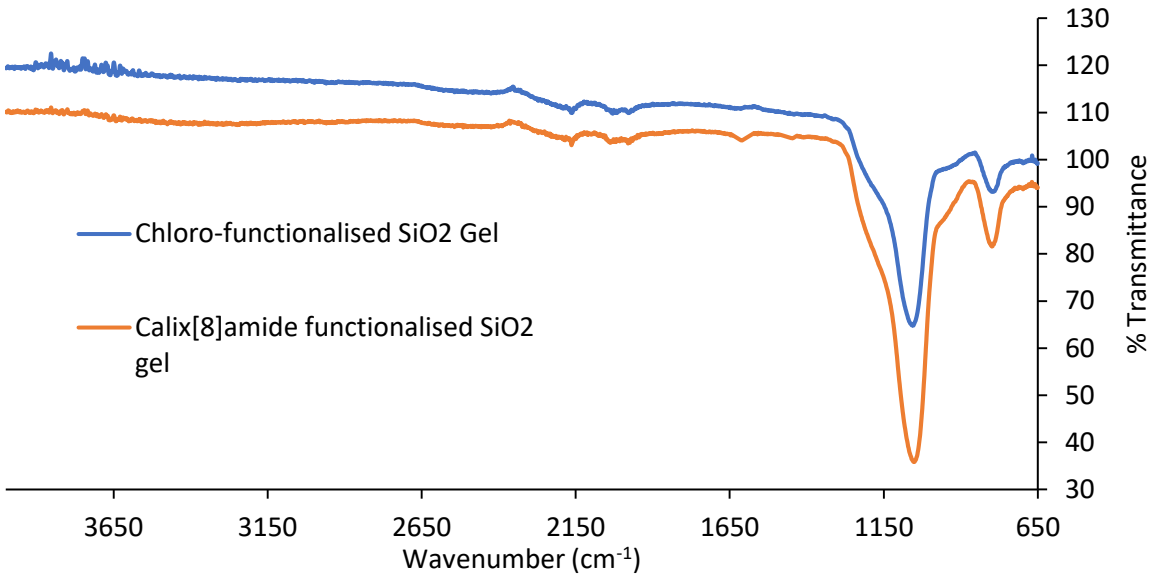

Figure 3.11 FT-IR of Chloro-functionalised SiO_2 gel **82** and calix[8]amide functionalised SiO_2 gel **89**

Energy dispersive X-ray spectroscopy was used to observe the percentage change of elements upon immobilisation. An increase of oxygen due to the calix[8]amide was observed as well as a decrease in Si and Cl (Table 3.2), which could indicate successful immobilisation of calix[8]amide into silica gel. However, as seen with calix[4]bis-crown-functionalised silica gel **83**, the percentage change in C doesn't correlate to ligand immobilisation and the margin of error for EDX (±0.1 for uniformly flat surfaces) may negate the decrease in Cl. If the ligand has been immobilised then this shows that EDX spectroscopy is not sensitive enough to quantify the percentage change of elements.

	Chloro-functionalised SiO_2 Gel ***82***	*Calix[8]amide functionalised SiO_2 Gel* ***89***
C (%)	21.34	21.86
O (%)	46.58	54.84
Si (%)	31.53	23.06
Cl (%)	0.55	0.24

Table 3.2 Energy dispersive X-ray spectroscopy of chloro-functionalised SiO_2 gel **82** and calix[8]amide functionalised SiO_2 gel **89**

TGA analysis of chloro-functionalised SiO_2 gel **82** showed an initial mass loss around 125 °C, probably relating to the loss of absorbed water, followed by a near linear loss between 250-700 °C most likely relating to decomposition of organic matter (Appendix A3). TGA analysis of calix[8]amide SiO_2 gel **89** showed a similar trend as the chloro-functionalised SiO_2 **82** (Appendix A1), with the near linear loss occurring at 350-600 °C relating to ~7% w/w loading. Surface morphology of chloro-functionalised SiO_2 gel **82** and calix[8]amide functionalised SiO_2 gel **89**, shown in Figure 3.12, was examined by SEM. Comparison of the SEM images highlights the increased surface roughness caused by the possible incorporation of calix[8]amide **87** onto the surface of the SiO_2.

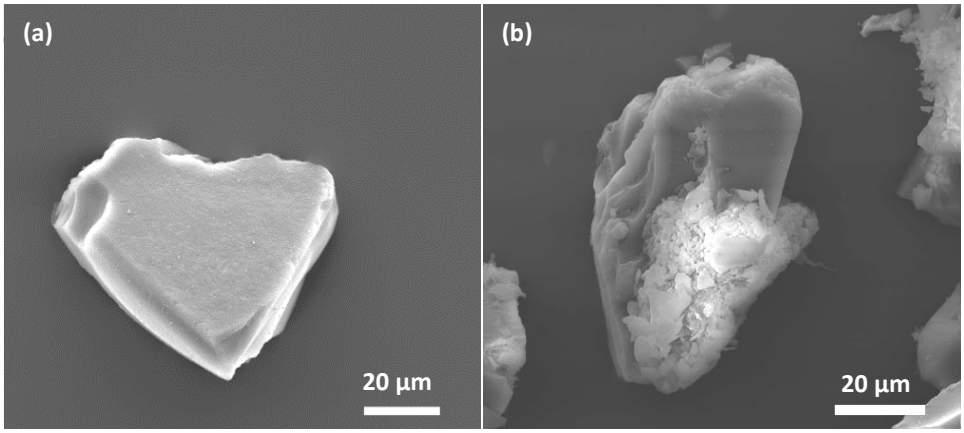

Figure 3.12 SEM images of a. chloro-functionalised SiO_2 gel **82** and b. calix[8]amide functionalised SiO_2 gel **89**

3.3.3 Extraction studies of Calix[8]amide functionalised SiO_2 gel 89.

The extraction capability of calix[8]amide functionalised SiO_2 gel **89** was investigated compared to chloro-functionalised SiO_2 gel **82**. A column extraction technique was trialled using both calix[8]amide functionalised SiO_2 gel **89** and chloro-functionalised SiO_2 gel **82** in separate columns. The columns were loaded with 500 mg of calix[8]amide functionalised SiO_2 gel **89** or chloro-functionalised SiO_2 gel **82** and these were eluted with 5 mL samples of Sr^{2+} (100 ppb) at pH 2 at a rate of 5 mL min^{-1}. However, as with the calix[8]amide functionalised SiO_2 MNPs **88** in Section 3.2, extraction of Sr^{2+} was poor with calix[8]amide functionalised SiO_2 gel **89**, while the chloro-functionalised SiO_2 gel **82** displayed no extraction. This highlights that the solid-state support is not the issue with extraction capabilities and that the ligand itself needs modification to improve extraction. Addition of functionality on the upper rim could help to stabilise complexation with alkali metals. Calix[8]amides with the benzyl protecting groups on the upper rim have been investigated in a liquid-liquid extraction of Sr^{2+} by Casnati *et al.* showing a high selectivity for Sr over Na.[93] The presence of the benzyl group could be crucial in providing additional electron density to stabilise complexation and prevent stripping from water molecules and other complexing anions. Another improvement, previously stated in Section 2.3.3, would be to improve immobilisation of calix[8]amide **87** to chloro-functionalised SiO_2 gel **82**. Utilising the Finkelstein reaction with the addition of potassium iodide or sodium iodide would produce iodo-functionalised SiO_2 gel which could improve the rate and yield of immobilisation as the iodo-functionalisation is a much better leaving group than the chloro-functionalisation.

Chapter 4 – Investigation of BTBP Functionalised MNPs for Extraction of Corrosion Products

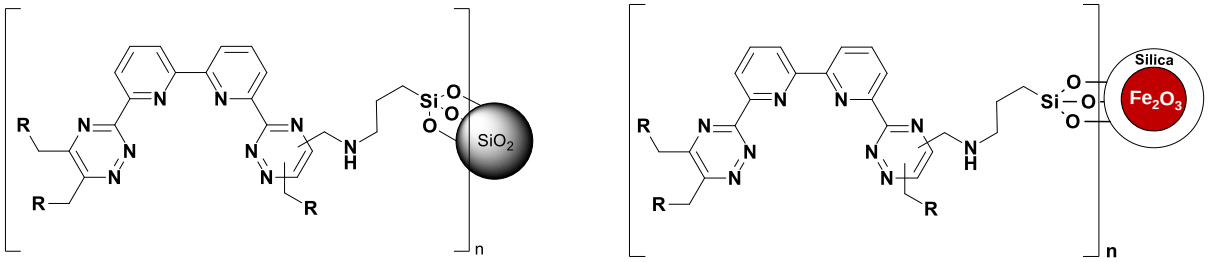

4.1 Introduction

The $CyMe_4$-BTBP ligand **25**, designed as a possible extractant of trivalent actinides in the presence of lanthanides and the current benchmark for the SANEX process in Europe was synthesised by the Harwood group from 2,2'-bypyridine **19**.[16,45] Separation of the minor actinides from lanthanides in spent nuclear fuel allows for a process called transmutation where the minor actinides are bombarded with neutrons, facilitating their conversion to shorter-lived isotopes.[15,16] The presence of lanthanides greatly inhibits transmutation because the lanthanides have high neutron capture cross sections that will absorb neutrons.[6] While BTBP cannot significantly differentiate the minor actinides from lanthanides, it is able to extract certain corrosion and fission products that complicate the separation process.[115] These corrosion and fission products could be removed utilising a two-column process involving BTBP immobilised SiO_2 gel to co-extract the problematic corrosion and fission products, while BTPhen immobilised SiO_2 gel could separate the minor actinides from lanthanides at 4M HNO_3.[115]

4.1.1 Synthesis of tetra-bromomethyl-BTBP functionalised SiO_2 gel

The synthesis of BTBP involves a 4-step route starting from 2,2'-bipyridine **19**, that is bis-*N*-oxidised using hydrogen peroxide and acetic acid resulting in bis-2,2'-bipyridine *N*-oxide. The dinitrile is synthesised using a Reissert-Henze cyanidation reaction with trimethylsilyl cyanide and benzoyl chloride. The dinitrile is then reacted with hydrazine in ethanol to form the bis-aminohydrazide.[134] A condensation reaction with bromomethyl diketone yields tetra-bromomethyl BTBP.

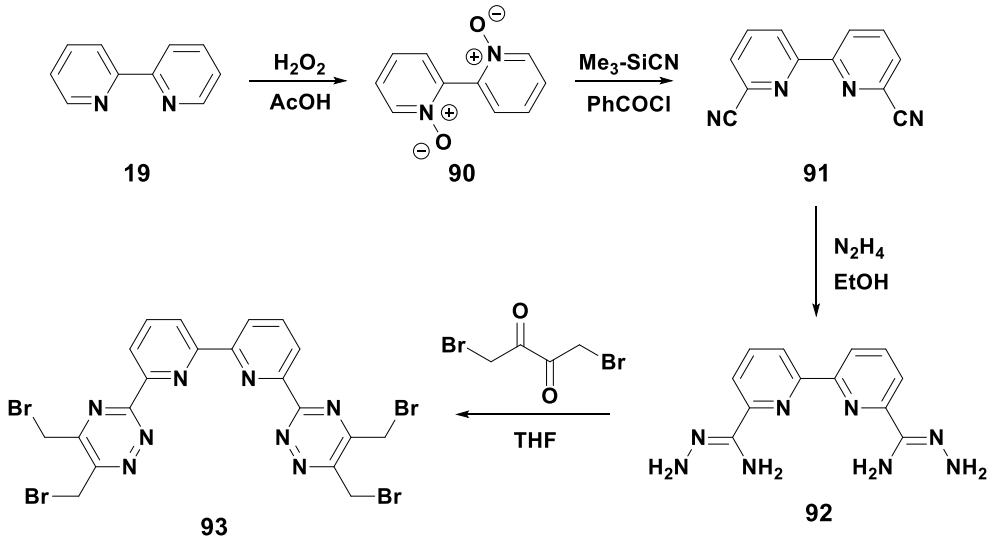

Scheme 4.1 Synthesis of tetra-bromomethyl BTBP **93**

Tetra-bromomethyl BTBP **93** is then directly immobilised onto aminopropyl-functionalized SiO_2 gel **94**.

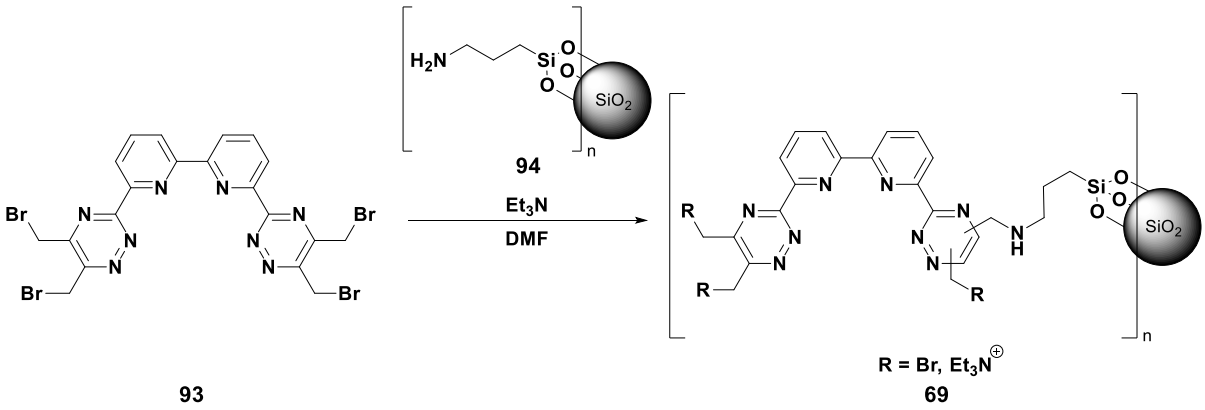

Scheme 4.2 Synthesis of tetra-bromomethyl-BTBP functionalised SiO_2 gel **69**

*4.1.2 Extraction studies of tetra-bromomethyl-BTBP functionalised SiO_2 gel **69***

Harwood and Afsar *et al.* studied the extraction ability of tetra-bromomethyl-BTBP immobilised SiO_2 gel **69** for transition metals in the presence of group I, II and III metals. BTBP functionalised SiO_2 gel **69** was loaded into a column and standard solutions at pH 0.5 containing a range of metals, each at 100 ppb concentration (100 mL) were passed through

the column.[115] Figure 4.1 shows the percentage extraction of different metals with this BTBP functionalised SiO_2 gel **69**.

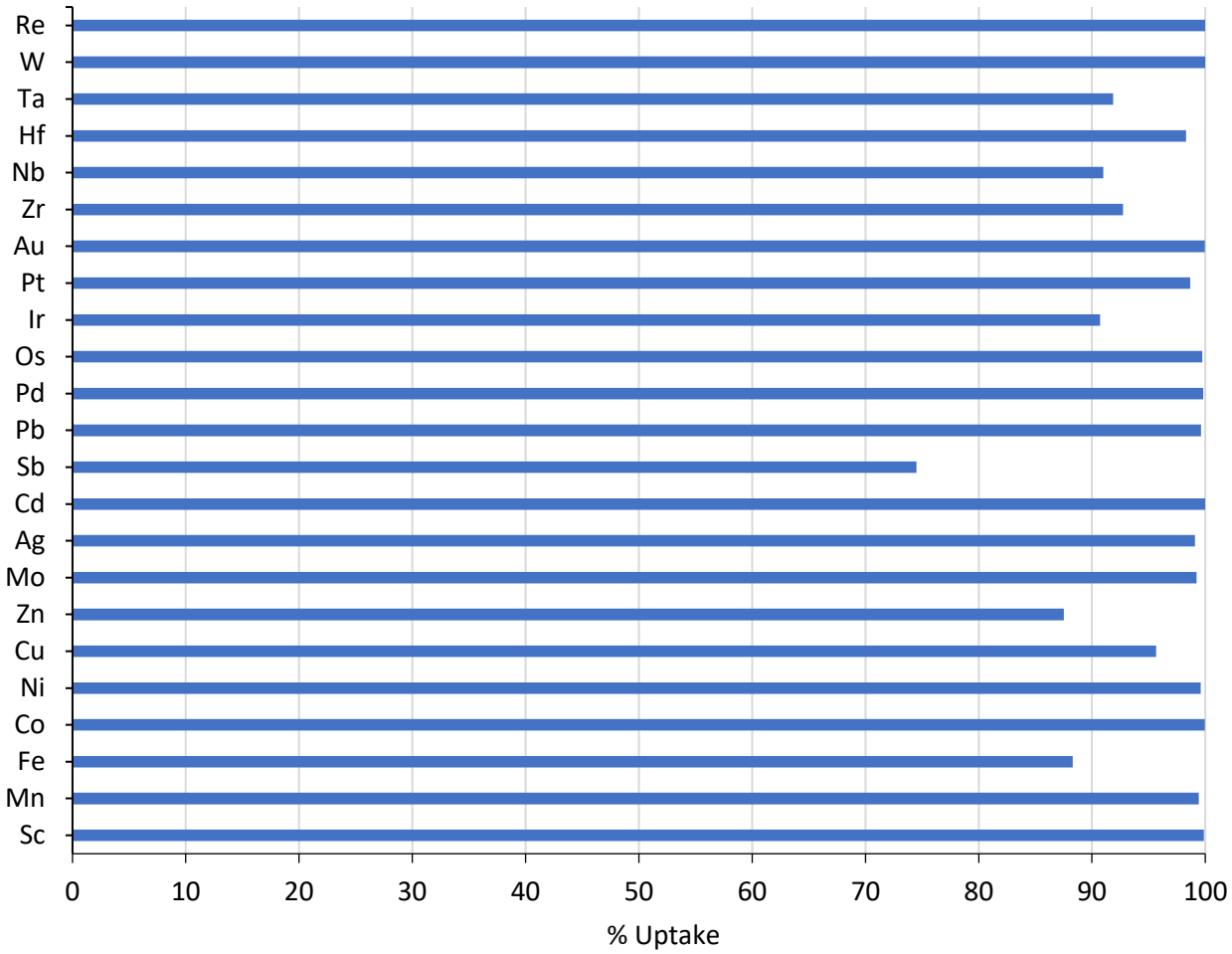

Figure 4.1 Percentage extraction of metal ions (100 ppb) from aqueous solution at pH 0.5 by BTBP functionalised SiO_2 gel **69**.[115]

The percentage extraction of various metal ions – Sc^{3+}, Mn^{2+}, Fe^{3+}, Co^{2+}, Ni^{2+}, Cu^{2+}, Zn^{2+}, Mo^{4+}, Ag^{+}, Cd^{2+}, Sb^{5+}, Pb^{2+}, Pd^{2+}, Os^{4+}, Ir^{3+}, Pt^{4+}, Au^{3+}, Zr^{4+}, Nb^{5+}, Hf^{4+}, Ta^{5+}, W^{6+} and Re^{4+} by tetra-bromomethyl-BTBP functionalized SiO_2 gel **69** showed >80% for all the metals except for Sb^{5+}.

4.2 Extraction studies of BTBP functionalised SiO_2 coated MNPs

4.2.1 Synthesis of BTBP functionalised SiO_2 coated MNPs ***96***

Extraction studies were carried out using previously immobilised tetra-bromomethyl BTBP onto SiO_2 coated MNPs. Tetra-bromomethyl BTBP was directly immobilised using triethylamine in DMF onto aminopropyl-SiO_2 coated MNPs.

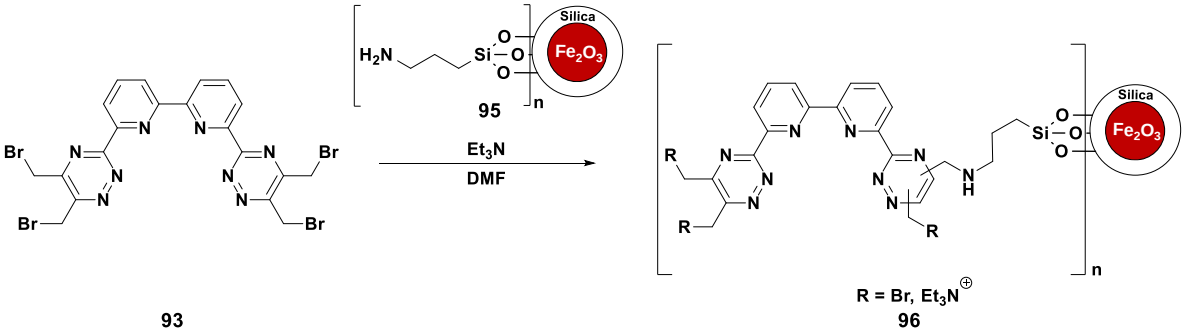

Scheme 4.3 Synthesis of BTBP functionalised SiO_2 coated MNPs **96**

Once immobilised the amine functionality can potentially undergo ring closure, displacing an adjacent bromide group.

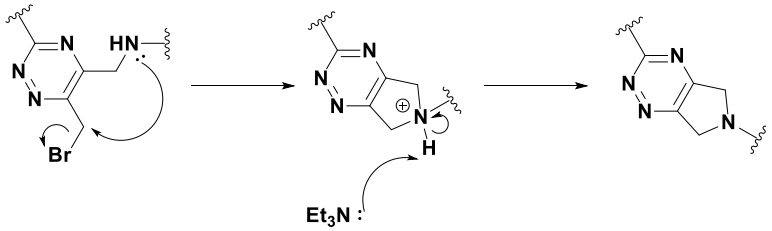

Figure 4.2 Possible ring closure of BTBP functionalised SiO_2 coated MNPs **96**.

4.2.2 Capacity Study of BTBP functionalised SiO_2 coated MNPs ***96***

The capacity of tetra-bromomethyl-BTBP functionalised SiO_2 coated MNPs **96** was investigated for comparison with BTBP functionalised SiO_2 gel **69**. Standard solutions at pH 0.5 containing various transition metals – Mn^{2+}, Fe^{3+}, Co^{2+}, Ni^{2+}, Cu^{2+}, Zn^{2+}, Ag^{+}, Cd^{2+}, V^{5+} and Cr^{3+}

each at 100 ppb concentration (100 mL) were used. The samples were mixed with BTBP functionalised SiO_2 coated MNPs **96** using a different dosage for each sample (10 mg, 100 mg, 200 mg, 500 mg). Figure 4.3 shows the percentage extraction of various transition metals by tetra-bromomethyl-BTBP functionalised SiO_2 coated MNPs **96**. Mn^{2+}, Fe^{3+} and Zn^{2+} were not extracted by these tetra-bromomethyl-BTBP functionalised SiO_2 coated MNPs **96** compared to >80% by the tetra-bromomethyl-BTBP functionalised SiO_2 gel **69**. The main difference is the extraction technique used, with tetra-bromomethyl-BTBP functionalised SiO_2 coated MNPs **96** utilising a batch extraction method and tetra-bromomethyl-BTBP functionalised SiO_2 gel **69** using a column extraction method. The column extraction technique actively forces metal ions through a higher concentration of functionalised solid-state support compared to the dispersion of MNPs in a sample However, the BTBP functionalised SiO_2 coated MNPs **96** have a high affinity for Cu^{2+}, Ag^{+} and Cd^{2+} even at the lowest dose (10 mg) almost recreating the extraction percentages achieved using BTBP functionalised SiO_2 gel.

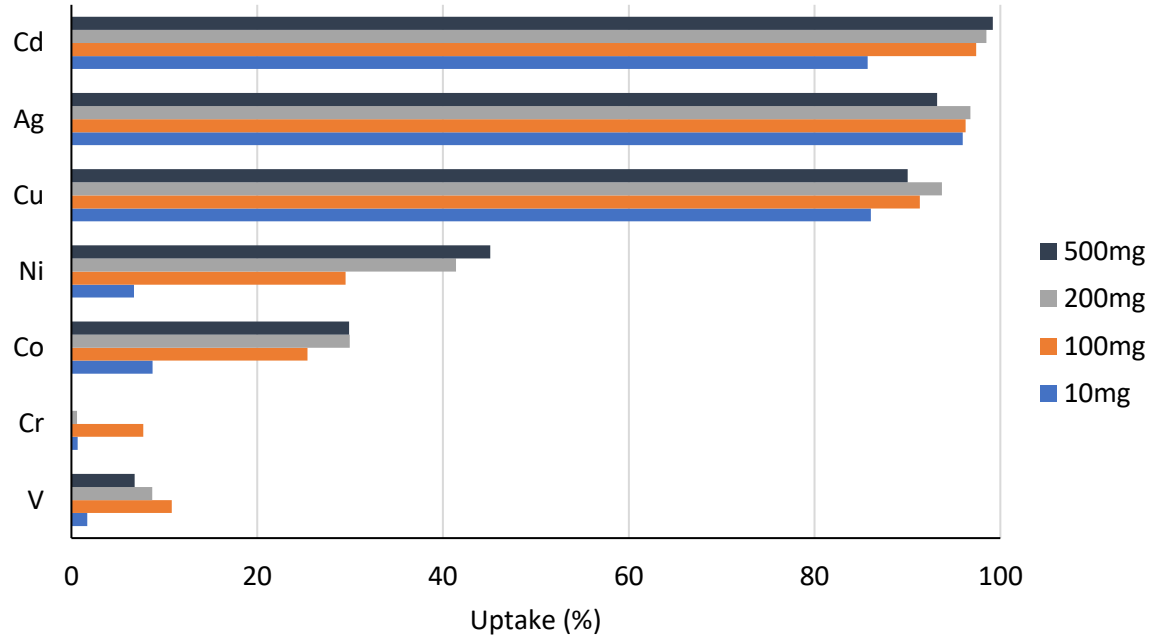

Figure 4.3 Percentage extraction of metal ions (100 ppb) from aqueous solution at pH 0.5 by BTBP functionalised SiO_2 coated MNPs **96**.

While the overall extraction percentages are lower than those of the BTBP functionalised SiO_2 gel **69**, specific selectivity was still observed, with the BTBP functionalised SiO_2 coated MNPs **96** extracting Cu^{2+}, Ag^{+} and Cd^{2+} >80% compared to the remaining transition metals showing <10% with the exception of Ni^{2+} and Co^{2+}.

*4.2.3 Kinetic Study of BTBP functionalised SiO_2 coated MNPs **96***

The kinetics of extraction were then tested to compare with the fast kinetics achieved with BTBP functionalised SiO_2 gel **69**, where samples were passed through the column at a rate of 10 mL min^{-1}.[115] The change in pH was also investigated, running kinetics tests at pH 0.5, 2 and 7. Standard solutions at containing various transition metals – Mn^{2+}, Co^{2+}, Ni^{2+}, Cu^{2+}, Zn^{2+}, Ag^{+}, Cd^{2+}, V^{5+} and Cr^{3+} each at 100 ppb concentration (100 mL) were made up at pH 0.5, 2 and 7 using nitric acid to achieve acidic conditions. The samples were mixed with BTBP functionalised SiO_2 coated MNPs **96** (10 mg) and mixed for 24 hours. Samples (5 mL) were taken at varying intervals (5 mins – 24 hours) to be analysed using ICP-MS.

Figure 4.4 shows the extraction kinetics of Cu^{2+}, Ag^{+} and Cd^{2+} all of which showed high extraction in the capacity study. The extraction kinetics show Ag^{+} achieving maximum extraction after 4 hours; whereas Cu^{2+} and Cd^{2+} extraction plateaued after 8 hours.

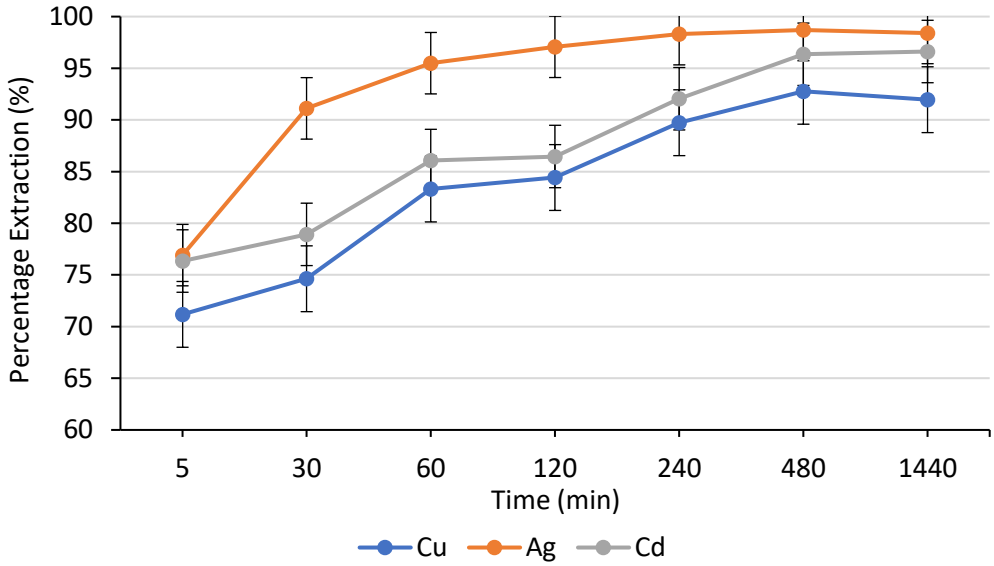

Figure 4.4 Extraction data at pH 0.5 for Cu^{2+}, Ag^{+} and Cd^{2+}

The extraction kinetics observed with BTBP functionalised SiO_2 coated MNPs **96** were noticeably slower than those achieved using BTBP functionalised SiO_2 gel **69**. Despite the large surface area of MNPs, the functionalised SiO_2 gel showed faster kinetics, while the less selectivity in the extraction could be because of the extraction technique used as the column method may be increasing contact time between the ligand and metal ions.

Comparing with the other transition metals shown in Figure 4.5, a much lower overall extraction was achieved ranging between 40-50%.

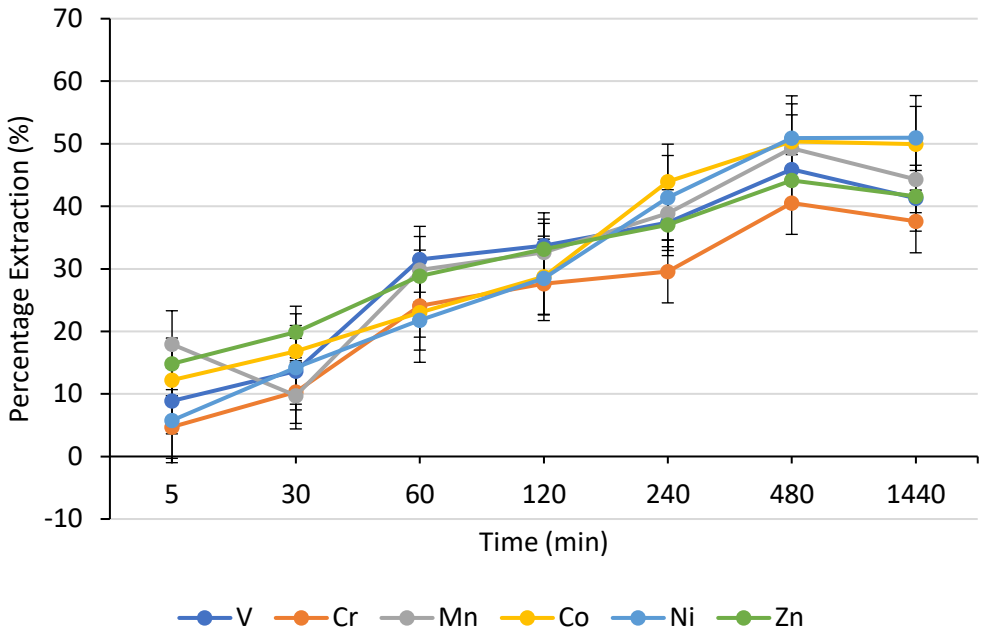

Figure 4.5 Kinetic extraction data at pH 0.5 for V^{5+}, Cr^{3+}, Mn^{2+}, Co^{2+}, Ni^{2+} and Zn^{2+}

The extraction of the remaining transition metals showed a near linear increase in extraction over time. However, V^{5+}, Cr^{3+}, Mn^{2+} and Zn^{2+} all showed a decrease in extraction between 480-1440 minutes.

With the samples at pH 2, similar results were found where Ag^{+} was extracted much faster than Cd^{2+} and Cu^{2+} as shown in Figure 4.6. However, compared to pH 0.5, Cd^{2+} and Cu^{2+} were extracted more slowly and resulted in a lower percentage extraction after 24 hours. This could be because the concentration of nitrate ion, which provides an effective counterion for the BTBP-metal ion complexes, is lower at pH 2 than pH 0.5.

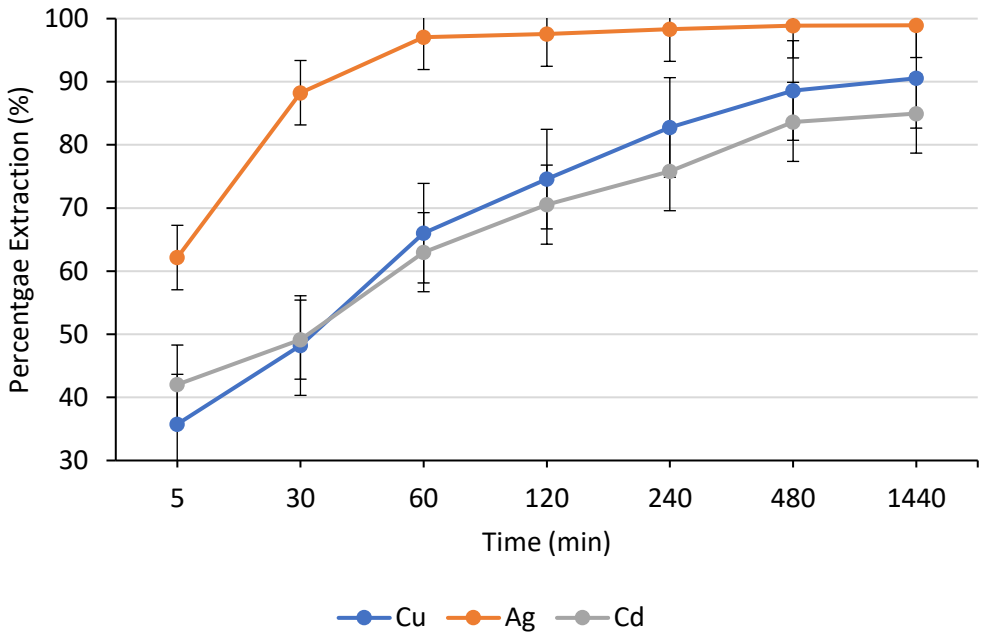

Figure 4.6 Kinetic extraction data at pH 2 for Cu^{2+}, Ag^{+} and Cd^{2+}

The remaining transition metal extraction data for pH 2 are shown in Figure 4.7. The extraction kinetics were slower and could well need longer than 24 hours to achieve maximum capacity. This further highlights the importance of the nitrate counterion, which is needed to stabilise the BTBP-metal ion complex.

At pH 7 Ag^{+} shows a slower rate of extraction but still achieves maximum extraction after 24 hours as shown in Figure 4.8. The decrease after 8 hours for Ag^{+}, Cd^{2+} and Cu^{2+} could be because of the precipitation of metal hydroxides.

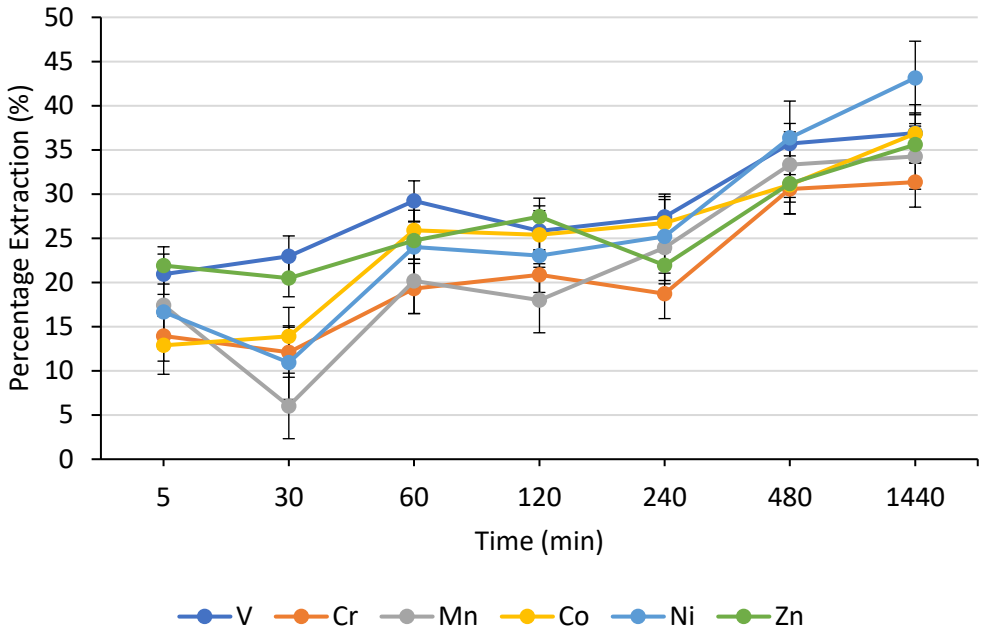

Figure 4.7 Kinetic extraction data at pH 2 for V^{5+}, Cr^{3+}, Mn^{2+}, Co^{2+}, Ni^{2+} and Zn^{2+}

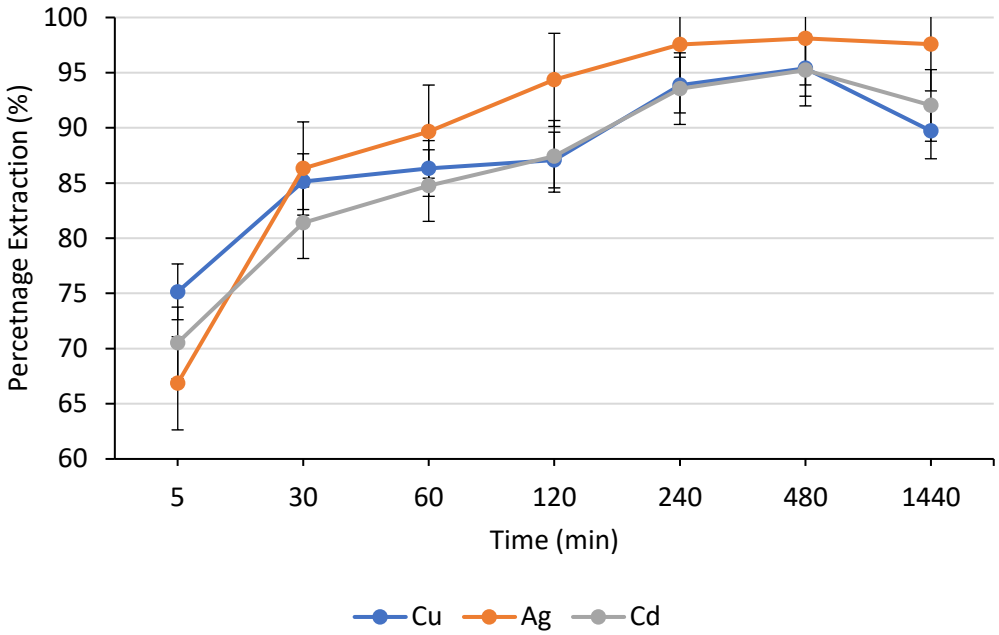

Figure 4.8 Kinetic extraction data at pH 7 for Cu^{2+}, Ag^{+} and Cd^{2+}

Figure 4.9 shows the remaining metal extraction data at pH 7. Initial extraction at 5 minutes was the lowest compared to extraction at pH 0.5 and 2, but after 24 hours, a similar percentage extraction was achieved compared to extraction of V^{5+}, Cr^{3+}, Mn^{2+} and Zn^{2+} after 24 hours at pH 2. Co^{2+} and Ni^{2+} showed an extraction percentage of 50% after 24 hours,

comparable to Co^{2+} and Ni^{2+} extraction after 24 hours at pH 0.5, while V^{5+} showed higher extraction before decreasing after 8 hours which could be due to precipitation of vanadium hydroxide complexes.

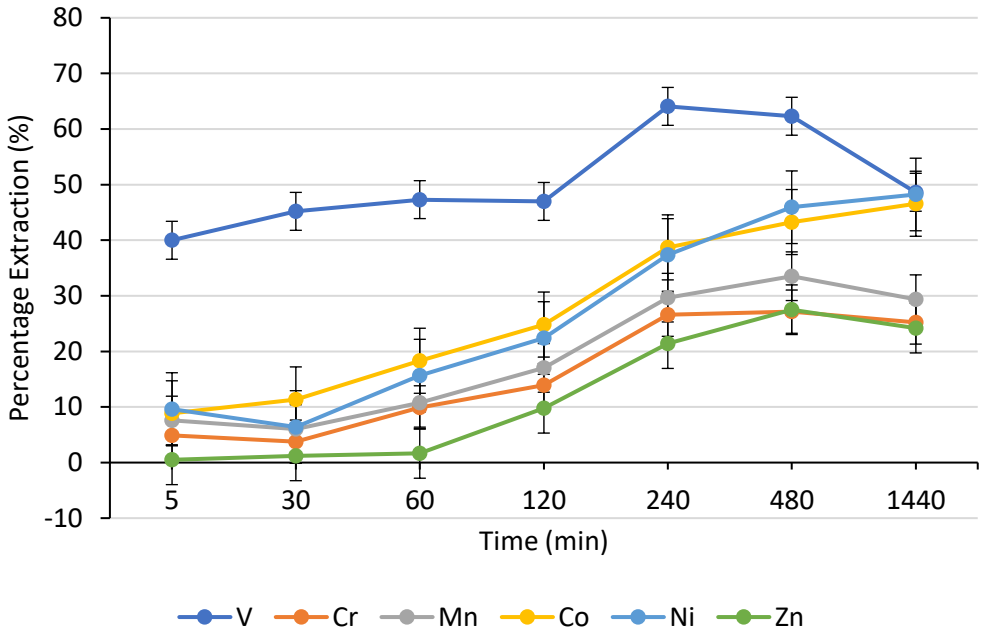

Figure 4.9 - Kinetic extraction data at pH 7 for V^{5+}, Cr^{3+}, Mn^{2+}, Co^{2+}, Ni^{2+} and Zn^{2+}

The concentration of nitrate counterion is the lowest in the samples at pH 7 compared to samples at pH 2 and 0.5. The low concentration of nitrate ions, an effective counterion for BTBP-metal ion complexes, causes the slow extraction kinetics observed at pH 7.

4.3 Conclusion

BTBP functionalised SiO_2 coated MNPs **96** show selectivity for Cu^{2+}, Ag^{+} and Cd^{2+}, which is not observed in the extraction data for BTBP functionalised SiO_2 gel **69**. High percentage extraction was achieved for Cu^{2+}, Ag^{+} and Cd^{2+} (>80%) after 24 hours; whereas poor extraction was observed for Mn^{2+}, Co^{2+}, Ni^{2+}, Zn^{2+}, V^{5+} and Cr^{3+}. The batch technique involving mixing BTBP functionalised SiO_2 coated MNPs **96** in sample solutions may have a reduced contact time between the BTBP ligand and metal ions compared to the column technique. As the MNPs

have a higher surface area and higher loading of BTBP onto the surface compared to the functionalised SiO_2 gel, using the BTBP functionalised SiO_2 coated MNPs **96** in a column method may achieve high extraction for all the transition metals and fast extraction kinetics. Higher extraction was observed in pH 0.5 owing to the higher concentration of nitrate anions which stabilise the cation-BTBP complex. The importance of nitrate anion concentration was observed from the reduction in extraction capabilities and decreased kinetics in pH 2 and 7.

Chapter 5 – Conclusions and Future Work

5.1 Conclusions

The introduction to this thesis outlined a review into current proposed processes for nuclear decommissioning. The development of selective ligands for caesium and strontium in the presence of other group I and II elements was discussed for extraction of fission products from SNF and environmental contamination. Advancements in solid support extraction and immobilisation of selective ligands onto the surface of magnetic nanoparticles and macroscopic silica gel was covered.

The reported synthesis of calix[4]bis-crown **47** was followed, with improved modifications developed for the synthesis of diol **72** and the tosylation reaction to afford ditosylate **78**. Utilising a Finkelstein reaction in the synthesis of diol **72** achieved a yield of 93% compared to the literature, where a 30% yield was reported.[85] The tosylation of diol **72** to ditosylate **78** was improved by means of sonication. The literature reported a yield of 86% after 6 days stirring in DCM with triethylamine and toluenesulfonyl chloride.[85] Using the same reagents, the reaction was sonicated affording ditosylate **78** after 5 hours with a yield of 92%. Using these improved synthetic routes, calix[4]bis-crown **47**, covalently bonded to silica-coated MNPs **81** or incorporated onto the surface of macroscopic silica gel **83**, was investigated for its ability to selectively extract Cs^+ in the presence of alkali metals (Li^+, Na^+, K^+), group II metals (Ca^{2+}, Mg^{2+}) and transition metals such as Fe^{3+} and Cu^{2+}.

Calix[4]bis-crown functionalised silica-coated MNPs **81** displayed high selectivity for Cs^+ over alkali metals, group II metals and transition metals at pH 7. Stripping of Cs^+ from calix[4]bis-crown MNPs **81** was exhibited in 2% HNO_3 solution allowing for recycling of calix[4]bis-crown MNPs **81**. A dose concentration of 0.5 mg mL^{-1} achieved high extraction (> 90%) of 100 ppb Cs^+, which upon extrapolation, infers that 250 g of calix[4]bis-crown functionalised MNPs

would be needed for 500 L of Cs contaminated water at 100 ppb Cs^+. This shows a potential for a vast reduction in secondary waste compared to liquid-liquid extraction methods. Calix[4]bis-crown functionalised silica gel **83** also exhibited high extraction (> 90%) of 100 ppb Cs^+. Calix[4]bis-crown silica gel **83** displayed fast extraction kinetics, achieving maximum capacity after 5 minutes compared to calix[4]bis-crown MNPs **81** where high extraction was reached after 1 hour of mixing.

Calix[8]amide **87** was synthesised for selective extraction of strontium from aqueous media present in PUREX raffinate or environmental contamination. The cyclic octamers were isolated from cyclic hexamers and heptamers by filtration from hot chloroform. Both cyclic hexamers and heptamers dissolved in hot chloroform, leaving insoluble cyclic octamer after filtration. An amide functionality was applied to the lower rim of the calix[8]arene, followed by deprotection of the benzoyl group to phenol in the upper rim. This functionalised calix[8]amide **87** was covalently bound to silica-coated MNPs **88** and immobilised onto the surface of macroscopic silica gel **89** for strontium extraction studies.

Unfortunately, calix[8]amide functionalised silica-coated MNPs **88** displayed poor extraction capabilities for strontium, only extracting < 10% at pH 2 and < 5% at pH 7. Calix[8]amide functionalised silica gel **89** also exhibited poor extraction capabilities. Higher extractions observed at pH 2 may be due to the presence of nitrate counter anions, able to stabilise complexation between strontium cations and the calix[8]amide. The amide functionality on the lower rim of calix[8]amide provides *N*-donor moiety that complexes with the strontium cations. However, the lack of functionality on the upper rim leaves the strontium cation susceptible to solvation by water molecules. Functionalisation of the upper rim could supply

addition electron density to stabilise the calix[8]amide-strontium cation complex and protect the strontium cation from 'stripping'.

Tetra-bromomethyl-BTBP functionalised silica-coated MNPs **96** were investigated and compared to tetra-bromomethyl-BTBP functionalised macroscopic silica gel **69** for uptake of problematic corrosion and fission products present in nuclear waste streams. Tetra-bromomethyl-BTBP functionalised silica-coated MNPs **96** were found to be selective for Ag^{+}, Cd^{2+} and Cu^{2+} achieving high extraction (> 80%) in batch studies at pH 0.5, 2 and 7. Increased extraction abilities and good kinetics of extraction were observed at pH 0.5, possibly because of the higher concentration of nitrate ions. The nitrate ions act as counter anions, stabilising the cation-BTBP complex. Better extraction kinetics and extraction efficiencies for all fission and corrosion products tested were observed with tetra-bromomethyl-BTBP functionalised silica gel **95** using a column extraction technique.

5.2 Future Work

Further investigation into ligand immobilised magnetic nanoparticles is necessary, particularly with regards to their use conditions in nuclear decommissioning. In such environments, magnetic separation must be examined in pipework of decommissioning process plants and nuclear plants. The use of solid supports over liquid-liquid techniques would allow for a vast decrease in secondary waste, allowing a more manageable process.

Calix[4]bis-crown **47** immobilised onto solid supports have led to positive extraction results for caesium. The synthetic route to calix[4]bis-crown **47** requires a slow macrocyclisation that needs to be improved in order to make calix[4]bis-crown **47** a desirable option for caesium extraction. Mitsunobu reactions are regularly used to form ether bonds from alcohols.[135–137]

A modified Mitsunobu reaction, coupling diol **72** to calix[4]arene **35**, could be beneficial to increase the overall yield of calix[4]bis-crown **47**.

Immobilisation of calix[4]bis-crown **47** onto silica gel displayed high extraction capabilities (> 90%) for caesium. Further study into the selectivity of calix[4]bis-crown functionalised silica gel **83** for caesium over sodium is needed. A column loaded with calix[4]bis-crown functionalised silica gel **83** would be subject to a multielement solution containing Cs^{+}, alkali metals (Li^{+}, Na^{+}, K^{+}), group II metals (Ca^{2+}, Mg^{2+}) and the transition metals such as Fe^{3+} and Cu^{2+}. ICP-MS analysis on samples before and after they are passed through the column would determine the selectivity of the functionalised silica gel **83**.

Incorporation of a vinyl functionality on calix[4]bis-crown **47** would allow for co-polymerisation with styrene. Co-polymerisation with styrene allows for more control of ligand loading by changing the ratio of ligand to styrene. Electro-spinning the resulting co-polymer would produce a fibrous network with a very high surface area capable of passive extraction.[138] The inert fibrous polymer network could be placed in a porous container into a contaminated sample, where the ligand immobilised onto the network could 'harvest' the target contaminant. This is ideal for areas where aggressive mixing or column extraction is not appropriate, such as remote areas where electrical power is not available or where concentrations of the desired metal are so low that it would be economically unfeasible to expend energy in the extraction (eg. precious metals from seawater).

Calix[8]amide **87** immobilised onto solid supports performed poorly in the extraction of strontium. Deprotection of the benzyl groups to phenols in the upper rim was employed to produce a means of immobilisation to solid supports. However this leaves the cavity of calix[8]amide exposed to stripping agents and solvating molecules such as ubiquitous water.

Calix[8]amide with the benzyl protecting groups on the upper rim has previously been investigated in a liquid-liquid extraction of Sr^{2+} showing a high selectivity for Sr over Na.[93] Replacement of the benzyl group with a functionalised benzyl group (e.g. 4-(chloromethyl)benzoic acid) would allow for immobilisation to solid supports and stabilise the cation-calix[8]amide complex. The presence of the benzyl group could be crucial in providing additional electron density to stabilise complexation and prevent stripping from water molecules and other complexing anions.

Chapter 6 – Experimental

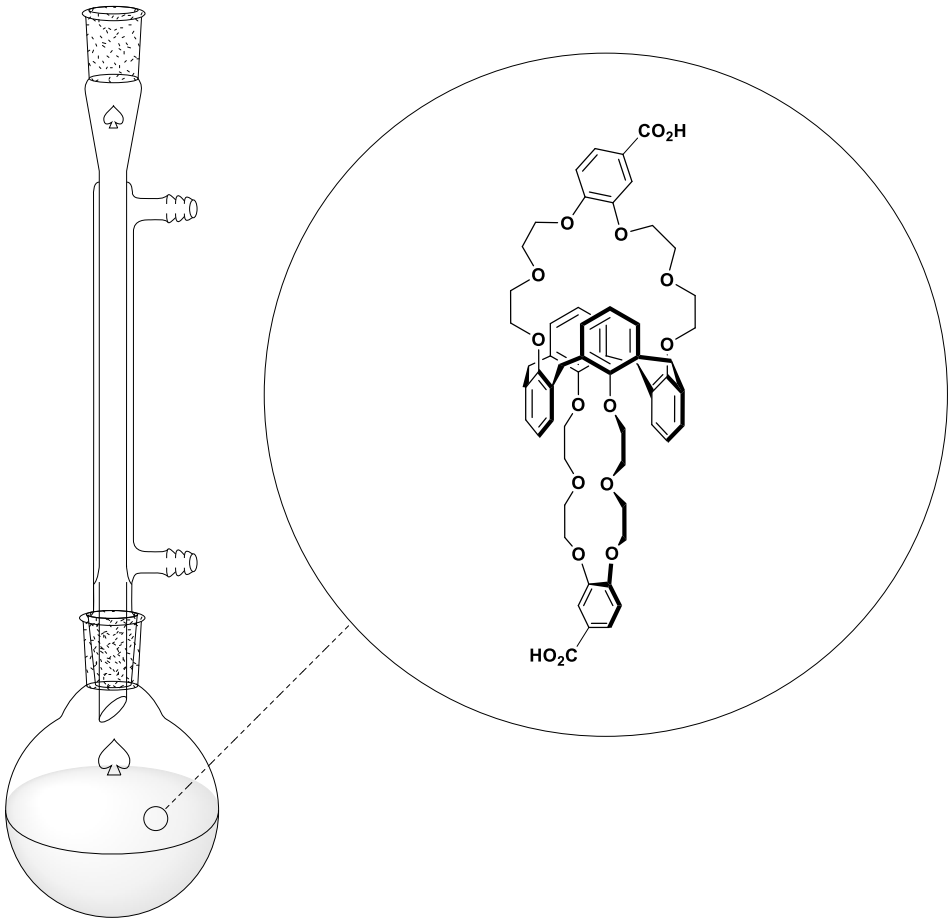

6.1 General Experimental Details

All reagents were supplied by Acros, Aldrich, Fisher or Fluorochem chemical suppliers and were used as supplied unless stated otherwise. All non-aqueous reactions, unless otherwise stated, were carried out in oven-dried glassware under dry nitrogen. Hotplates were used for heated reactions and stirred magnetically in oil baths. Cooling to 0 °C was achieved using an ice-water bath.

NMR spectra were recorded using either a Bruker AMX400 or an Advance DFX400 instrument. Deuterated chloroform ($CDCl_3$) or deuterated dimethyl sulfoxide (DMSO-d_6) were used as solvents. Chemical shifts (δ) were reported in parts per million (ppm) with the abbreviations s, d, t, q, dd, dt and m denoting singlet, doublet, triplet, quartet, double doublet, double triplet and unresolved multiplet resonance respectively. All coupling constants (*J*) were recorded in Hertz (Hz). Assignments were made using chemical shift and coupling constant data using DEPT-90, COSY, HSQC and HMBC experiments where required.

IR spectra were recorded on a Perkin-Elmer Spectrum One FT-IR spectrometer instrument with peak intensities abbreviated to: w, weak; m, medium; s, strong; br, broad.

All melting point were determined on a Stuart SMP10 melting point apparatus and were uncorrected.

Mass spectra were recorded under conditions of electrospray ionisation (ESI) on a Thermo Scientific LTQ-Orbitrap XL with a Thermo Scientific Accela HPLC.

The morphology of MNPs and silica gel were observed by Miss Amanpreet Kaur in the EMLab. Images were obtained using an FEI Quanta 600 FEG scanning electron microscope (SEM) and a

JEOL 2100 Plus transmission electron microscope (TEM). Elemental analysis was carried out using Energy Dispersive X-ray Spectroscopy (EDX) in conjunction with SEM.

Thermogravimetric (TGA) analyses were performed using a TGA-Q50 thermogravimetric analyser.

6.2 Synthesis of Ligands

*6.2.1 Synthesis of Ethyl 3,4-bis(2-(2-hydroxyethoxy)ethoxy)benzoate **72***[85]

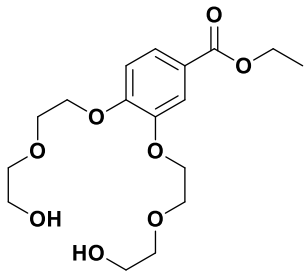

72

Method 1:

Potassium carbonate (31.5 g, 225 mmol) was added to a suspension of ethyl 3,4-dihydroxybenzoate **7** (10.0 g, 54 mmol) and the mixture stirred at room temperature in acetonitrile (270 mL) for 2 hours. The mixture was then heated to reflux and 2-(2-chloroethoxyl)ethanol **71** (13.4 mL, 127 mmol) was added. After 3 days, additional potassium carbonate (12.002 g, 86 mmol) and 2-(2-chloroethoxy)ethanol **71** (7.0 mL, 66 mmol) were added and the mixture was returned to reflux for a further 4 days. The solvent was then removed by rotary evaporation. The residue was dissolved in dichloromethane (100 mL) and washed successively with 1M HCl (2 x 50 mL), water (2 x 50 mL) and brine (2 x 50 mL). The mixture was then dried over $MgSO_4$, filtered and concentrated via rotary evaporation to afford diol **72** (7.99 g, 41%) as a yellow oil.

Method 2:

Potassium carbonate (33.56 g, 243.2 mmol, 4 e.q) and potassium iodide (25.20 g, 151.8 mmol, 2.5 e.q) were added to a suspension of ethyl 3,4-dihydroxybenzoate **70** (11.06 g, 60.7 mmol) in acetonitrile (250 mL). After stirring at RT for 2 hours, 2-(2-chloroethoxy)ethanol **71** (15.83 mL, 151.8 mmol) was added to the suspension and the mixture heated to reflux under

nitrogen. After 3 days, additional potassium carbonate (16.50 g, 119 mmol), potassium iodide (12.50g, 75 mmol) and 2-(2-chloroethoxy)ethanol **71** (7 mL, 66 mmol) were added to the suspension and reflux under nitrogen was maintained for a further 3 days. The suspension was then cooled to RT, deionised water (100 mL) was added and the product was extracted into dichloromethane (2 x 200 mL). The combined organic layers were washed with 1M HCl (200 mL), deionised water (200 mL) and brine (200 mL). The organic phase was dried over magnesium sulfate, filtered and concentrated *in vacuo* to afford diol **72** (20.23 g, 93%) as a brown oil.

Method 3:

Potassium carbonate (33.56 g, 243.2 mmol, 4 e.q) and potassium iodide (25.20 g, 151.8 mmol, 2.5 e.q) were added to a suspension of ethyl 3,4-dihydroxybenzoate **70** (11.06 g, 60.7 mmol) in acetonitrile (250 mL). After stirring at RT for 2 hours, 2-(2-chloroethoxy)ethanol **71** (15.83 mL, 151.8 mmol) was added to the suspension and the mixture heated to reflux under nitrogen. After 3 days, additional potassium carbonate (16.50 g, 119 mmol), potassium iodide (12.50g, 75 mmol) and 2-(2-chloroethoxy)ethanol **71** (7 mL, 66 mmol) were added to the suspension and reflux under nitrogen was maintained for a further 3 days. The suspension was then cooled to RT, deionised water (100 mL) was added and the product was extracted into dichloromethane (2 x 200 mL). The combined organic layers were washed with 1M HCl (200 mL), deionised water (200 mL) and brine (200 mL). The organic phase was dried over magnesium sulfate, filtered and concentrated *in vacuo* to afford diol **72** (20.23 g, 93%) as a brown oil. FT-IR (ATR) ν_{max} / cm^{-1} 3433br, 2865w, 1708m, 1600w, 1512w, 1427w, 1267s, 1210s, 1123s, 1024s.

δ_H (400 MHz, $CDCl_3$) 7.66 (dd, *J* = 2.0, 8.5 Hz, 1H, Ar*H*), 7.56 (d, *J* = 2.0 Hz, 1H, Ar*H*), 6.89 (d, *J* = 8.5 Hz, 1H, Ar*H*), 4.34 (q, *J* = 7.0 Hz, 2H, CH_2CH_3), 4.24 – 4.16 (m, 4H, OCH_2CH_2O), 3.97 (br s, 2H, OH), 3.94 – 3.86 (m, 4H, OCH_2CH_2O), 3.77 – 3.70 (m, 4H, OCH_2CH_2O), 3.70 – 3.63 (m, 4H, OCH_2CH_2O), 1.38 (t, *J* = 7.0 Hz, 3H, CH_2CH_3); δ_C (100 MHz, $CDCl_3$) 166.16 (C=O), 152.20, 147.71, 123.80 (Ar*C*), 123.20, 113.84, 111.72 (Ar*C*H), 72.79, 72.76, 69.10, 68.93, 68.40, 68.26, 61.41, 61.40 (OCH_2CH_2O), 60.83 (OCH_2CH_3), 14.23 (OCH_2CH_3); (FTMS + pESI) cald $C_{17}H_{27}O_8$ $[M+H]^+$: 359.1661; observed 359.1702; cald $C_{17}H_{26}O_8Na$ $[M+Na]^+$: 381.1525; observed 381.1520

*6.2.2 Synthesis of Ethyl 3,4-bis(2-(2-(tosyloxy)ethoxy)ethoxy)benzoate **78**[85]*

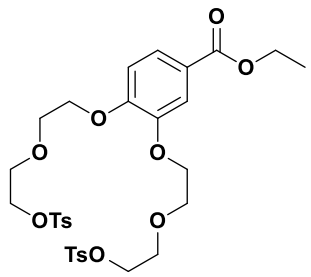

78

Method 1:

Diol **72** (5.80 g, 8 mmol) and toluenesulfonyl chloride (14.9 g, 78 mmol) were added to dichloromethane (150 mL) at 0 °C. Triethylamine (10.7 mL, 76 mmol) in dichloromethane (50 mL) was added dropwise and the mixture was then stirred at RT for 6 days. Deionised water (100 mL) was then added to the mixture, the organic layer was separated, dried over magnesium sulfate, filtered and concentrated *in vacuo*. The crude yellow oil was then purified by silica gel chromatography (99: 1 $CHCl_3$: methanol) to give ditosylate **78** (10.01 g, 93%) as a yellow oil.

Method 2:

Diol **72** (19.59 g, 54 mmol) and toluensulfonyl chloride (19.81 g, 104 mmol) were added to chloroform (200 mL) at 0 °C under N_2. A solution of triethylamine (15.1 mL, 108 mmol) and DMAP (0.66 g, 5.4 mmol) in chloroform (100 mL) was added dropwise and the mixture was then stirred at room temperature for 4 days under N_2. Deionised water (200 mL) was then added to the mixture, the organic layer was washed with sat. copper sulfate solution (100 mL). The organic layer was dried over magnesium sulfate, filtered and concentrated *in vacuo* to afford ditosylate **78** (33.42 g, 92%) as a brown oil.

Method 3:

Diol **72** (1.00 g, 2.79 mmol) and tosylchloride (1.06 g, 5.58 mmol) were added to chloroform (15 mL) at 0 °C. Triethylamine (0.8 mL, 5.74 mmol) in chloroform (15 mL) was added dropwise and the mixture was then sonicated at 45 °C for 5 hours under N_2. Deionised water (30 mL) was then added to the mixture. The organic layer was dried over magnesium sulfate, filtered and concentrated *in vacuo* to afford ditosylate **78** as a brown oil (1.69 g, 91%).

FT-IR (ATR) ν_{max} / cm^{-1} 2865w, 1707m, 1595w, 1509w, 1452w, 1429w, 1267s, 1211s, 1128s.

δ_H (400 MHz, $CDCl_3$) 7.77 (d, *J* = 8.0 Hz, 4H, ArH_{tosyl}), 7.66 (d, *J* = 8.5 Hz, 1H, Ar*H*), 7.53 (s, 1H, Ar*H*), 7.29 (d, *J* = 8.0 Hz, 4H, ArH_{tosyl}), 6.85 (d, *J* = 8.5 Hz, 1H, Ar*H*), 4.34 (q, *J* = 7.0 Hz, 2H, C$H_2$$CH_3$), 4.24 – 4.14 (m, 4H, OC$H_2$$CH_2$O), 4.14 – 4.05 (m, 4H, OC$H_2$$CH_2$O), 3.84 – 3.73 (m, 8H, OCH_2CH_2O), 2.39 (s, 6H, CH_3), 1.38 (t, *J* = 7.0 Hz, 3H, $OCH_2$$CH_3$); δ_C (100 MHz, $CDCl_3$) 166.07 (C=O), 152.76, 148.07, 144.83, 132.85 (Ar*C*), 129.83, 127.85 (Ar*C*H), 123.90 (Ar*C*), 123.29, 114.74, 112.54 (Ar*C*H), 69.52, 69.50, 69.46, 68.86, 68.81, 68.52 (O$CH_2$$CH_2$O), 60.75 (O$CH_2$$CH_3$), 21.51 ($CH_3$), 14.23 ($OCH_2$$CH_3$); (FTMS + pESI) cald $C_{31}H_{39}O_{12}S_2$ $[M+H]^+$: 667.1877; observed 667.1877; cald $C_{31}H_{38}O_{12}S_2Na$ $[M+Na]^+$: 689.1697; observed 689.1692

*6.2.3 Synthesis of Calix[4]arene-bis-[(4-ethoxycarbonyl-1,2-phenylene)crown-6] **79**[85]*

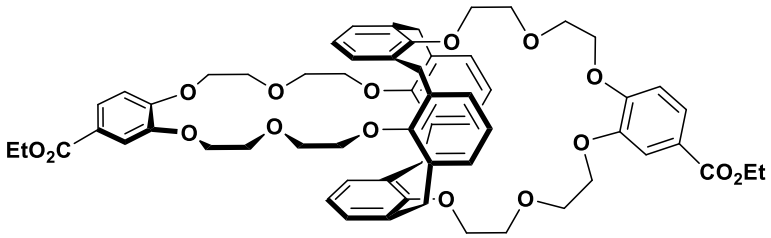

79

Calix[4]arene **35** (1.75 g, 4.12 mmol), potassium carbonate (5.7 g, 41.29 mmol) and ditosylate **78** (2.82 g, 4.22 mmol) in dry acetonitrile (150 mL) were heated to reflux under nitrogen for 7 days. Additional potassium carbonate (5.70 g, 41.29 mmol) and ditosylate **78** (2.82 g, 4.22 mmol) were then added and the mixture heated to reflux for a further 7 days. The mixture was then cooled to RT and filtered to remove residual potassium carbonate. The solvent was then removed by rotary evaporation, affording an orange solid. The orange solid was dissolved in DCM (100 mL) and neutralised with 1M HCl. The organic layer was washed with water (100 mL) and brine (100 mL), dried over magnesium sulfate, filtered and concentrated *in vacuo* to give the crude product as an orange solid. The crude product was purified by silica gel chromatography (95 : 5 $CHCl_3$: MeOH, Rf = 0.6) to afford calix[4]bis-crown **79** as a white solid (2.50 g, 57%) m.p. 84-86 °C; FT-IR (ATR) ν_{max} / cm^{-1} 2870w, 1709m, 1599w, 1512w, 1427w, 1354m, 1269s, 1174s, 1133s

δ_H (400 MHz, $CDCl_3$) 7.74 (dd, *J* = 8.5, 2.0 Hz, 2H, Ar*H*), 7.66 (d, *J* = 2.0 Hz, 2H, Ar*H*), 7.07 (m, 8H, Ar*H*), 6.97 (d, *J* = 8.5 Hz, 2H, Ar*H*), 6.67 (t, *J* = 7.5 Hz, 4H, Ar*H*), 4.37 (q, *J* = 7.1 Hz, 4H, CH_2CH_3), 4.24 – 4.14 (m, 8H, OCH_2CH_2O), 3.81 – 3.71 (m, 16H, OCH_2CH_2O, $ArCH_2Ar$), 3.64 – 3.51 (m, 16H, OCH_2CH_2O), 1.40 (t, *J* = 7.0 Hz, 6H, OCH_2CH_3); δ_C (100 MHz, $CDCl_3$) 166.34 (C=O), 156.40, 153.02, 148.33, 134.07 (Ar*C*), 130.27 (Ar*C*H), 124.27 (Ar*C*), 123.69, 122.43, 115.58,

113.01 (Ar*C*H), 70.42, 70.37, 70.24, 70.19, 69.96, 69.84, 69.53 (O*C*H_2*C*H_2O), 60.87 (O*C*$H_2$$CH_3$), 37.74 (Ar*C*$H_2$Ar), 14.46 (OC$H_2$*C*$H_3$); (FTMS + pESI) cald $C_{62}H_{69}O_{16}$ $[M+H]^+$: 1069.4580; observed 1069.4599; cald $C_{62}H_{68}O_{16}Na$ $[M+Na]^+$: 1091.4400; observed 1091.4410

6.2.4 Synthesis of Calix[4]arene-bis-[(4-carboxyl-1,2-phenylene)-crown-6] ***47***[85]

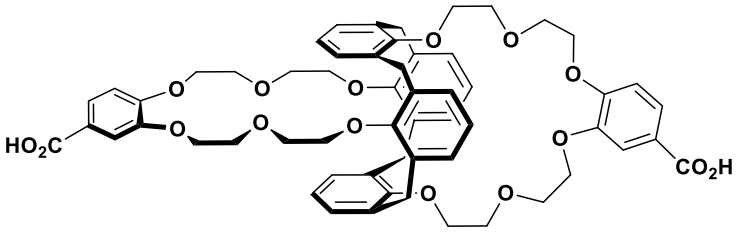

47

A mixture of calix[4]bis-crown **79** (0.4 g, 0.38 mmol) and potassium hydroxide (0.09 g, 1.66 mmol) in ethanol (15 mL) was stirred at reflux for 3 hours. The mixture was then cooled to RT and deionised water (15 mL) was added, followed by concentrated HCl (1.5 mL) and additional deionised water (15 mL). A white precipitate was formed, which was filtered off and washed with deionised water (50 mL). The precipitate was then dissolved in chloroform, dried over magnesium sulfate, filtered and concentrated *in vacuo* to afford calix[4]bis-crown **47** as a white solid (0.226 g, 59%) m.p. 111-113 °C; FT-IR (ATR) ν_{max} / cm^{-1} 3379br, 2926w, 1704m, 1601w, 1513w, 1453m, 1266s, 1205s, 1130s, 1024s.

δ_H (400 MHz, DMSO) 12.73 (s, 2H, O*H*), 7.64 (dd, *J* = 8.5, 2.0 Hz, 2H, Ar*H*), 7.54 (d, *J* = 2.0 Hz, 2H, Ar*H*), 7.15 (d, *J* = 8.5 Hz, 2H, Ar*H*), 7.05 (d, *J* = 7.0 Hz, 8H, Ar*H*), 6.59 (t, *J* = 7.0 Hz, 4H, Ar*H*), 4.17 (t, *J* = 4.0 Hz, 4H, OC*H*$_2$CH$_2$O), 4.11 (t, *J* = 4.0 Hz, 4H, OC*H*$_2$CH$_2$O), 3.77 (s, 8H, ArC*H*$_2$Ar), 3.72 (t, *J* = 4.0 Hz, 4H, OC*H*$_2$CH$_2$O), 3.63 (t, *J* = 4.0 Hz, 4H, OC*H*$_2$CH$_2$O), 3.56 – 3.44 (m, 8H, OCH$_2$C*H*$_2$O), 3.40 – 3.29 (m, 8H, OCH$_2$C*H*$_2$O); δ_C (100 MHz, $CDCl_3$) 167.00 (C=O), 156.07, 152.60, 147.73, 133.55 (Ar*C*), 129.48 (Ar*C*H), 123.82 (Ar*C*), 123.39, 121.83, 115.22, 113.19 (Ar*C*H), 69.47, 69.28, 69.20, 68.22 (OCH$_2$*C*H$_2$O), 37.74 (Ar*C*H$_2$Ar); (FTMS + pESI) cald $C_{58}H_{61}O_{16}$ $[M+H]^+$: 1013.3954; observed 1013.3970; cald $C_{58}H_{60}O_{16}Na$ $[M+Na]^+$: 1035.3774; observed 1035.3784

*6.2.5 Synthesis of 3,4-bis(2-(2-hydroxyethoxy)ethoxy)benzaldehyde **97***

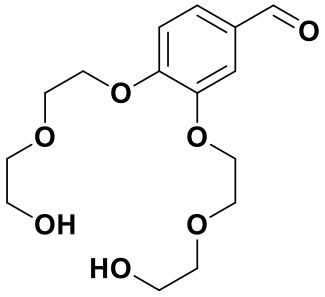

97

Potassium carbonate (20.00 g, 145 mmol, 2 eq) and potassium iodide (24.00 g, 145 mmol, 2 e.q) were added to a suspension of 3,4-dihydroxybenzaldehyde (10.00 g, 72.5 mmol) in acetonitrile (200 mL). After stirring at RT for 1 hour, 2-(2-chloroethoxy)ethanol (15 mL, 145 mmol) was added to the suspension and the mixture heated to reflux under nitrogen. After 3 days the suspension was cooled to RT, deionised water (100 mL) was added and the product was extracted into dichloromethane (2 x 200 mL). The combined organic extracts were washed with 1M HCl (200 mL), deionised water (200 mL) and brine (200 mL). The organic phase was dried over magnesium sulfate, filtered and concentrated *in vacuo* to afford diol **97** (18.89 g, 83%) as a brown oil. FT-IR (ATR) ν_{max} / cm^{-1} 3378br, 2871w, 1679m, 1584m, 1508m, 1435m, 1263s, 1118s, 1046s.

δ_H (400 MHz, $CDCl_3$) 9.84 (s, 1H, C*H*CO), 7.46 (dd, *J* = 8.0, 2.0 Hz, 1H, ArC*H*), 7.42 (d, *J* = 2.0 Hz, 1H, ArC*H*), 6.98 (d, *J* = 8.0 Hz, 1H, ArC*H*), 4.27 – 4.20 (m, 4H, OC*H*$_2$CH$_2$O), 3.98 – 3.91 (m, 4H, OC*H*$_2$CH$_2$O), 3.80 – 3.73 (m, 4H, OCH$_2$C*H*$_2$O), 3.73 – 3.66 (m, 4H, OCH$_2$C*H*$_2$O); δ_C (100 MHz, $CDCl_3$) 190.62 (C=O), 153.62, 148.61, 130.17 (Ar*C*), 126.97, 111.63, 110.44 (Ar*C*H), 72.90, 72.85, 68.95, 68.81, 68.35, 68.21 (O*C*H$_2$*C*H$_2$O), 61.39 (OCH$_2$*C*H$_2$OH); (FTMS + pESI) cald $C_{15}H_{23}O_7$ $[M+H]^+$: 315.1438; observed 315.1444; cald $C_{15}H_{22}O_7Na$ $[M+Na]^+$: 337.1258; observed 337.1258

*6.2.6 Synthesis of 5,11,17,23,29,35,41,47-Octakis(benzyloxy)-49,50,51,52, 53,54,55,56-octahydroxycalix[8]arene **85***

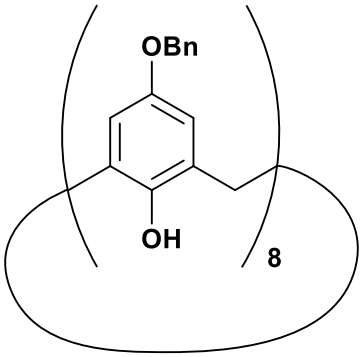

85

Paraformaldehyde (6 g) and potassium *tert*-butoxide (0.5 g, 4.5 mmol) were added to a suspension of 4-benzyloxyphenol **84** (15 g, 74.9 mmol) in *p*-xylene (300 mL) under N_2. The suspension was heated at 110 °C for 16 hours under N_2. Additional paraformaldehyde (2 g) was added and the suspension was heated at 135 °C for a further 16 hours. The suspension was then cooled and the solid residue filtered. The crude solid was washed with acetone to afford calix[8]arene **85** as a white powder (8.3 g, 52%) m.p. >300 °C; FT-IR (ATR) ν_{max} / cm^{-1} 3194br, 2924w, 1602w, 1481w, 1452w, 1383w, 1237s, 1089s, 905s.

δ_H (400 MHz, DMSO) 7.47 – 7.22 (m, 40H, ArH_{benzyl}), 6.69 (m, 16H, Ar*H*), 4.90 (m, 16H, OCH_2Ar), 3.77 (s, 16H, ArCH_2Ar); δ_C (101 MHz, DMSO) Insufficiently soluble to obtain a meaningful spectrum; (FTMS + pESI) cald $C_{112}H_{95}O_{16}$ $[M-H]^-$: 1695.6662; observed 1695.6626

6.2.7 Synthesis of 5,11,17,23,29,35,41,47-Octakis(benzyloxy)-49,50,51,52, 53,54,55,56-octakis[(N,N-diethylaminocarbonyl)methoxy]calix[8]arene ***64***[133]

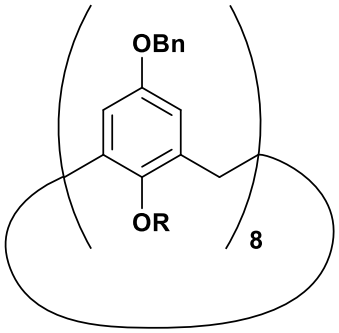

R = CH_2CONEt_2

64

Calix[8]arene **85** (2.80 g, 1.65 mmol) was dissolved in dry DMF (100 mL), caesium carbonate (18.82 g, 57.8 mmol) and 2-chloro-*N*,*N*-diethylacetamide **86** (13.6 mL, 99.0 mmol) were added and the suspension was heated to 90 °C for 16 hours. Once cooled the suspension was quenched with 1M HCl (300 mL). The crude product was filtered and washed with deionised water, dissolved in minimal DCM, methanol was added and the solution left at -5 °C for 16 hours. The precipitate was filtered to afford calix[8]amide **64** as a pale yellow powder (2.02 g, 50%) m.p. >300 °C; FT-IR (ATR) ν_{max} / cm^{-1} 2933w, 1638m, 1585m, 1452m, 1198m, 1037m.

δ_H (400 MHz, $CDCl_3$) 7.20 – 7.04 (m, 40H), 6.54 (s, 16H, ArC*H*), 4.53 (s, 16H,OCH_2Ar), 4.42 (s, 16H, OCH_2CO), 4.04 (s, 16H, ArCH_2Ar), 3.34 – 3.03 (m, 32H, NCH_2CH_3), 1.09 – 0.84 (m, 48H, NCH_2CH_3); δ_C (101 MHz, $CDCl_3$) 167.05 (CO), 155.10, 149.31, 137.07, 134.63 (Ar*C*), 128.20, 127.62, 127.52, 115.05 (Ar*C*H), 72.23 (OCH_2CO), 69.55 (OCH_2Ar), 41.22, 40.00 (NCH_2CH_3), 30.58 (ArCH_2Ar), 14.20, 12.85 (NCH_2CH_3); (FTMS + pESI) cald $C_{160}H_{184}N_8O_{24}Na$ $[M+Na]^+$: 2624.3204; observed 2624.3316

*6.2.8 Synthesis of 5,11,17,23,29,35,41,47-Octahydroxy-49,50,51,52, 53,54,55,56-octakis[(N,N-diethylaminocarbonyl)methoxy]calix[8]arene **87***[133]

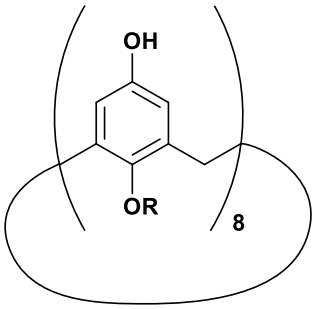

$R = CH_2CONEt_2$

87

Pearlman's catalyst ($Pd(OH)_2/C$, 0.7 g) and cyclohexene (18 mL) were added to a suspension of calix[8]amide **64** (1.00 g, 0.38 mmol) in ethanol (150 mL) at 90 °C under N_2. After 16 hours the mixture was cooled, and the catalyst filtered off. The filtrate was concentrated *in vacuo* to afford the crude product that was triturated with methanol to afford pure calix[8]amide **87** as a pale yellow powder (0.73 g, 76%) m.p. >300 °C; FT-IR (ATR) ν_{max} / cm^{-1} 3197br, 2971w, 1621s, 1452s, 1193s, 1010m.

δ_H (400 MHz, DMSO) 8.79 (s, 8H, OH), 6.27 (s, 16H, ArC*H*), 4.33 (s, 16H, OCH_2CO), 3.86 (s, 16H, ArCH_2Ar), 3.20 – 3.09 (m, 32H, NC$H_2$$CH_3$), 0.91 (dt, *J* = 13.0, 7.0 Hz, 48H, NCH_2CH_3); δ_C (101 MHz, DMSO) 166.56 (CO), 153.23 (Ar*C*OH), 147.72, 134.27 (Ar*C*), 114.98 (Ar*C*H), 71.65 (O*C*H_2CO), 40.67 (N*C*$H_2$$CH_3$), 13.94, 12.67 ($NCH_2CH_3$); (FTMS + pESI) cald $C_{104}H_{136}N_8O_{24}Na$ $[M+Na]^+$: 1903.9560; observed 1903.9573

6.3 Synthesis of Immobilised Magnetic Nanoparticles

6.3.1 Synthesis of iodoalkyl-functionalised SiO_2-coated Fe_2O_3 MNPs ***67***[107,109]

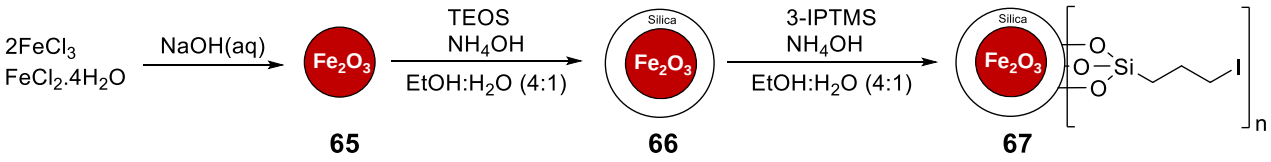

$FeCl_2.4H_2O$ (0.8 g, 4.0 mmol) and $FeCl_3$ (1.3 g, 8.0 mmol) were dissolved in degassed deionised water (40 mL) and the solution added dropwise to 2M NaOH solution (200 mL) with vigorous stirring. Stirring was maintained for 1 hour and the resulting Fe_2O_3 MNPs **65** were separated using an external neodymium magnet and decanting the supernatant. The MNPs were washed with degassed deionised water (200 mL) and 0.01M HCl (100 mL) to remove unreacted iron salts. The Fe_2O_3 MNPs **65** were dispersed in a mixture of degassed ethanol (400 mL) and degassed deionised water (100 mL) by sonication for 10 minutes. Ammonium hydroxide (35%, 36 mL) and tetraethyl orthosilicate (3.6 mL, 16 mmol) were consecutively added to the suspension and the mixture sonicated at RT for 2 hours. (3-Iodopropyl)trimethoxysilane (6.3 mL, 32 mmol) was then added and the reaction mixture was sonicated for a further 3 hours. The resulting functionalised MNPs **67** were collected by magnetic separation and washed with degassed ethanol (200 mL). The resultant MNPs **67** (2.37 g) were dried at 120 °C.

6.3.2 Immobilisation of Calix[4]arene-bis-[(4-carboxyl-1,2-phenylene)-crown-6] onto SiO_2-MNPs

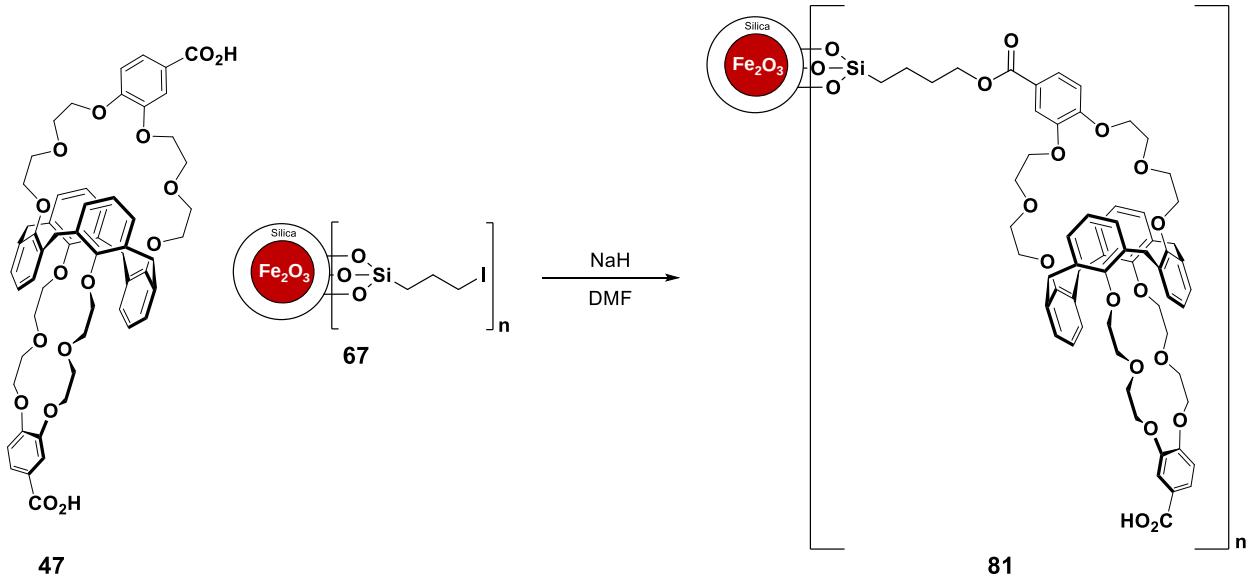

47 **67** **81**

Sodium hydride (60% dispersion in mineral oil, 0.03 g, 0.9 mmol, 1.8 eq) was added to a suspension of calix[4]bis-crown **47** (0.5 g, 0.5 mmol) in DMF (100 mL) at 120 °C and the mixture stirred for 30 minutes. Iodoalkyl-functionalized SiO_2-coated MNPs **67** (0.5 g) were slowly added and the suspension was stirred at 120 °C for 16 hours. The calix[4]bis-crown functionalised MNPs were separated using an external neodymium magnet and washed with degassed ethanol (200 mL). The functionalised MNPs **81** (0.45 g) were dried at 120 °C.

6.3.3 Immobilisation of Calix[8]amide onto SiO_2-coated MNPs

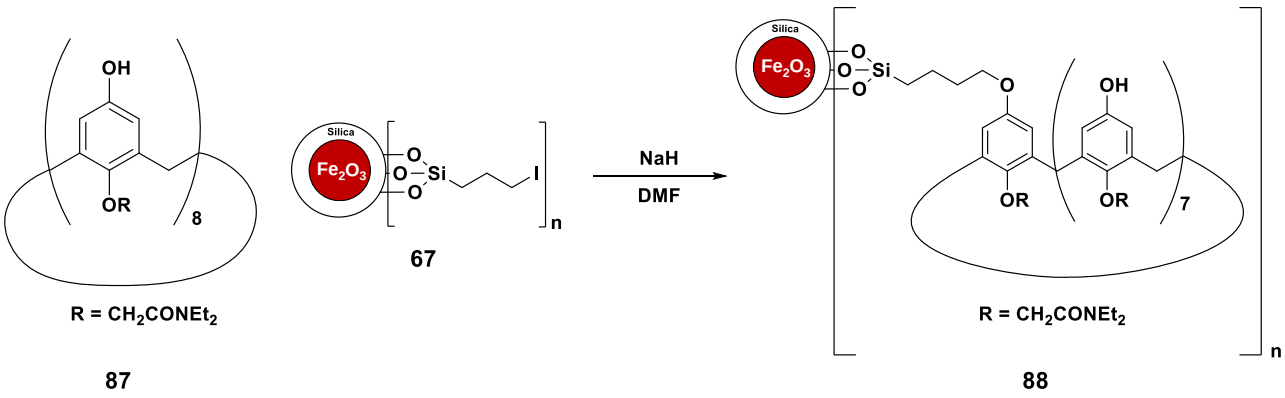

Sodium hydride (60% dispersion in mineral oil, 0.04 g, 1.1 mmol, 2 eq) was added to a suspension of calix[8]amide **87** (1.0 g, 0.53 mmol) in DMF (100 mL) at 120 °C and the mixture stirred for 30 minutes. Iodoalkyl-functionalised SiO_2-coated MNPs **67** (1.0 g) were slowly added and the suspension was stirred at 120 °C for 16 hours. The calix[8]amide functionalised MNPs **88** were separated using an external neodymium magnet and washed with degassed ethanol (200 mL) and dried at 120 °C (0.63 g).

6.4 Synthesis of Immobilised SiO_2 gel

6.4.1 Immobilisation of Calix[4]arene-bis-[(4-carboxyl-1,2-phenylene)-crown-6] onto SiO_2 gel

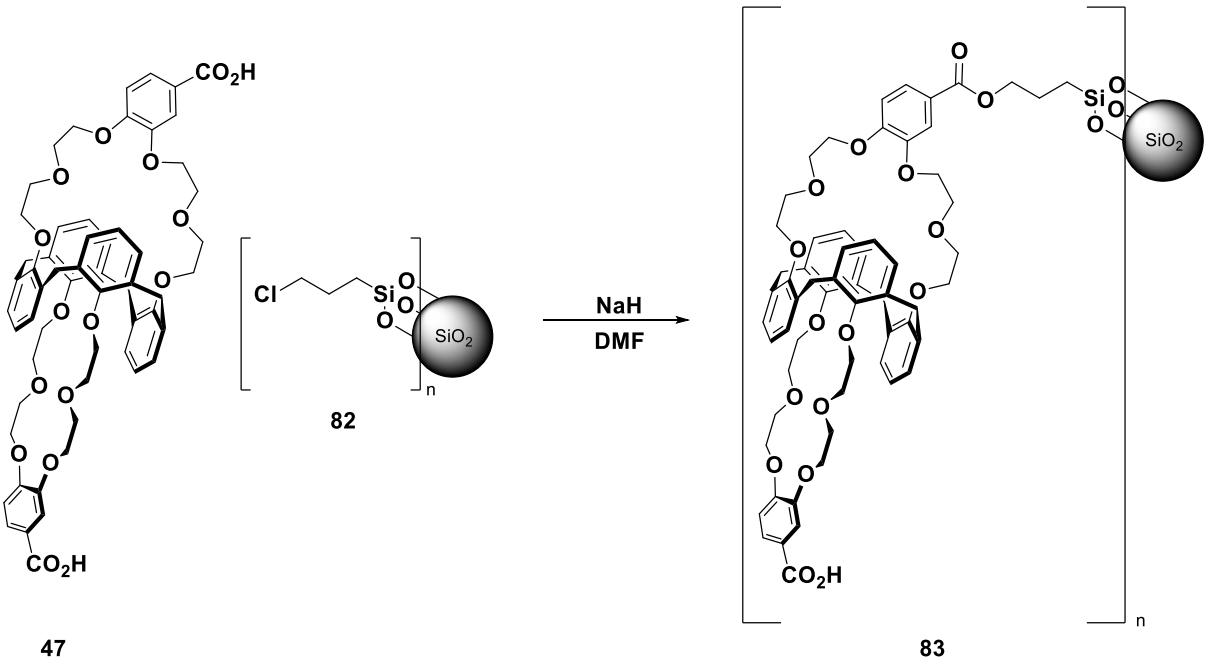

47 82 83

Sodium hydride (60% dispersion in mineral oil, 0.08 g, 1.96 mmol, 2 eq) was added to a suspension of calix[4]bis-crown **47** (1.02 g, 0.98 mmol) in DMF (100 mL) at 120 °C and the mixture stirred for 30 minutes. Chloropropyl-functionalized SiO_2 gel **82** (2.03 g, ~ 2.5 mmol/g loading) was slowly added and the suspension was stirred at 120 °C for 16 hours. The calix[4]bis-crown functionalised SiO_2 gel **83** was separated by filtration and washed with deionised water (100 mL) and ethanol (200 mL). The functionalised SiO_2 gel **83** was dried at 120 °C (1.87 g).

6.4.2 Immobilisation of calix[8]arene onto SiO_2 gel

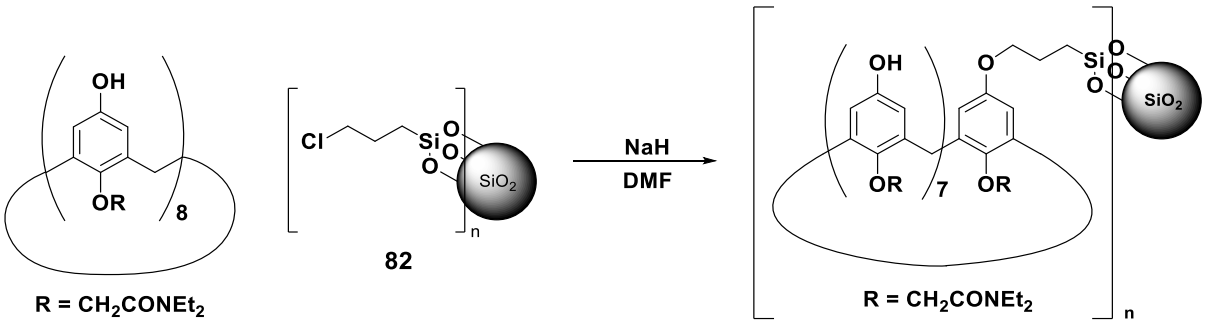

Sodium hydride (60% dispersion in mineral oil, 0.06 g, 1.50 mmol, 2.5 eq) was added to a suspension of calix[8]amide **87** (1.01 g, 0.59 mmol) in DMF (100 mL) at 120 °C and the mixture stirred for 30 minutes. Chloropropyl-functionalised SiO_2 gel **82** (2.12 g, ~ 2.5 mmol/g loading) was slowly added and the suspension was stirred at 120 °C for 16 hours. The calix[8]arene functionalised SiO_2 gel **89** was separated by filtration and washed with deionised water (100 mL) and ethanol (200 mL). The functionalised SiO_2 gel **89** was dried at 120 °C (2.04 g).

6.5 ICP-MS Extraction Studies

6.5.1 ICP-MS General Procedure

ICP-MS analysis was carried out using a Thermo-Fisher iCAP Q ICP-MS with Rh as the internal standard. A stock solution of 2% HNO_3 spiked with 5 ppb Rh was prepared using ultra-pure water and HNO_3 (70%, purified by redistillation, ≥ 99.999% trace metals basis). All standard solutions were prepared using the stock solution of 2% HNO_3 spiked with 5 ppb Rh. Standards were prepared using metal mixes purchased from Sigma-Aldrich as TraceCERT (Traceable Certified Reference Materials). Standards used to calibrate the ICP-MS were at concentrations of 5, 10, 25, 50 and 100 ppb. All extraction samples were normalised to 2% HNO_3 and spiked with 5 ppb Rh before testing. Samples (5 mL) were taken before and after extractions to provide true initial and end concentrations. An average of three readings was taken with all samples.

6.5.2 Examination of Calix[4]bis-crown MNPs Extraction Ability

Six samples of Cs solution (10 mL) were made to approx. 10 ppb using a stock Cs solution (1000 ppm). Three samples were subjected to mixing with calix[4]bis-crown functionalised MNPs **81** (5 mg) and the other three with iodo-functionalised MNPs **67** (5 mg). Mixing was carried out for 24 hours and the mixtures were then placed onto neodymium magnets to ensure separation of nanoparticles. The samples were then centrifuged and passed through a 0.22 micron filter to ensure all large particles had been removed before ICP-MS analysis. After filtration, 5 mL aliquots were subjected to ICP-MS analysis.

6.5.3 Capacity study of Calix[4]bis-crown functionalised MNPs

Five samples of Cs solution (100 mL) were made to approx. 100 ppb using a stock Cs solution (1000 ppm) at pH 7. The samples were mixed with calix[4]bis-crown MNPs **81** using different

dosages for each sample (2 mg, 5 mg, 10 mg, 50 mg, 100 mg). Mixing was carried out for 24 hours and the samples were then placed onto neodymium magnets to ensure separation of nanoparticles. Small samples (10 mL) were then taken from each test and were subjected to centrifuging and passed through a 0.22 micron filter to ensure all solid particles had been removed. After filtration, 5 mL aliquots were subjected to ICP-MS analysis.

6.5.4 Kinetics Study of calix[4]bis-crown MNPs

A sample of Cs solution (200 mL) was made to approx. 100 ppb using a stock Cs solution (1000 ppm) at pH 7. The sample was mixed with calix[4]bis-crown MNPs **81** (100 mg) for 24 hours. Small samples (10 mL) were taken at intervals (5, 30, 60, 120, 240, 480 and 1440 mins) and placed onto neodymium magnets to ensure separation of nanoparticles. Samples were subjected to centrifuging and passed through a 0.22 micron filter to ensure all solid particles had been removed. After filtration, 5 mL aliquots were subjected to ICP-MS analysis.

6.5.5 Competing Ion study of calix[4]bis-crown MNPs

Three samples of Cs/multi-element solution (100 mL) were made to approx. 100 ppb using a stock Cs solution (1000 ppm) at pH 7. The multi-element stock contained Al, Sb, Ba, Pb, B, Ca, Cd, Cr, Co, Fe, K, Cu, Li, Mg, Mo, Na, Ni, P, Si, Ti, V and Zn (all at 100 ppm). Each sample was made to a different concentration of multi-elements (10 ppb, 250 ppb and 1000 ppb) using the multi-element stock solution. The samples were mixed with calix[4]bis-crown functionalised MNPs **81** (50 mg) for 120 minutes and samples (100 mL) were placed onto neodymium magnets to ensure separation of nanoparticles from the samples. Small samples (10 mL) were then taken from each test and were subjected to centrifuging and passed through a 0.22 micron filter to ensure all solid particles had been removed. After filtration, 5 mL aliquots were subjected to ICP-MS analysis.

6.5.6 Examination of Calix[4]bis-crown SiO_2 gel Extraction Ability

A column was loaded with calix[4]bis-crown SiO_2 gel **83** (500 mg). A sample of Cs solution (100 ppb) at pH 7 (5 mL) was passed through the column with a flow rate of 5 mL min^{-1}. The eluent was subjected to centrifuging and passed through a 0.22 micron filter to ensure no silica that may have passed through the column was in the eluent. A sample (5 mL) was then taken for ICP-MS analysis. Extraction was repeated with a new sample of Cs solution (100 ppb) which was passed through a chloro-functionalised SiO_2 gel loaded column to compare extraction capabilities of the two solid phases.

6.5.7 Capacity study of calix[4]bis-crown SiO_2 gel

Calix[4]bis-crown SiO_2 gel **83** (500 mg) was loaded onto a column. Seven samples of Cs solution (100 ppb) at pH 7 (5 mL) were passed through the column with a flow rate of 5 mL min^{-1}. Each 5 mL sample was subjected to centrifuging and passed through a 0.22 micron filter to ensure no silica that may have passed through the column was in the eluent. The samples were then subjected to ICP-MS analysis.

6.5.8 Examination of Calix[8]amide MNPs Extraction Ability

Six samples of Sr solution (10 mL) were made to approx. 10 ppb using a stock Sr solution (1000 ppm). Three samples were subjected to mixing with calix[8]amide functionalised MNPs **88** (5 mg) and the final three with iodo-functionalised MNPs (5 mg). Mixing was carried out for 24 hours and samples (10 mL) were placed onto neodymium magnets to ensure separation of nanoparticles. The samples were centrifuged and passed through a 0.22 micron filter to ensure all solid particles had been removed before ICP-MS analysis. After filtration, aliquots (5 mL) were subjected to ICP-MS analysis.

6.5.9 Examination of Calix[8]amide SiO_2 gel Extraction Ability

A column was loaded with calix[4]bis-crown SiO_2 gel **89** (500 mg). A sample of Cs solution (100 ppb) at pH 7 (5 mL) was passed through the column with a flow rate of 5 mL min^{-1}. The eluent was subjected to centrifuging and passed through a 0.22 micron filter to ensure no silica that may have passed through the column was in the eluent. A sample (5 mL) was then subjected to ICP-MS analysis. Extraction was repeated with a new sample of Cs solution (100 ppb), which was passed through a chloro-functionalised SiO_2 gel loaded column and treated in the same way to compare extraction capabilities.

6.5.10 Capacity study of BTBP functionalised SiO_2 coated MNPs

Four samples of 100 mL transition metal mix (V, Cr, Mn, Fe, Co, Ni, Cu, Zn, Ag, Cd) were made to approx. 100 ppb using a stock transition metal mix (100 ppm) at pH 2. The samples were mixed with different doses of BTBP-functionalised SiO_2 coated MNPs **97** (10 mg, 100 mg, 200 mg, 500 mg). Mixing was achieved for 8 hours and the samples were then placed onto neodymium magnets to ensure separation of nanoparticles. Small samples (10 mL) were then taken from each test and were subjected to centrifuging and passed through a 0.22 micron filter to ensure all solid particles had been removed. After filtration, 5 mL aliquots were subjected to ICP-MS analysis.

6.5.11 Kinetics study of BTBP functionalised SiO_2 coated MNPs

Three samples of 100 mL transition metal mix (V, Cr, Mn, Fe, Co, Ni, Cu, Zn, Ag, Cd) were made to approx. 100 ppb using a stock transition metal mix (100 ppm) at pH 0.5, 2 and 7. The sample was mixed with BTBP-functionalised SiO_2 coated MNPs **97** (10 mg) for 24 hours. Small samples (5 mL) were taken at intervals (5, 30, 60, 120, 240, 480 and 1440 mins) and placed onto neodymium magnets to ensure separation of nanoparticles. Samples were subjected to

centrifuging and passed through a 0.22 micron filter to ensure all solid particles had been removed. After filtration, 5 mL aliquots were subjected to ICP-MS analysis.

Appendices

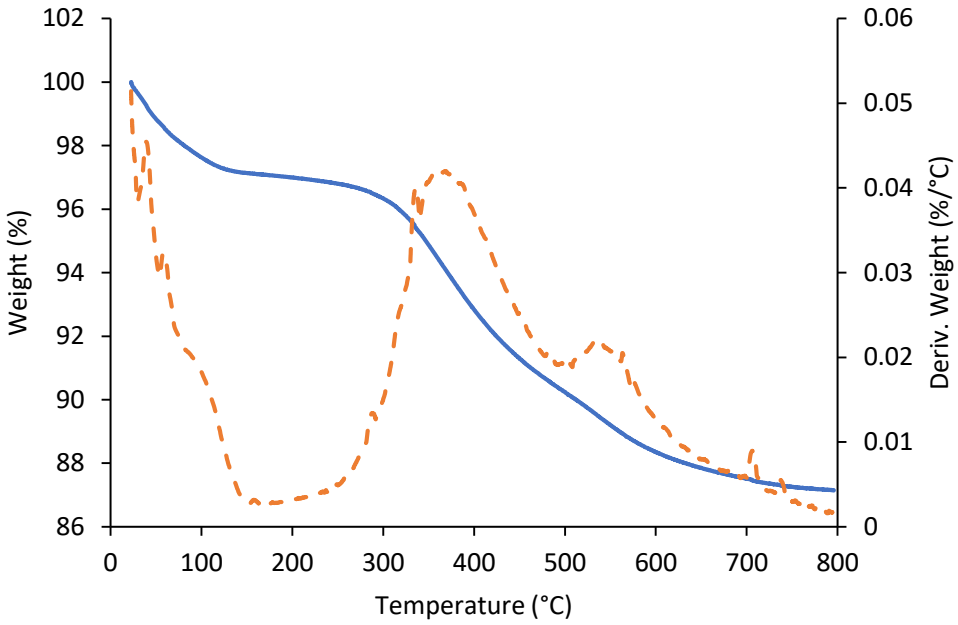

Appendix A1 – TGA for chloropropyl-functionalized SiO_2 gel **82**

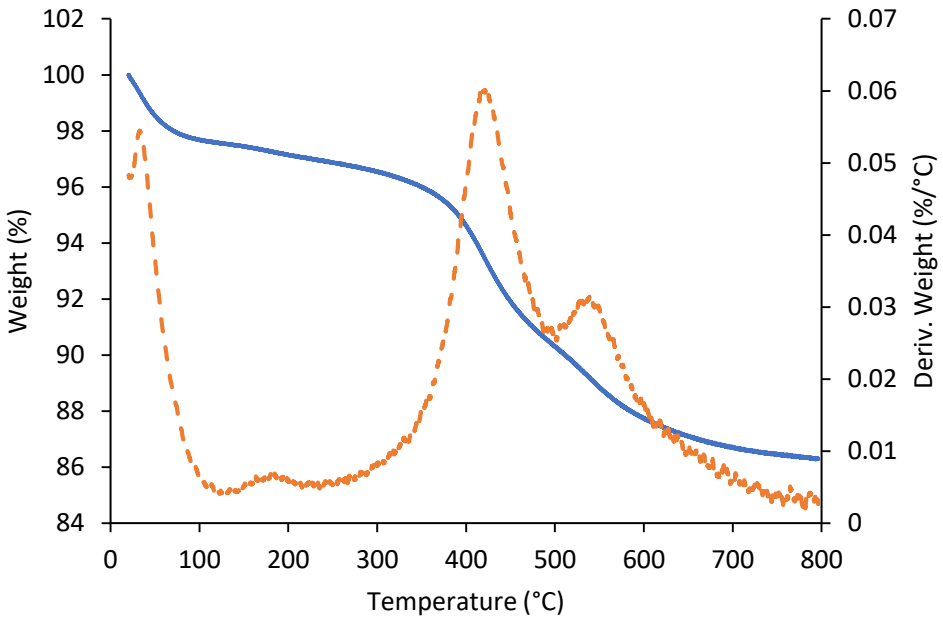

Appendix A2 – TGA for calix[4]bis-crown functionalised SiO_2 gel **83**

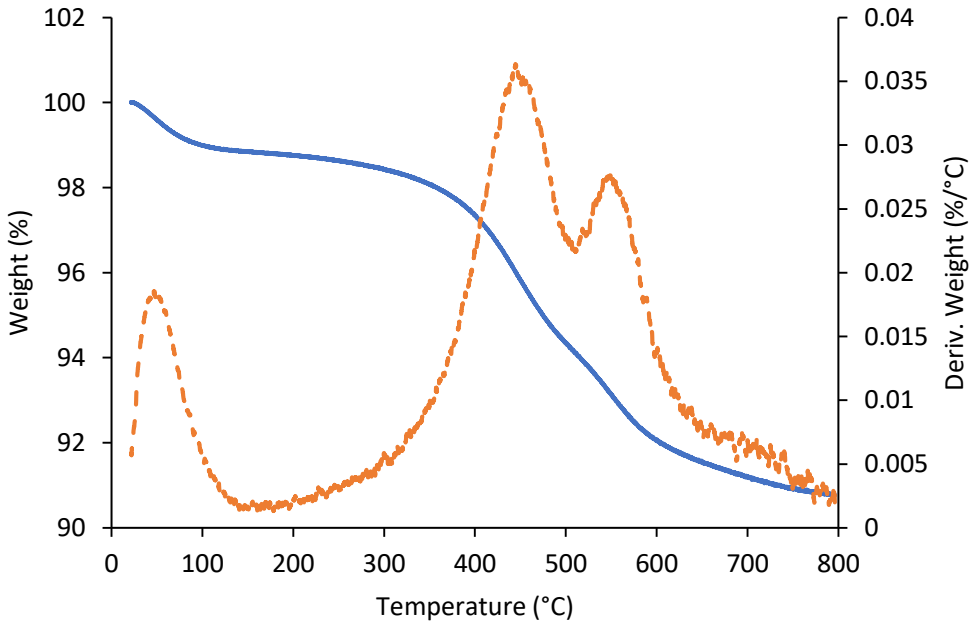

Appendix A3 – TGA for calix[8]arene functionalised SiO_2 gel **89**

References:

1 V. Smil, *Energy Transitions: Global and National Perspectives*, 2017.

2 J. M. V. Antonio Erias, Cansu Karaka, Corinna Grajetzki, James Carton, Mekalia Paulos, Pirjo Jantunen, Prajwal Baral, Samal Bex, *World Energy Resources 2016*, 2016.

3 A. Verbruggen and E. Laes, *Environ. Sci. Policy*, 2015, **51**, 170–180.

4 L. Borges Silverio and W. D. Q. Lamas, *Energy Policy*, 2011, **39**, 281–289.

5 IAEA, *IAEA Nucl. Energy Ser.*, 2018, **NW-T-1.14**, 74.

6 F. W. Lewis, M. J. Hudson and L. M. Harwood, *Synlett*, 2011, 2609–2632.

7 C. E. Housecroft and A. G. Sharpe, *Inorganic chemistry*, Pearson Prentice Hall, 2008.

8 L.R., *Nuclear engineering handbook*, 1959, vol. 11.

9 V. S. Yemel'yanov and A. I. Yevstyukhin, *Metall. Nucl. Fuel*, 1969, **101**, 1–571.

10 D. D. Sood and S. K. Patil, *J. Radioanal. Nucl. Chem. Artic.*, 1996, **203**, 547–573.

11 J. E. Birkett, M. J. Carrott, O. D. Fox, C. J. Jones, C. J. Maher, C. V. Roube, R. J. Taylor and D. A. Woodhead, *Chim. Int. J. Chem.*, 2005, **59**, 898–904.

12 The Royal Society, *Fuel cycle stewardship in a nuclear renaissance*, 2011.

13 F. W. Lewis, L. M. Harwood, M. J. Hudson, M. G. B. Drew, J. F. Desreux, G. Vidick, N. Bouslimani, G. Modolo, A. Wilden, M. Sypula, T. H. Vu and J. P. Simonin, *J. Am. Chem. Soc.*, 2011, **133**, 13093–13102.

14 S. Cotton, *Lanthanide and Actinide Chemistry and Spectroscopy*, Wiley, 2006.

15 M. J. Hudson, F. W. Lewis and L. M. Harwood, *The circuitous journey from malonamides to BTPhens: Ligands for separating actinides from lanthanides*, Elsevier Ltd., 1st edn., 2013, vol. 9.

16 F. W. Lewis, L. M. Harwood, M. J. Hudson, P. Distler, J. John, K. Stamberg, A. Núñez, H. Galán and A. G. Espartero, *European J. Org. Chem.*, 2012, **2012**, 1509–1519.

17 A. E. V Gorden, M. A. DeVore and B. A. Maynard, *Inorg Chem*, 2013, **52**, 3445–3458.

18 C. Madic, B. Boullis, P. Baron, F. Testard, M. J. Hudson, J.-O. Liljenzin, B. Christiansen, M. Ferrando, A. Facchini, A. Geist, G. Modolo, A. G. Espartero and J. De Mendoza, *J. Alloys Compd.*, 2007, **444**, 23–27.

19 L. Nigond, N. Condamines, P. Y. Cordier, J. Livet, C. Cuillerdier, C. Musikas, L. Nigond, N. Condamines, P. Y. Cordier, J. Livet, C. Madic, C. Cuillerdier, C. Musikas and M. J. Hudson, *Sep. Sci. Technol.*, 1995, **30**, 2075–2099.

20 C. Cuillerdier, C. Musikas, P. Hoel, L. Nigond and X. Vitart, *Sep. Sci. Technol.*, 1991, **26**, 1229–1244.

21 S. A. Ansari, P. Pathak, P. K. Mohapatra and V. K. Manchanda, *Chem. Rev.*, 2012, **112**, 1751–1772.

22 S. Tachimori, Y. Sasaki and S. I. Suzuki, *Solvent Extr. Ion Exch.*, 2002, **20**, 687–699.

23 H. Narita, T. Yaita and S. Tachimori, *Solvent Extr. Ion Exch.*, 2004, **22**, 135–145.

24 T. Yaita, A. W. Herlinger, P. Thiyagarajan and M. P. Jensen, *Solvent Extr. Ion Exch.*, 2004, **22**, 553–571.

25 Y. Sasaki, P. Rapold, M. Arisaka, M. Hirata, T. Kimura, C. Hill and G. Cote, *Solvent Extr. Ion Exch.*, 2007, **25**, 187–204.

26 Z. X. Zhu, Y. Sasaki, H. Suzuki, S. Suzuki and T. Kimura, *Anal. Chim. Acta*, 2004, **527**, 163–168.

27 H. Galán, C. A. Zarzana, A. Wilden, A. Núñez, H. Schmidt, R. J. M. Egberink, A. Leoncini, J. Cobos, W. Verboom, G. Modolo, G. S. Groenewold and B. J. Mincher, *Dalt. Trans.*, 2015, **44**, 18049.

28 K. L. Nash, *Solvent Extr. Ion Exch.*, 1993, **11**, 729–768.
29 K. L. Nash and G. R. Choppin, *Sep. Sci. Technol.*, 1997, **32**, 255–274.
30 K. L. Nash, *Handb. Phys. Chem. Rare Earths*, 1994, **18**, 197–238.
31 N. Kaltsoyannis, *Inorg. Chem.*, 2013, **52**, 3407–3413.
32 A. Afsar, L. M. Harwood, M. J. Hudson, P. Distler and J. John, *Chem. Commun*, 2014, **50**, 15082.
33 C. Adam, P. Kaden, B. B. Beele, U. Müllich, S. Trumm, A. Geist, P. J. Panak and M. A. Denecke, *Dalt. Trans.*, 2013, **42**, 14068–14074.
34 A. Leoncini, J. Huskens and W. Verboom, *Chem. Soc. Rev.*, 2017, **46**, 7229–7273.
35 H. H. Dam, D. N. Reinhoudt and W. Verboom, *Chem. Soc. Rev.*, 2007, **36**, 367–377.
36 P. J. Panak and A. Geist, *Chem. Rev.*, 2013, **113**, 1199–1236.
37 Z. Kolarik, *Chem. Rev.*, 2008, **108**, 4208–4252.
38 Z. Kolarik, U. Mullich, F. Gassner and F. Karlsruhe, *Solvent Extr. Ion Exch.*, 1999, **17**, 1155–1170.
39 J. E. Dixon and T. C. Bruice, *J. Am. Chem. Soc*, 1972, **94**, 2052–2056.
40 B. F. Filippini and R. F. Hudson, *A General Treatment of Enhanced Nucleophilic Reactivity*, 1972.
41 W. P. Jencks, J. Carriuolo Vol, B. P. William Jencks, J. Carriuolo and K. J. Laidler, *Reactivity of Nucleophilic Reagents toward Esters*, Faraday Soc, 1952, vol. 74.
42 E. Aneheim, C. Ekberg, A. Fermvik, M. R. S. J. Foreman, T. Retegan and G. Skarnemark, *Solvent Extr. Ion Exch.*, 2010, **28**, 437–458.
43 M. J. Hudson, L. M. Harwood, D. M. Laventine and F. W. Lewis, *Inorg. Chem.*, 2013, **52**, 3414–3428.
44 M. Nilsson, C. Ekberg, M. Foreman, M. Hudson, J. O. Liljenzin, G. Modolo and G. Skarnemark, *Solvent Extr. Ion Exch.*, 2006, **24**, 823–843.
45 D. Magnusson, B. Christiansen, M. R. S. Foreman, A. Geist, J. P. Glatz, R. Malmbeck, G. Modolo, D. Serrano-Purroy and C. Sorel, *Solvent Extr. Ion Exch.*, 2009, **27**, 97–106.
46 L. M. Harwood, F. W. Lewis, M. J. Hudson, J. John and P. Distler, *Solvent Extr. Ion Exch.*, 2011, **29**, 551–576.
47 A. Afsar, P. Distler, L. M. Harwood, J. John and J. Westwood, *J. Org. Chem.*, 2016, **3**, 8–11.
48 T. Koubský, H. Schmidt, G. Modolo and L. Kalvoda, *Procedia Chem.*, 2016, **21**, 509–516.
49 A. Geist, C. Hill, G. Modolo, M. R. S. J. Foreman, M. Weigl, K. Gompper, M. J. Hudson and C. Madic, *Solvent Extr. Ion Exch.*, 2006, **24**, 463–483.
50 M. S. H. Bader, *J. Hazard. Mater.*, 2001, **82**, 139–182.
51 W. J. Weber, A. Navrotsky, S. Stefanovsky, E. R. Vance and E. Vernaz, *MRS Bull.*, 2009, **34**, 46–53.
52 P. K. Mohapatra, D. S. Lakshmi, A. Bhattacharyya and V. K. Manchanda, *J. Hazard. Mater.*, 2009, **169**, 472–479.
53 P. K. Mohapatra, S. A. Ansari, A. Sarkar, A. Bhattacharyya and V. K. Manchanda, *Anal. Chim. Acta*, 2006, **571**, 308–314.
54 M. V Ernest, J. P. Bibler, R. D. Whitley and N.-H. H. L. Wang, *Ind. Eng. Chem. Res.*, 1997, **36**, 2775–2788.
55 E. Blasius, W. Klein and U. Schön, *J. Radioanal. Nucl. Chem. Artic.*, 1985, **89**, 389–398.
56 G. Ye, F. Bai, J. Wei, J. Wang and J. Chen, *J. Hazard. Mater.*, 2012, **225**–**226**, 8–14.
57 M. Yamada, *Radiat. Emerg. Med.*, 2012, **1**, 33–39.
58 Y. A. Izrael, M. De Cort, A. R. Jones, I. M. Nazarov, S. D. Fridman, E. V. Kvasnikova, E. D.

Stukin, G. N. Kelly, I. I. Matveenko, Y. M. Pokumeiko, L. Y. Tabatchnyi and Y. Tsaturon, *Radiol. consequences Chernobyl Accid.*, 1996, 1–10.

59 A. Paasikallio, A. Rantavaara and J. Sippola, *the Science of the Total Environment tin. The transfer of cesium-137 and strontium-90 from soil to food crops after the Chernobyl accident*, 1994, vol. 155.

60 S. M. Vakulovsky, A. I. Nikitin, V. B. Chumichev, I. Y. Katrich, O. A. Voitsekhovich, V. I. Medinets, V. V Pisarev, L. A. Bovkum and E. S. Khersonsky, *Cesium-137 and Strontium-90 Contamination of Water Bodies in the Areas Affected by Releases from the Chernobyl Nuclear Power Plant Accident: An Overview*, 1994, vol. 23.

61 W. H. Hallenbeck, *Radiation protection*, Lewis Publishers, 1994.

62 M. Laraia, *Radioactive contamination and other environmental impacts of waste from nuclear and conventional power plants, medical and other industrial sources*, Elsevier Ltd, 2015.

63 K. Anzai, N. Ban, T. Ozawa and S. Tokonami, *J. Clin. Biochem. Nutr*, 2012, **50**, 2–8.

64 F. A. Cotton and G. Wilkinson, *Advanced Inorganic Chemistry*, Wiley-Blackwell, 3rd edn., 1972.

65 F. A. Cotton, G. Wilkinson, C. J. Pedersen,) T R Stengle and J. D. Baldeschwieler, *J. Chem. Phys*, 1966, **55**, 307.

66 C. J. Pedersen, D. G. Stewart, D. Y. Waddan, E. T. Borrows, B. Patent, J. L. Down, J. Lewis, B. Moore, G. W. Wilkinson and J. Chem, *J. Am. Chem. Soc*, 1967, **2**, 57.

67 J. W. Steed, *Coord. Chem. Rev.*, 2001, **215**, 171–221.

68 D. J. Cram, *Angew. Chemie Int. Ed. English*, 1986, **25**, 1039–1057.

69 R. D. Hancock, *J. Chem. Educ.*, 1992, **69**, 615–621.

70 J. D. Dunitz, M. Dobler, P. Seiler and R. P. Phizackerley, *Acta Cryst.*, 1974, **30**, 2733–2738.

71 D. Bright and M. R. Truter, *J. Chem. Soc. B*, 1970, 1544–1550.

72 M. A. Bush, M. R. Truter, P. H. Ribbe, H. D. Megaw and W. H. Taylor, *J. Chem. Soc. B*, 1971, **13**, 1503.

73 J. W. Steed and P. C. Junk, *J. Chem. Soc*, 1999, 2141–2146.

74 M. Mercer and M. R. Truter, *J. Chem. Soc*, 1973, 2215–2220.

75 G. J. Lumetta, R. D. Rogers and A. S. Gopalan, *Calixarenes for Separations*, American Chemical Society, 2000, vol. 757.

76 C. D. Gutsche, *Calixarenes*, Royal Society of Chemistry, 2008.

77 A. Zinke and E. Ziegler, *Berichte der Dtsch. Chem. Gesellschaft (A B Ser.*, 1944, **77**, 264–272.

78 J. W. Cornforth, P. D'acry Hart, G. A. Nicholls, R. J. W. Rees and J. A. Stock, *Br. Pharmacol. Soc.*, 1955, **10**, 73–86.

79 C. D. Gutsche, B. Dhawan, M. Leonis and D. Stewart, in *Organic Syntheses*, John Wiley & Sons, Inc., Hoboken, NJ, USA, 2003, pp. 77–77.

80 C. D. Gutsche and L. J. Bauer, *J. Am. Chem. Soc*, 1985, **107**, 6052–6059.

81 P. R. Martínez-Alanis and I. Castillo, *Tetrahedron Lett.*, 2005, **46**, 8845–8848.

82 R. M. Izatt, J. D. Lamb, R. T. Hawkins, P. R. Brown, S. R. Izatt and J. J. Christensen, *J. Am. Chem. Soc*, 1983, **105**, 1782–1785.

83 S. R. Izatt, R. T. Hawkins, J. J. Christensen and R. M. Izatt, *J. Am. Chem. Soc*, 1985, **107**, 63–66.

84 L. H. Delmau, P. V Bonnesen, N. L. Engle, T. J. Haverlock, F. V Sloop Jr. and B. A. Moyer, *Solvent Extr. Ion Exch.*, 2006, **24**, 197–217.

85 S. Pellet-Rostaing, F. Chitry, J. A. Spitz, A. Sorin, A. Favre-Réguillon and M. Lemaire, *Tetrahedron*, 2003, **59**, 10313–10324.

86 C. Xu, J. Wang and J. Chen, *Solvent Extr. Ion Exch.*, 2012, **30**, 623–650.

87 V. S. Talanov, G. G. Talanova, M. G. Gorbunova and R. A. Bartsch, *J. Chem. Soc. Perkin Trans.,* 2002, **2**, 209–215.

88 V. S. Talanov, G. G. Talanova and R. A. Bartsch, *Tetrahedron Lett.*, 2000, **41**, 8221–8224.

89 T. J. Haverlock, P. V Bonnesen, R. A. Sachleben and B. A. Moyer, *J. Incl. Phenom. Macrocycl. Chem.*, 2000, **36**, 21–37.

90 G. Arena, A. Contino, A. Magri, D. Sciotto and J. D. Lamb, *Supramol. Chem.*, 1998, **10**, 5–15.

91 M. G. Gorbunova, P. V Bonnesen, N. L. Engle, E. Bazelaire, L. H. Delmau and B. A. Moyer, *Tetrahedron Lett.*, 2003, **44**, 5397–5401.

92 S. Fanni, F. Arnaud-Neu, M. A. McKervey, M. J. Schwing-Weill and K. Ziat, *Tetrahedron Lett.*, 1996, **37**, 7975–7978.

93 A. Casnati, S. Barboso, H. Rouquette, M. J. Schwing-Weill, F. Arnaud-Neu, J. F. Dozol and R. Ungaro, *J. Am. Chem. Soc.*, 2001, **123**, 12182–12190.

94 H. Y. Lee, D. R. Bae, J. C. Park, H. Song, W. S. Han and J. H. Jung, *Angew. Chemie - Int. Ed.*, 2009, **48**, 1239–1243.

95 P. Xu, M. Zeng, D. L. Huang, C. L. Feng, S. Hu, M. H. Zhao, C. Lai, Z. Wei, C. Huang, G. X. Xie and Z. F. Liu, *Sci. Total Environ.*, 2012, **424**, 1–10.

96 Y. Pang, G. Zeng, L. Tang, Y. Zhang, Y. Liu, X. Lei, Z. Li, J. Zhang, Z. Liu and Y. Xiong, *Chem. Eng. J.*, 2011, **175**, 222–227.

97 Y. Feng, J.-L. Gong, G.-M. Zeng, Q.-Y. Niu, H.-Y. Zhang, C.-G. Niu, J.-H. Deng and M. Yan, *Chem. Eng. J.*, 2010, **162**, 487–494.

98 X. Liu, Q. Hu, Z. Fang, X. Zhang and B. Zhang, *Langmuir*, 2009, **25**, 3–8.

99 N. J. Williams, J. Dehaudt, V. S. Bryantsev, H. Luo, C. W. Abney and S. Dai, *Chem. Commun.*, 2017, **53**, 2744–2747.

100 C. F. Poole, *Trends Anal. Chem.*, 2003, **22**, 362–373.

101 J. M. Gladis and T. Prasada Rao, *Anal. Lett.*, 2002, **35**, 501–515.

102 K. Pyrzyñska and M. Trojanowicz, *Crit. Rev. Anal. Chem.*, 1999, **29**, 313–321.

103 A. Junker-Buchheit and M. Witzenbacher, *J. Chromatogr. A*, 1996, **737**, 67–74.

104 X. Chang, N. Jiang, H. Zheng, Q. He, Z. Hu, Y. Zhai and Y. Cui, *Talanta*, 2007, **71**, 38–43.

105 L. Nunez, M. Kaminski, C. Bradley, B. A. Buchholz, S. Landsberger, S. B. Aase, H. E. Tuazon and G. F. Vandegrif, *Chem. Technol. Div.*, 1995

106 M. D. Kaminski and L. Nunez, *Sep. Sci. Technol.*, 2000, **35**, 2003–2018.

107 W. Wu, Z. Wu, T. Yu, C. Jiang and W. S. Kim, *Sci. Technol. Adv. Mater.*, 2015, **16**, 23501.

108 A. Afsar, L. M. Harwood, M. J. Hudson, M. E. Hodson and E. J. Shaw, *Chem. Commun. (Camb).*, 2014, **50**, 7477–80.

109 M. Nazrul Islam, L. Van Phong, J. R. Jeong and C. Kim, *Thin Solid Films*, 2011, **519**, 8277–8279.

110 Y. Zhu, T. Ikoma, N. Hanagata and S. Kaskel, *Small*, 2010, **6**, 471–478.

111 J. G. Shao, X. C. Xie, Y. J. Xi, X. N. Liu and Y. X. Yang, *Glas. Phys. Chem.*, 2013, **39**, 329–335.

112 Z. Cao, L. Yang, Q. Ye, Q. Cui, D. Qi and U. Ziener, *Langmuir*, 2013, **29**, 6509–6518.

113 F. W. Lewis, L. M. Harwood, M. J. Hudson, M. G. B. Drew, A. Wilden, M. Sypula, G. Modolo, T.-H. Vu, J.-P. Simonin, G. Vidick, N. Bouslimani and J. F. Desreux, *Procedia Chem.*, 2012, **7**, 231–238.

114 G. Z. Fang, J. Tan and X. P. Yan, *Anal. Chem.*, 2005, **77**, 1734–1739.

115 A. Afsar, P. Distler, L. M. Harwood, J. John and J. Westwood, *Chem. Commun.*, 2017, **53**, 4010–4013.

116 P. K. Jal, S. Patel and B. K. Mishra, *Talanta*, 2004, **62**, 1005–1028.

117 A. Afsar, P. Distler, L. M. Harwood, J. John and J. Westwood, *Chem. Commun.*, 2017, **53**, 4010–4013.

118 L. M. Harwood, A. Afsar, P. Distler, J. John, J. S. Babra, Z. Y. Selfe, J. Cowell and J. Westwood, *Separation of Minor Actinides from Lanthanides Using Immobilized Ligand Systems: The Role of the Counterion*, 2018, vol. 99.

119 Z. Wang, *Comprehensive Organic Name Reactions and Reagents*, 2010.

120 M. B. Smith and J. March, *March's advanced organic chemistry*, 2007.

121 G. W. Kabalka, M. Varma and R. S. Varma, 1986, 2386–2388.

122 Y. Ju, D. Kumar and R. S. Varma, *J. Org. Chem.*, 2006, **71**, 6697–6700.

123 H. Jia, Q. Li, A. Bayaguud, S. She, Y. Huang, K. Chen and Y. Wei, *Sci. Rep.*, 2017, **7**, 1-9

124 S. Xu, I. Held, B. Kempf, H. Mayr, W. Steglich and H. Zipse, *Chem. - A Eur. J.*, 2005, **11**, 4751–4757.

125 P.-E. Danjou, D. Wallyn, F. Cazier-Dennin and F. Delattre, *Ultrason. Sonochem.*, 2012, **19**, 1201–1204.

126 G. Brown and F. Nystrom, *Reduction of Organic Compounds by Lithium Aluminium Hydride*, 1947, vol. 1199.

127 K. E. Wiegers and S. G. Smith, *J. Org. Chem.*, 1978, **43**, 1126–1131.

128 K. Maaz, S. Karim, A. Mumtaz, S. K. Hasanain, J. Liu and J. L. Duan, *J. Magn. Magn. Mater.*, 2009, **321**, 1838–1842.

129 A. H. Lu, E. L. Salabas and F. Schüth, *Angew. Chemie - Int. Ed.*, 2007, **46**, 1222–1244.

130 R. Z. D. A. L. Andrade, D. M. Souza, M. C. Pereira, J. D. Fabris, *Cerâmica*, 2009, **55**, 420–424.

131 A. Morel, S. I. Nikitenko, K. Gionnet, A. Wattiaux, J. Lai-kee-him, C. Labrugere, B. Chevalier, G. Deleris, C. Petibois, A. Brisson, M. Simonoff, I. Bordeaux, L. H. Vigneau and A. Faculte, *ACS Nano*, 2008, **2**, 847–856.

132 M. Yamaura, R. L. Camilo, L. C. Sampaio, M. A. Mac# Edo, M. Nakamura and H. E. Toma, *J. Magn. Magn. Mater.*, 2004, **279**, 210–217.

133 A. Casnati, R. Ferdani, A. Pochini and R. Ungaro, 1997, **3263**, 6236–6239.

134 A. Afsar, P. Distler, L. M. Harwood, J. John and J. Westwood, *J. Org. Chem.*, 2016, **81**, 10517–10520.

135 O. Mitsunobu and M. Yamada, *Bull. Chem. Soc. Jpn.*, 2006, **40**, 2380–2382.

136 D. Hirose, M. Gazvoda, J. Košmrlj and T. Taniguchi, *Chem. Sci.*, 2016, **7**, 5148–5159.

137 K. C. K. Swamy, N. N. B. Kumar, E. Balaraman and K. V. P. P. Kumar, *Chem. Rev.*, 2009, **109**, 2551–2651.

138 A. Afsar, J. Westwood, P. Distler, L. M. Harwood, S. Mohan, J. John and F. J. Davis, *Tetrahedron*, 2018, **74**, 5258–5262.